ROCK-MASS BEHAVIOR IN THE TRANSITIONAL ZONE BETWEEN STRONG AND WEAK ROCK CONDITIONS

Prepared for

Nuclear Regulatory Commission
Contract NRC–02–97–009

Prepared by

Mikko P. Ahola
Sui-Min (Simon) Hsiung
Amitava Ghosh

Center for Nuclear Waste Regulatory Analyses
San Antonio, Texas

September 1999

CONTENTS

FIGURES

FIGURES (cont'd)

TABLES

ACKNOWLEDGMENTS

This report was prepared to document work performed by the Center for Nuclear Waste Regulatory Analyses (CNWRA) for the Nuclear Regulatory Commission (NRC) under Contract No. NRC-02-97-009. The activities reported here were performed on behalf of the NRC Office of Nuclear Material Safety and Safeguards, Division of Waste Management. The report is an independent product of the CNWRA and does not necessarily reflect the views or regulatory position of the NRC.

The authors thank R. Chen and P. Mackin for their reviews of this report. The authors are thankful to L. Selvey and J. Wike for skillful typing of the report and to C. Gray who provided a full range of expert editorial services in the preparation of the final document.

QUALITY OF DATA

All CNWRA-generated original data contained in this report meet quality assurance (QA) requirements described in the CNWRA Quality Assurance Manual. Sources for other data should be consulted for determining the level of quality for those data.

SOFTWARE QUALITY ASSURANCE

The distinct element code UDEC (Version 3.0) used for the analysis contained in this report, is controlled under the CNWRA software QA procedure (QAP) (TOP-018, Development and Control of Scientific and Engineering Software). Several simple software packages developed at the CNWRA were used for analyses of data contained in this report. These computational software packages fall under the categories covered by QAP-014, Documentation and Verification of Routine Calculations, and are not controlled by configuration management procedure TOP-018.

EXECUTIVE SUMMARY

The Yucca Mountain (YM) area is characterized by north to northwest-trending mountain ranges composed of volcanic strata that dip eastward. The strata are broken into *en echelon* fault blocks. The geomechanical conditions at the site are characterized by a highly fractured rock mass with prominent vertical and subvertical faults and joints that transgress the site environs. The proposed repository location is in the densely welded, devitrified part of the Topopah Spring (TSw2 unit) member of the Paintbrush tuff and is about 350 m below the ground surface.

Stability of underground openings, including emplacement drifts, would primarily depend on thermal-mechanical (TM) effects. The TM effects include those due to *in situ* and excavation-induced stresses; dynamic motions including the cumulative effect of repeated seismic motions; and thermally induced stresses and deformations. Movement along joints in the disturbed jointed rock mass would form the primary mode of deformation of the near-field rock mass (Kana et al., 1991, 1995; Hsiung et al., 1992). In addition to the TM effects, behavior of the joints would also be influenced by the presence of water (Jaeger and Cook, 1979; Hoek and Brown, 1982), temperature, and time-dependent degradation of mechanical properties of rock matrix and joints (Kemeny and Cook, 1990; Price et al., 1987). Furthermore, the rock-mass responses would likely be different in the regions of rock-mass strength transition. The rock-mass quality throughout the exploratory studies facility (ESF) derived from the scan-line and full-peripheral fracture mapping (Civilian Radioactive Waste Management System Management and Operating Contractor, 1997) indicates substantial variation.

A series of TM simulations were performed using the distinct element code UDEC Version 3.0 (Itasca Consulting Group, Inc., 1996) to investigate the effect on underground waste emplacement drifts at YM of a rock-mass transitional zone between strong and weak rock conditions. The analysis focused on the TM effects induced by *in situ*, excavation, and thermally induced stresses. The strong and weak rock-mass zones were simulated by varying the joint frequency in either region for the two joint sets modeled.

Results of these simulations indicate that, for emplacement drifts intersecting a transitional zone between strong and weak rock conditions, the shearing along joints is more extensive in the transitional zone than where no transitional zone is present. The effect does not appear to be significant for tensile and shear failure zones around the emplacement drifts. However, the effects of a transitional zone between strong and weak rock masses appear to be more pronounced if there is degradation to the rock block and rock joints/joint asperities due to a prolonged high temperature environment (a high-temperature environment enhances microfracturing and geochemical and geohydrologic changes within the rock).

The potential for rock-mass strength reduction under long-term thermal loading should be confirmed through heater tests currently being conducted within the ESF. Under degraded strength conditions, the adverse effects in the transitional zone are predicted to be in the form of zones of increased rock tension around drifts directly within the transitional zone as well as within adjacent drifts on the weak rock-mass side of the transitional zone, and increased rock failure from both yield and tension around the entire perimeter of such drifts. In addition, much larger joint shear displacements are predicted to occur along subhorizontal, and to some extent, subvertical joints around drifts located directly within the transition and within adjacent drifts on the weak rock-mass side of the transition. The larger degree of shearing along joints indicates the need for rock-bolt reinforcement that not only has a high axial strength, but also a high resistance to shearing at the joint intersections. The predicted rock failure in tension or yield around these drifts indicates the need for

additional rock reinforcement between the grouted rock bolts (e.g., wire mesh or steel straps). Finally, the floors of such drifts are not exempt from rock failure and joint shearing. Rock bolting into the floor of such drifts might be prudent to prevent shifting or uplift of the floor which could damage the pedestals on which the waste canisters rest. Although several base case simulations assuming both strong rock and weak rock conditions were analyzed, such base case simulations could not be run for all the transitional zone models analyzed. As a result, it cannot be confirmed that all the rock-mass behavioral effects identified in this report are solely due to the presence of a transitional zone. The effects might also be related to the different degree of jointing within each region.

1 INTRODUCTION

Yucca Mountain (YM), in southern Nevada, has been designated by the United States Congress for characterization as a potential repository site for high-level nuclear waste (HLW) disposal. The YM area is characterized by north to northwest-trending mountain ranges composed of volcanic strata that dip eastward. The strata are broken into *en echelon* fault blocks. The geomechanical conditions at the site are characterized by a highly fractured rock mass with prominent vertical and subvertical faults and joints that transgress the site environs. The potential repository location is in the densely welded, devitrified part of the Topopah Spring (TSw2 unit) member of the Paintbrush tuff and is about 350 m below the ground surface.

The fractured rock mass will be perturbed in several ways. First, construction of the proposed repository would alter the state of stress, which in turn would cause mechanical deformation of the rock including joint normal and shear deformations. Joint normal and shear deformations would affect excavation stability. Second, emplaced nuclear waste would provide an active heat source for an extended time period. This thermal load would induce rock expansion. Rock expansion could cause dilation, closure, and shear failure of fractures. The thermal load could also cause degradation of the mechanical properties of the rock mass (Price et al., 1987). Third, dynamic ground motions could induce additional stresses. The dynamic ground motions, including the cumulative effect of repeated seismic motions, could cause further dilation, closure, and shear of fractures (Hsiung et al., 1992; Kana et al., 1991, 1995). Designing for the preclosure or operations period ($\approx$ 100 yr) requires an understanding of the thermal-mechanical (TM) response of the jointed rock mass as it would impact drift stability and retrievability.

Stability of underground openings, including emplacement drifts, would primarily depend on TM effects. The TM effects would be caused by *in situ* and excavation-induced stresses, dynamic motions, including the cumulative effect of repeated seismic motions, and thermally induced stresses and deformations (Hsiung et al., 1992; Ghosh et al., 1996). Movement along joints in the disturbed, jointed rock mass would form the primary mode of deformation of the near-field rock mass (Kana et al., 1991, 1995; Hsiung et al., 1992). Excessive slippage of a rock block along failed joints may affect performance of the waste canisters inside emplacement drifts. In addition to the TM effects, behavior of the joint would also be influenced by the presence of water (Jaeger and Cook, 1979; Hoek and Brown, 1982), temperature, and time-dependent degradation of mechanical properties of rock matrix and joints (Kemeny and Cook, 1990; Price et al., 1987).

It is well recognized that rock strength and joint properties are a function of time (or stress) and temperature. That is, rock mass deteriorates as time passes and/or temperature increases (Martin, 1972; Hsiung and Shih, 1979; Price et al., 1987; Carter, 1975, 1976). Time-dependent decrease in shear strength of joints may be due to (i) fracture wall-rock alteration as a result of extended exposure to heat and moisture and (ii) slow deformation of asperities as a result of sustained stress concentration. The time-dependent decrease in strength of rock blocks is generally associated with (i) gradual slip on grain contacts under sustained stress concentration, (ii) subcritical crack growth due to sustained stress concentration at microcrack tips, and (iii) possible increase in ductility (decrease in viscosity) of minerals due to exposure to heat.

The rock-mass responses would be complicated further in the region where the rock-mass transitions from strong to weak. The stability of the transitional area under sustained heated conditions is not well understood. The rock-mass quality throughout the Exploratory Studies Facility (ESF) derived from the scan-line and full-peripheral fracture mapping (Civilian Radioactive Waste Management System Management and Operating Contractor, 1997) indicates substantial variation. Transition of rock mass from strong to weak

exists within small regions. Consequently, it may be necessary to better understand how the rock mass in these transitional regions behaves. This report was prepared with this objective in mind.

A series of TM simulations was performed using the distinct element method to investigate the effect on underground waste emplacement drifts at YM of a rock transitional zone between strong and weak rock conditions. The focus of the TM simulations was *in situ*, excavation, and thermally induced stresses. Effects of dynamic motion were not included in this analysis. Two vertical rock transitional zone locations were investigated: one directly through the centerline of a waste emplacement drift (3-drift TM model), and the other midway between two waste emplacement drifts (4-drift TM model). The strong and weak rock-mass zones were simulated by varying the joint frequency for the two joint sets modeled. The mean joint spacings in the weak rock-mass regions were set to roughly one-half those in the strong rock mass, considering computer code limitations and computer run times. Little information was available in the literature to define an approach to adjust the rock-mass properties of the rock blocks (i.e., moduli, etc.) based on the block sizes in each rock-mass region to take into account fractures/fissures that are not explicitly modeled. As a result, properties for these rock blocks were those obtained from test data on small intact cores from the proposed repository host rock (TSw2 unit), even though the blocks in the TM model for both regions were significantly larger than the core samples. The rock block was modeled as an elastic-plastic material. To the extent possible, the TM calculations were carried out for 150 yr, roughly the duration of the proposed repository preclosure period.

Additional TM simulations assumed either strong rock or weak rock conditions prevailed throughout the model domain as base cases to compare with the rock transitional zone models. To simulate the likely scenario of gradual degradation of the rock mass with time (i.e., from thermal or other effects), computer runs were conducted for the transitional zone models using reduced rock block and joint strength parameters. The effects of varying joint normal and joint shear stiffnesses in the transitional zone were also investigated. Finally, reinforcement using fully grouted rock bolts was simulated to investigate axial forces and failure of the steel bolts, shear forces and related failure of the grout, and effects on the behavior/yielding of the rock mass surrounding the emplacement tunnels in each rock-mass region. The number of discrete elements and finite difference zones within discrete elements as well as their irregular shapes and sizes considering standard deviations used in the generation of the joint patterns, resulted in severe restrictions on maximum thermal time steps and caused long computer run times. As a result, a limited number of TM runs was conducted to investigate the effects addressed. Table 1-1 shows a matrix of TM runs that were performed, the results of which are discussed in later sections of this report.

Table 1-1. Matrix of thermal-mechanical computer simulations

Case #	Model Type*		Joint Spacing†			Rock/Joint Strength‡		Joint Normal and Shear Stiffness§			Rock Bolt Reinforcement	
			Base Cases		Transition							
	3-Drift	4-Drift	Large	Small	Large/ Small	Ref.	Reduced	Ref.	Low	High	No	Yes
1	✔		✔			✔		✔			✔	
2	✔			✔		✔		✔			✔	
3	✔				✔	✔		✔			✔	
4		✔			✔	✔		✔			✔	
5	✔				✔		✔	✔			✔	
6		✔			✔		✔	✔			✔	
7	✔				✔	✔				✔	✔	
8	✔				✔	✔			✔		✔	
9	✔				✔		✔	✔				✔

* Model types (3-drift model has vertical rock transition through the middle of the drift, 4-drift model has vertical rock transition midway between the drifts). Note: Base case simulations have no transitional zone.
† Large spacing is twice the small spacing.
‡Reference rock/joint mechanical properties refer to U.S. Department of Energy laboratory test values on small cores (see tables 2-2, 2-3). Reduced strength parameter values are half of the reference parameter values.
§High joint normal and shear stiffness values are a factor of 10 higher than the reference values. Low joint normal and shear stiffness values are one-tenth the reference values.

2 DATA INPUT AND MODEL GEOMETRY

The TM analyses were conducted with the distinct element code UDEC Version 3.0 (Itasca Consulting Group, Inc., 1996). Two types of models were developed depending on the location of the rock-mass transitional zone. The first type included a transitional zone along the vertical centerline through an emplacement drift separating a strong rock-mass strength region from a weak rock-mass strength region (figure 2-1). The second type included a transitional zone located along a vertical line midway between two waste emplacement drifts (figure 2-2). As shown in figures 2-1 and 2-2, the waste emplacement drifts are spaced 28 m apart [based on U.S. Department of Energy (DOE) (1998a) Viability Assessment (VA) thermal loading strategy in section 2.2] and have a diameter of 5 m. For each analysis, additional emplacement tunnels were incorporated on either side of the transitional zone to minimize boundary effects, since the jointing included in the models was not symmetric about the transitional zone. The models extended vertically to the ground surface (approximately 300 m above the waste emplacement drift horizon) as well as over 200 m below the waste emplacement horizon to accommodate the temperature changes from the 150-yr thermal loading period.

Fracture geometry information (e.g., inclination angles, trace lengths) for the UDEC analyses was taken from previous distinct element TM analyses of the waste emplacement drifts in the TSw2 unit, namely Chen (1999). These data are based on fracture characteristics information collected at YM by the DOE through site characterization activities, including borehole exploration (Brechtel et al., 1995; Lin et al., 1993), surface

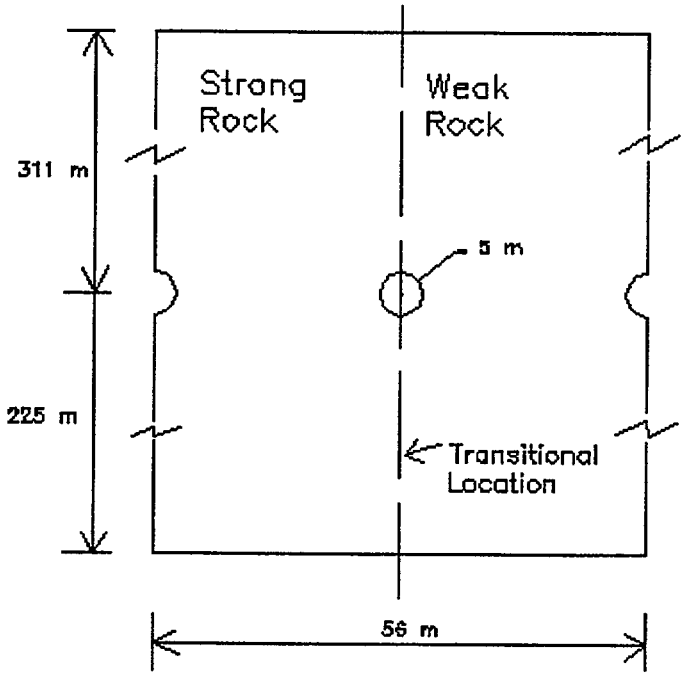

Figure 2-1. UDEC thermal-mechanical model with transitional zone located along vertical centerline through waste emplacement drift

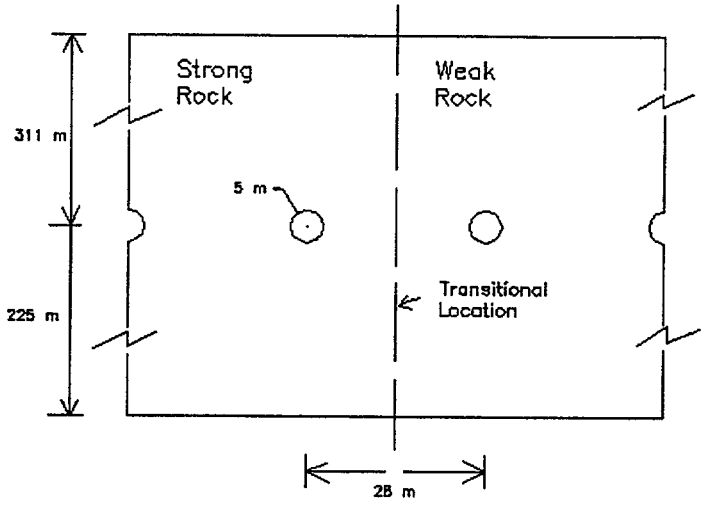

Figure 2-2. UDEC thermal-mechanical model with transitional zone located along vertical line midway between two waste emplacement drifts

mapping, and full-periphery geological mapping and detailed line survey in the ESF (Beason and Hoeg, 1997; Anna, 1998; Pye et al., 1997). Although three primary fracture sets were identified in the TSw2 unit using stereographic projections (Pye et al., 1997), only two primary fracture sets were included in the present TM analyses. As shown in table 2-1, these included a fracture set with a mean inclination of 85 degrees measured from the horizontal, and a second fracture set with a mean inclination of 20 degrees. Additional fracture parameters are listed in table 2-1. To simulate the difference between a strong and weak rock-mass strength on either side of the transitional zone, the fracture spacing was varied. For the weak rock, the subvertical fracture spacing was set to 0.5 m, and the subhorizontal spacing was set to 1.0 m [slightly larger than those used for the TSw2 horizon by Chen (1999) of 0.4 and 0.75 m for the subvertical and subhorizontal fracture spacings]. Since the present TM analysis incorporated a much larger fractured domain (i.e., multiple emplacement drifts), the fracture spacings needed to be increased slightly for the analysis to run in a reasonable time. For the strong rock region, the fracture spacing for both joint sets was increased by a factor of two. The rock blocks were similar for both regions. Estimates of the equivalent rock-mass moduli on either side of the rock transitional zone are provided in section 2.1.

Figure 2-3 shows the block mesh generated using the fracture information presented in table 2-1 for the strong and weak rock-mass regions for the 3-tunnel model with the transitional zone along the vertical centerline through the central tunnel. The UDEC code deletes portions of a fracture that only partially penetrate a block prior to zone generation. Therefore, the block mesh shown in figure 2-3 has such partial fracture segments deleted.

The fractured zone extends over the full lateral extent of the model, but only extends 15 m above and below the emplacement drifts to keep the number of blocks in the model and corresponding computer run times reasonable. The remainder of the far field is modeled as a continuum. This approximation does not appear to affect modeling results for the rock-mass behavior immediately around emplacement drifts. However, a slight discontinuity in the horizontal stress field was observed at the discontinuum and continuum boundary at a longer time. Figure 2-4 shows the UDEC block mesh generated for the 4-tunnel model from the fracture parameters in table 2-1, with the rock transitional zone along a vertical line midway between the two central tunnels. It was necessary to slightly overlap the joint generation regions between the strong and weak rock-mass

Table 2-1. UDEC parameters used to generate fracture pattern

Rock-Mass Strength	Joint Set	Angle*		Trace Length		Gap Length		Fracture Spacing	
		Mean	Deviation†	Mean	Deviation†	Mean	Deviation†	Mean	Deviation†
Weak Rock	1st	85.0	10.0	7.5	1.0	0.2	0.0	0.5	0.0
	2nd	20.0	5.0	5.0	1.0	0.2	0.0	1.0	0.0
Strong Rock	1st	85.0	10.0	7.0	1.0	0.2	0.0	1.0	0.0
	2nd	20.0	5.0	5.0	1.0	0.2	0.0	2.0	0.0

*The angle is measured counter-clockwise from the horizontal axis.
†The deviation is the standard deviation from the mean, assuming a uniform probability distribution.

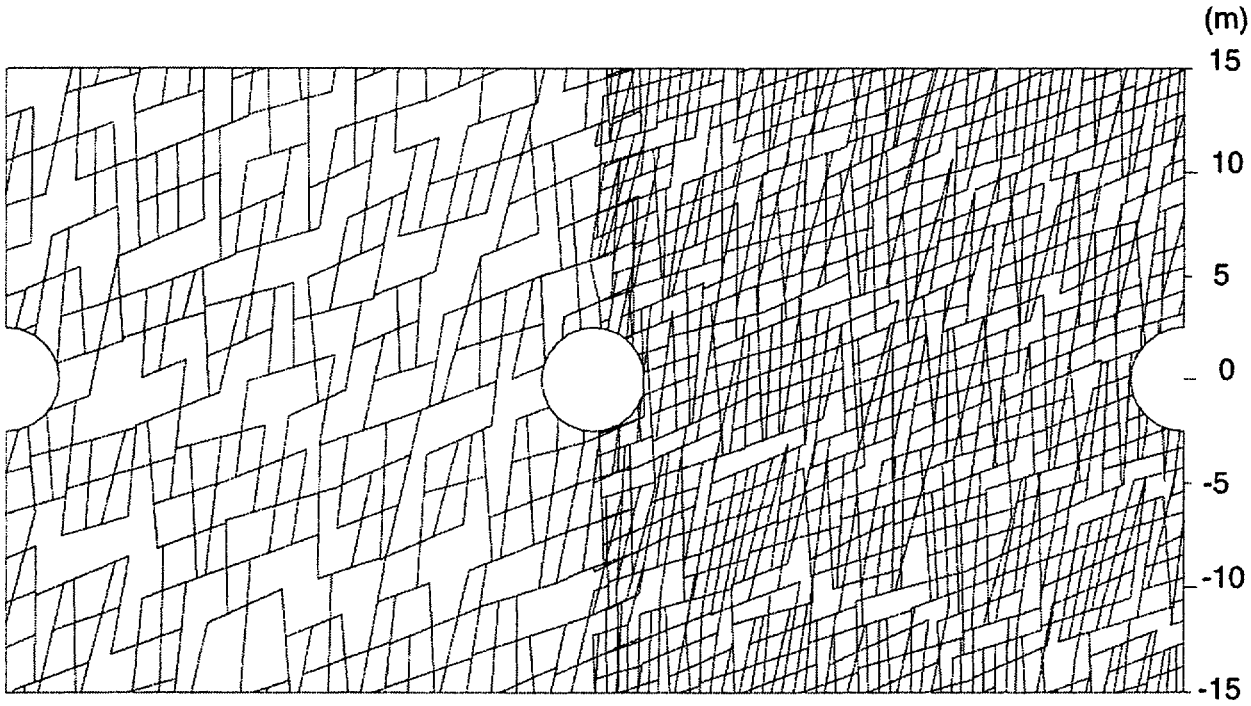

Figure 2-3. UDEC block plot for the 3-tunnel model with rock transitional zone along vertical centerline through the middle tunnel

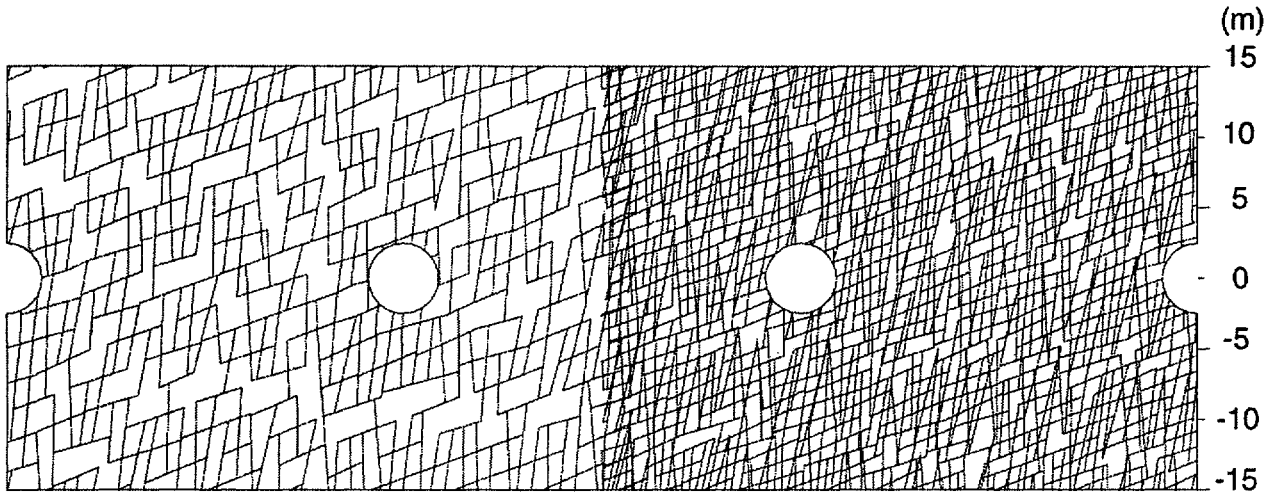

Figure 2-4. UDEC block plot for 4-tunnel model with rock transitional zone along vertical line midway between emplacement tunnels

regions, because UDEC automatically deletes joint segments that do not completely intersect a block or connect with other fracture traces. The result is that there would have been a narrow region with very little jointing. Overlapping the two joint regions eliminated this problem, although it added a few extra fractures over this narrow strip (i.e., 2.5 m) than would have resulted otherwise. Even with this narrow band of slightly higher joint density, an abrupt transition between a strong and weak rock mass exists at the intended locations.

2.1 MECHANICAL DATA INPUT

The reference rock mechanical property data for the TSw2 unit at the waste emplacement drift horizon was extracted from DOE VA studies of the underground facility (U.S. Department of Energy, 1997). This rock block property data was used in the UDEC analysis (table 2-2). Other rock units with different intact mechanical properties existing above and below the TSw2 host repository rock unit were not included in the analyses as they are sufficiently far away (i.e., approximately 100 m above or below waste emplacement drifts) that their impact on the TM results was assumed to be negligible. The reference mechanical properties of the fractures included in the UDEC analysis are listed in table 2-3 (U.S. Department of Energy, 1997, p. 14). The fractures were modeled with small cohesion and zero tensile strength and dilation.

Table 2-2. Reference rock block mechanical property data Topopah Spring (TSw2 unit)

Parameter	Value	Units
Bulk Modulus	18.39E+03	MPa
Shear Modulus	13.22E+03	MPa
Friction Angle	46.0	Degrees
Cohesion	36.9	MPa
Tensile Strength	8.91	MPa
Uniaxial Compressive Strength	166.0	MPa
Density	2297.0	Kg/m^3

Table 2-3. Reference rock joint mechanical property data Topopah Spring (TSw2 unit)

Parameter	Value	Unit
Friction Angle	41.0	Degrees
Cohesion	0.03	MPa
Tensile Strength	0.0	MPa
Dilation Angle	0.0	Degrees
Normal Stiffness	5.0E+04	MPa/m
Shear Stiffness	5.0E+04	MPa/m

Although the fracture spacings depicted in figures 2-3 and 2-4 are not uniform as a result of deviations in the input for the fracture inclination, the rock-mass modulus in a direction normal to a particular fracture orientation can be estimated. For a uniform joint spacing, a relation between the overall rock-mass modulus normal to the joint orientation can be developed in terms of the rock block Young's modulus, the joint spacing, and joint normal stiffness as follows (Itasca Consulting Group, Inc., 1996)

$$\frac{1}{E_m} = \frac{1}{E_r} + \frac{1}{K_n S} \qquad (2\text{-}1)$$

where

E_m — rock-mass modulus normal to fracture inclination (MPa)
E_r — rock block Young's modulus (MPa)

K_n — joint normal stiffness (MPa/m)
S — joint spacing (m)

An estimate of the rock-mass modulus in the subhorizontal direction (i.e., perpendicular to the subvertical joint set and the direction of highest thermal loading) for the UDEC TM analysis can be computed from Eq. (2-1) for both the strong and weak rock regions in the model. The thermal loading applied within the waste emplacement drifts results in the highest compressive stresses in this lateral direction. For the strong rock region [based on a mean subvertical fracture spacing (S) of 1.0 m, a fracture normal stiffness (K_n) of 50 GPa/m, and a rock block Young's modulus (E_r)] of 32 GPa, the equivalent horizontal rock-mass modulus (E_m) is computed to be approximately 20 GPa. Likewise, for the weak rock region [based on a mean subvertical fracture spacing (S) of 0.5 m, and the same parameter values for (K_n) and (E_r)] the equivalent horizontal rock-mass modulus (E_m) is computed to be approximately 14 GPa. Thus, by reducing the joint spacing by one-half between the strong and weak rock regions, the rock-mass modulus is reduced by approximately one-third. The DOE classifies the TSw2 repository block in terms of five rock categories, the weakest (category 1) having an estimated rock-mass modulus of 6.37 GPa, and the strongest (category 5) having an estimated rock-mass modulus of 23.51 GPa (U.S. Department of Energy, 1997, pp. 6–7). As such, the rock-mass moduli in this modeling analysis do not represent the extremes contained in DOE rock categories; however, the values used are believed sufficient to investigate whether a transition between strong and weak rock has increased detrimental effects on the emplacement drift performance during the preclosure period. Incorporating a larger transition in the rock-mass moduli into the UDEC models would require either increasing the joint frequency in the weak rock region (which may not be computationally feasible with UDEC) or reducing the rock block Young's modulus or joint normal stiffness. These considerations will be examined in a future study.

The effect of varying the joint normal and shear stiffnesses from their reference values (table 2-3) was evaluated in this TM study. Two cases were investigated, the first increasing both the joint normal and shear stiffnesses by a factor of 10 (i.e., to 5.0×10^5 MPa/m) from their reference values and the second decreasing the joint normal and shear stiffnesses by a factor of 10 (i.e., to 5.0×10^3 MPa/m). Using Eq. (2-1), with the lower value for the joint normal stiffness (i.e., $K_n = 5.0 \times 10^3$ MPa/m), the equivalent rock-mass modulus in the horizontal direction is calculated to be roughly 4.3 GPa in the strong rock-mass region and 2.3 GPa in the weak rock-mass region, using values of *S* equal to1.0 and 0.5 m, respectively.

Reduced rock block and joint strength parameters were used for several of the TM simulations. While the overall rock-mass moduli and joint stiffness remained the same for these simulations, the reduced rock and joint strength values of the rock block (simulating material degradation) result in faster onset to either yielding or tensile failure and subsequent plastic deformation and slip along joints. For these simulations, the joint friction and cohesion values listed in table 2-3 were reduced by one-half. The uniaxial compressive and tensile strengths of the rock block and rock block friction angle listed in table 2-2 were also reduced by one-half. The reduced rock block cohesion was determined from these above values using the following equation (Itasca Consulting Group, Inc., 1996)

$$q_u = S_i[\tan(45 + \varphi / 2)] \qquad (2\text{-}2)$$

where

q_u — uniaxial compressive strength (MPa)
S_i — rock cohesion (MPa)
φ — rock friction angle (degrees)

Fully grouted reinforced rock bolt properties used in several of the TM simulations are presented in table 2-4. Reinforcing steel properties (i.e., moduli and tensile yield strength) for an assumed 1.9 cm diameter bolt were obtained from Spiegel and Limbrunner (1998). A 20 MPa (3,000 psi) compressive strength cement was assumed for the grout. The grout modulus based on this compressive strength cement was also obtained from Spiegel and Limbrunner (1998). The value for the grout stiffness (K_{bond}) in table 2-4 is approximated from the following equation (Itasca Consulting Group, Inc., 1996)

$$K_{bond} = \frac{2\pi G}{10 \ln[1 + \frac{2t}{D}]} \qquad (2\text{-}3)$$

where

t — annulus thickness of the grout (m)
D — bolt diameter (m)
G — grout shear modulus (MPa)

Table 2-4. Rock bolt/grout reinforcement property data

Parameter	Value	Unit
Grout compressive strength	20.0	MPa
Grout shear modulus (G)	9.0E+03	MPa
Grout Poisson's ratio	0.19	Not applicable
Grout stiffness (K_{bond})	8.158E+03	MPa
Grout cohesive capacity(S_{bond})	0.6	MN/m
Bolt diameter (D)	1.9E-03	m
Hole diameter	3.8E-03	m
Bolt Young's modulus (E)	2.0E+05	MPa
Bolt tensile yield strength (F_y)	0.1375	MN

Likewise, the value for the grout cohesive capacity (S_{bond}), assuming failure that takes place at the grout/rock interface, is estimated from the following equations (Itasca Consulting Group, Inc., 1996)

$$S_{bond} = p(D + 2t)t_{peak} \tag{2-4}$$

and

$$\tau_{peak} = \tau_I Q_B \tag{2-5}$$

where

τ_I — one-half the grout compressive strength (MPa)
Q_B — quality of bond between grout and rock (assumed $Q_B = 1$ for perfect bonding)

The use of equations such as (2-4) and (2-5) was necessary to estimate the grout stiffness and strength properties, since no pull-test data could be found in the literature.

For all analyses, the applied *in situ* loading conditions at the waste emplacement horizon (i.e., y = −311 m depth) included a vertical compressive stress of approximately 7.0 MPa and a lateral or horizontal compressive stress of approximately 1.9 MPa, assuming a purely Poisson's effect (Chen, 1999). A vertical stress gradient of 0.022 MPa/m was used. Mechanical boundary conditions consisted of fixed vertical displacement at the base of the model and fixed lateral or x-displacement along the two vertical boundaries.

2.2 THERMAL DATA INPUT

The thermal rock property data for the TSw2 repository hoist rock formation were extracted from the DOE VA study reports (U.S. Department of Energy, 1997) and are listed in table 2-5. One limitation in the UDEC analysis is that the thermal properties cannot vary as a function of temperature, and mean values were used. The impact of this constraint on the results is not evaluated in this report..

The thermal calculations in UDEC are based on a rock continuum. Thus, fractures simulated in the model domain have no influence on the resulting temperature field. The DOE thermal loading strategy used the concept of areal mass loading (AML) in metric tons of uranium per acre, or MTU/acre. In the VA, DOE used 85 MTU/acre as the design AML that will satisfy the repository thermal goals (U.S. Department of Energy, 1998b). Therefore, for this TM modeling analysis, an 85-MTU/acre AML was utilized. The DOE

Table 2-5. Rock block thermal property data Topopah Spring (TSw2 Unit)

Parameter	Value	Units
Thermal conductivity	2.1	W/m-K
Thermal expansion coefficient	6.0E-06	K^{-1}
Specific heat	932.0	J/Kg-K

analysis shows that, to maintain an 85-MTU/acre AML, a uniform drift spacing of 28 m is needed. For a 28-m drift spacing, the waste package (WP) spacing is calculated to be 13.26 m (U.S. Department of Energy, 1998a,b; Chen, 1999). The VA design is evolving and DOE is evaluating an Enhanced Design Alternative (EDA) for the repository as a Site Recommendation Design (Civilian Radioactive Waste Management System, Management and Operating Contractor, 1999). This EDA uses a 60-MTU/acre thermal load. The drift spacing and WP spacing for the new design are 81 and 0.1 m, respectively. The emplacement drift stability for the new design will be investigated in the future. To simplify the two-dimensional (2D) UDEC analysis, the initial heat load from a WP is applied as a heat flux (W/m^2) directly to the drift wall, taking into account the drift wall circumference and the center-to-center spacing of the WPs. The initial heat output (Q_0) and average thermal decay for the WP assembly are provided in table V-1 of DOE (1998b). Assuming that the heat is uniformly distributed over the drift wall, the initial heat flux (q_0) is calculated as (Chen, 1999)

$$q_0 = \frac{Q_0}{\pi D L_{wp}} \tag{2-6}$$

where D is the drift diameter (5 m) and L_{wp} is the center-to-center spacing between two adjacent WPs (13.26 m). The thermal load is input into the UDEC model as a simple exponentially decaying flux boundary condition with a single decay coefficient of the form

$$q(t) = q_0 \exp(-\alpha t) \tag{2-7}$$

where q_0 (W/m^2) is the initial WP heat flux applied to the drift wall at the time of emplacement and α is the decay constant (s^{-1}). The initial heat flux was estimated to be 43.18 W/m^2, and the decay constant was estimated to be 3.22×10^{-10} (Chen, 1999).

Thermal boundary conditions utilized in the UDEC TM analysis consisted of zero heat flux along the two vertical boundaries (adiabatic), a fixed ground surface temperature of 18.7 °C, a fixed base temperature of 29.5 °C (i.e., 225 m below waste emplacement drift horizon), and a vertical temperature gradient of 0.02 °C/m.

2.3 MODEL SETUP

The UDEC TM analyses consisted of the following steps: (i) obtain model equilibrium under the *in situ* stress and gravity loading conditions, (ii) excavate the waste emplacement drifts and reach a new mechanical equilibrium state, and (iii) apply thermal loading as a decaying heat flux to the circular waste emplacement drift walls. The TM solution is performed as a decoupled process. In this approach, the thermal conduction is run for a short period followed by the mechanical calculations, to equilibrate with the new thermal state. The thermal time increment was specified on the order of days, weeks, and then months during the first portion of the TM analysis. It was then increased to years for the later portions of the analysis where the thermal gradients were much lower. The TM analyses were carried out for 150 yr after waste emplacement in most cases. All TM runs were conducted on a Micron Millennia Xku 300 MHz PC computer running Windows NT 4.0. Run times for the 150-yr thermal period were several days to a week, depending on the particular TM model run. The thermal calculations were the longest part of the run time, since UDEC used the same mechanical finite

difference mesh containing many small, irregular, and/or narrow finite difference zones for the thermal mesh, resulting in very slow thermal convergence. The UDEC implicit thermal time stepping scheme was used almost exclusively in the analyses, as the explicit time steps for the types of models run were calculated by UDEC to be too small for practical purposes.

To have a reference for comparison of the TM analyses with a rock transition, additional UDEC models were run assuming both strong rock or weak rock throughout the region around the waste emplacement drifts. The strong rock base case simulation assumed the fracture pattern represented by the left side of figures 2-3 and 2-4 existed throughout the model (i.e., no transitional zone). Likewise, the weak rock base case simulation assumed the fracture pattern represented by the right side of figures 2-3 and 2-4 existed throughout the lateral extent of the model.

3 MODELING RESULTS AND DISCUSSION

The UDEC TM analyses were conducted to investigate the impact of a transition between weak and strong rocks at two different locations: directly along the vertical centerline of a waste emplacement drift, and along a vertical line midway between two emplacement drifts. Different UDEC models were generated to analyze these two situations. UDEC input files for 3- and 4-drift rock transitional zone models are provided in appendixes A and B, respectively. As the UDEC TM analyses are 2D, a rock transition across a drift or series of drifts in the tunnel cross-sectional plane could be analyzed; however, a rock-mass strength transition along the length or axis of the tunnel could not be addressed. TM results are presented first for the case in which no rock transitional zone exists in the model (section 3.1). In this case, the entire modeled region had only one rock type. Two separate analyses were made using properties of both strong and weak rocks. Each rock type was modeled based on the representative fracture pattern (see table 2-1). TM results with a transitional zone are presented in section 3.2 along with the impact of a rock transitional zone on drift TM behavior. Sections 3.3, 3.4, and 3.5 discuss the impact of varying the joint stiffness, reducing the joint and rock block strength properties, and adding fully grouted reinforced rock bolts, respectively, on the effects of a transitional zone.

3.1 WITHOUT TRANSITIONAL ZONE

The parameters of interest in the UDEC TM analyses with and without a rock transitional zone include joint closure and joint shear displacements, stresses (including zones of tension), and failure or yield zones. Results presented in this section do not include a rock transitional zone and assume either a strong or weak rock, representative of the left-hand or right-hand side fracture geometry as shown in figure 2-3, exists throughout the lateral extent of the model. All results are shown after 150 yr of thermal loading and are plotted to the same scale for comparison.

Figures 3-1a and 3-1b show plots of joint shear displacements after 150 yr assuming weak and strong rock-mass strengths throughout the model, respectively. Figure 3-1a (weak rock) shows a maximum shear displacement of 8.58×10^{-3} m (8.58 mm) in the immediate floor of the center drift, and joint shear displacements are localized around the waste emplacement drifts. Figure 3-1b (strong rock) shows the maximum shear displacement to be slightly lower at approximately 6.06×10^{-3} m (6.06 mm) and, in addition to joint shear around the drifts, there is some shearing along the subhorizontal joints away from the immediate vicinity of the drifts. A small amount of shearing along the subvertical joints takes place close to the drift wall. The shearing along the subvertical joints occurred before the thermal load was applied (i.e., due to drift excavation alone), whereas the shearing along the subhorizontal joints occurred almost entirely from the thermal loading. The baseline cutoff for plotting the shear displacements was 5.0×10^{-4} m (0.5 mm).

Plots of joint closure show a more definite contrast between the weak rock and strong rock base case simulations as shown in figures 3-2a and 3-2b, respectively. Figure 3-2a for the weak rock base case, a maximum joint closure of 2.79×10^{-3} m (2.79 mm) is calculated, and the region of high joint closure is restricted primarily to the subvertical joints in the immediate roof and floor of the drifts (i.e., ± 5 m vertically above and below the drift centerline). However, figure 3-2b shows that, while the maximum joint closure for the strong rock simulation is slightly lower [i.e., 1.92×10^{-3} m (1.91 mm)], the region over which significant joint closure occurs is much larger. It extends approximately 10 to 15 m into the roof or floor of the drift as well as between the drifts, again only on the subvertical joints based on a joint closure cutoff of 5.0×10^{-4} m (0.5 mm) in the plots.

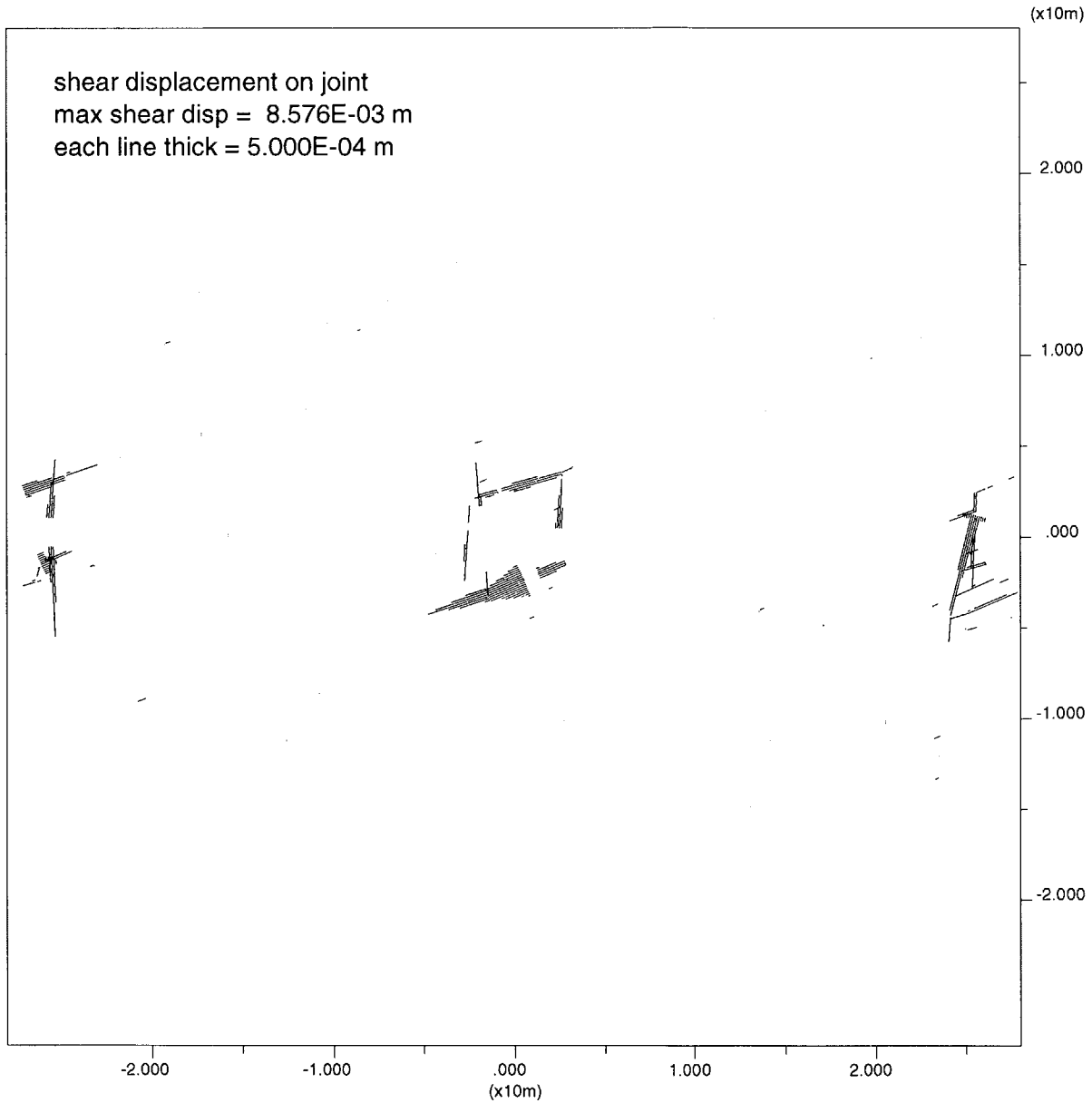

Figure 3-1a. Joint shear displacements (m) after 150 yr of thermal loading for base case weak rock-mass model

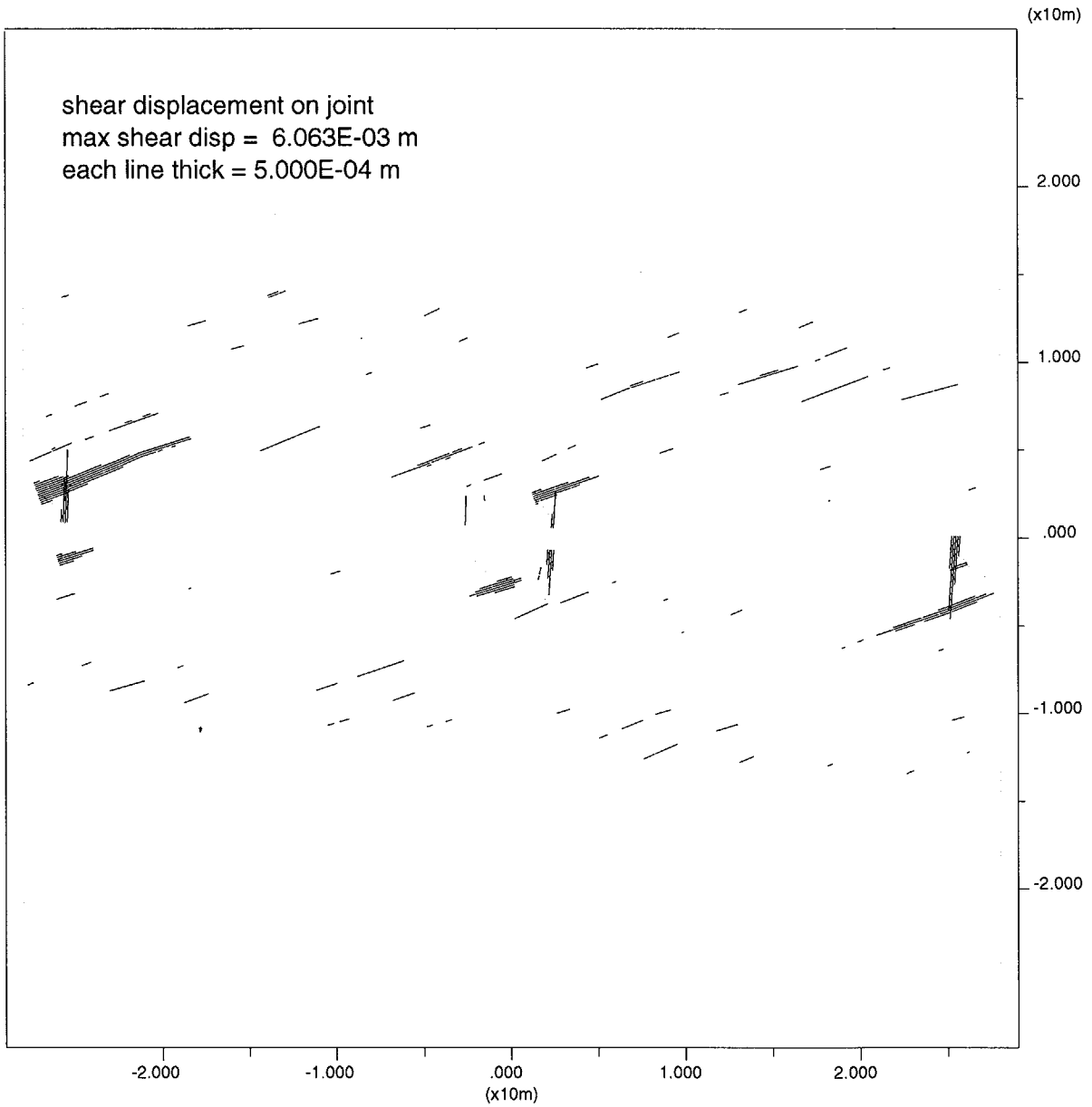

Figure 3-1b. Joint shear displacements (m) after 150 yr of thermal loading for base case strong rock-mass model

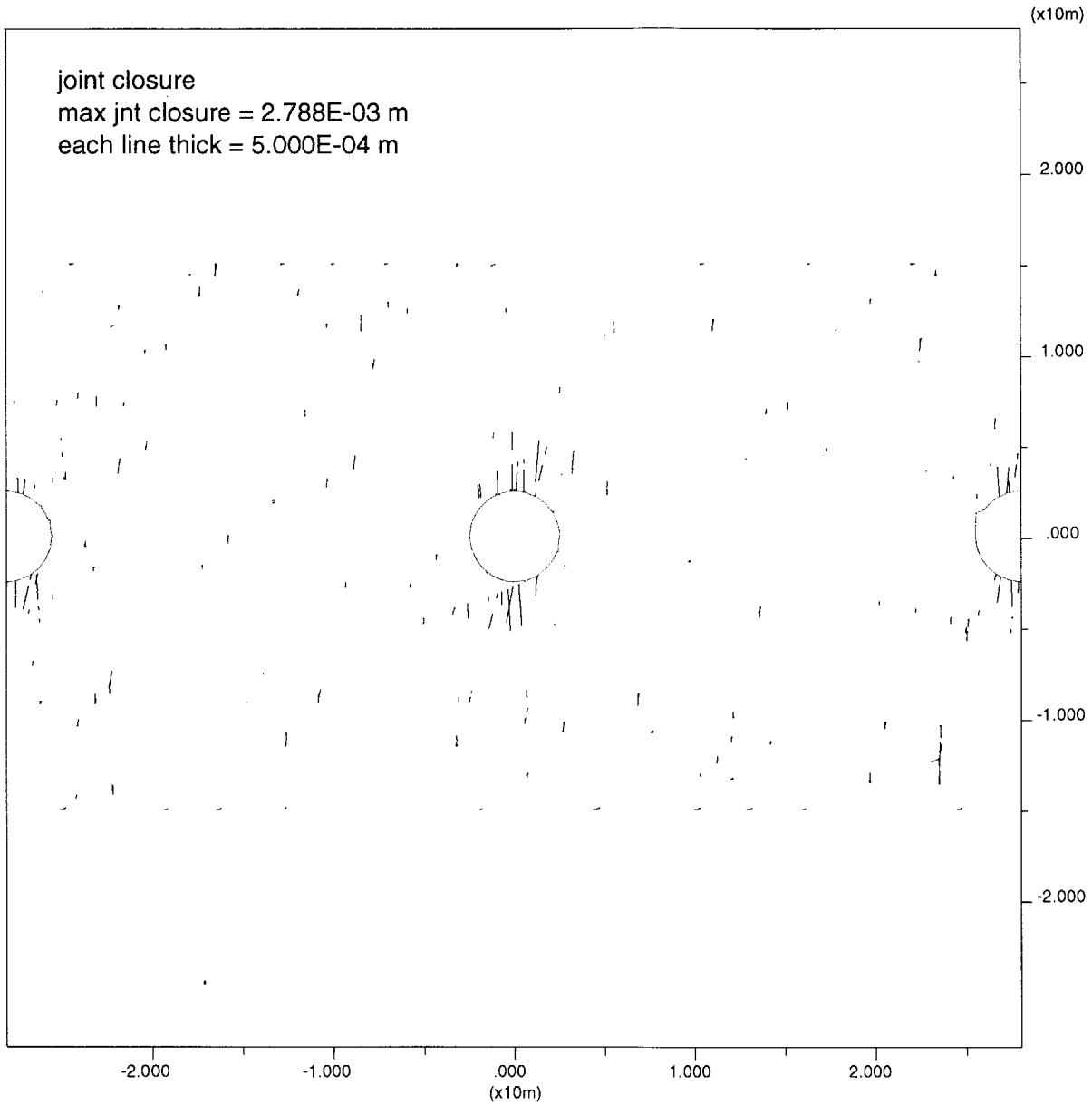

Figure 3-2a. Joint closure (m) after 150 yr of thermal loading for base case weak rock-mass model

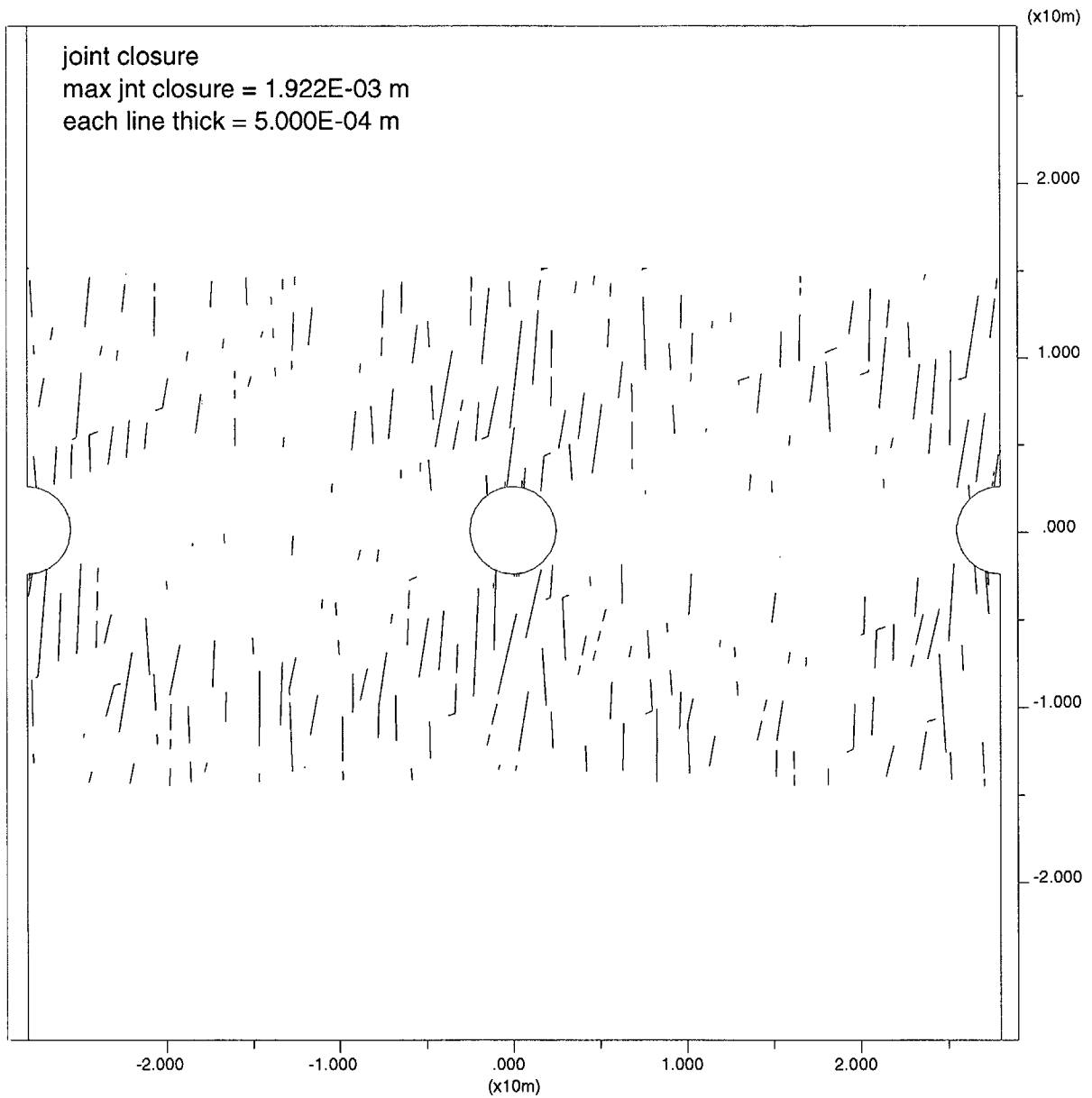

Figure 3-2b. Joint closure (m) after 150 yr of thermal loading for base case strong rock-mass model

Zones of tension around the central drift for the weak and strong rock base case simulations are depicted in figures 3-3(a) and (b), respectively. Although significant differences in tensile regions is not evident, the weak rock simulation shows somewhat more tension in the floor of the drift. Maximum tensile stress values are on the order of 6.5 to 7.5 MPa in both models (recall from table 2-2 the rock block tensile strength input value was 8.91 MPa). Based on the intact TSw2 rock strength parameters used in the analyses (see table 2-2), only a few rock zones along the perimeter walls of the waste emplacement drifts showed indications of rock yielding based on the Mohr-Coulomb failure criterion and no tensile rock failure after 150 yr of heating as shown in figures 3-4(a) and (b) for the base case strong and base case weak rock simulations, respectively. From monitoring points tracking time histories of various parameters, the horizontal compressive stress within the crown of the center tunnel peaks out between 60 to 65 MPa at around the period 80 to 100 yr after the start of heating for both base case models. Figures 3-5a and 3-5b show plots of major principal stress contours (compression negative) at a thermal time of 100 yr and near the time of maximum compression from the thermal load for the base case strong and base case weak rock masses, respectively. While the major principal stress magnitudes directly above the center tunnel are similar (as indicated also above from the monitoring points of horizontal stress at this location), the general major principal stress field is lower for the weak rock-mass model (figure 3-5b) than the strong rock-mass model (figure 3-5a). Maximum values for principal stresses, displacements, joint shear and closure values, etc., over the entire modeled domain are given in table 3-1 after drift excavation and 150 yr of thermal loading (end of simulation). Maximum rock temperatures calculated around the drift perimeter peak out at approximately 230°C at a time of approximately 60 yr after the start of heating.

3.2 WITH TRANSITIONAL ZONE

Effects of the rock transitional zone are presented, first for the case with a vertical transitional zone located along the centerline of the middle emplacement drift, and then for the case with the vertical transitional zone located midway between two emplacement drifts. Results are again plotted after 150 yr of thermal loading and at the same scale as those results presented in the previous section.

3.2.1 Vertical Rock Transitional Zone Along Centerline of Emplacement Drift (3-Drift Transitional Zone Model)

Figures 3-6 and 3-7 show plots of joint shear displacement and joint closure around the waste emplacement drifts after 150 yr of heating assuming a vertical transitional zone about the centerline of the middle drift (see figure 2-1 and figure 2-3). Figure 3-6 shows that the maximum shear displacement (21.2 mm) around the central drift where the transition occurs is higher than either that computed for the two base case simulations (figure 3-1a and b). Also, the effect of this transitional zone appears to concentrate the measurable shear displacements around the central drift and decrease the joint shear displacement along the subhorizontal joints in the adjacent drifts. As discussed in the previous section, the shear along the subvertical joints took place primarily after drift excavation and before heating.

Figure 3-7 shows that the maximum joint closure after 150 yr of heating for the UDEC model with the transitional zone is much smaller (1.47 mm) than for either the two base case TM simulations. The maximum joint closure is approximately one-half that calculated from the base case weak rock-mass simulation (figure 3-2a) and approximately three-quarters that of the base case strong rock simulation (figure 3-2b) after 150 yr of thermal loading. As shown in figure 3-6, the region of high joint closures is somewhat more extensive along the subvertical joints above and below the central tunnel where the transition occurs, than either the drifts

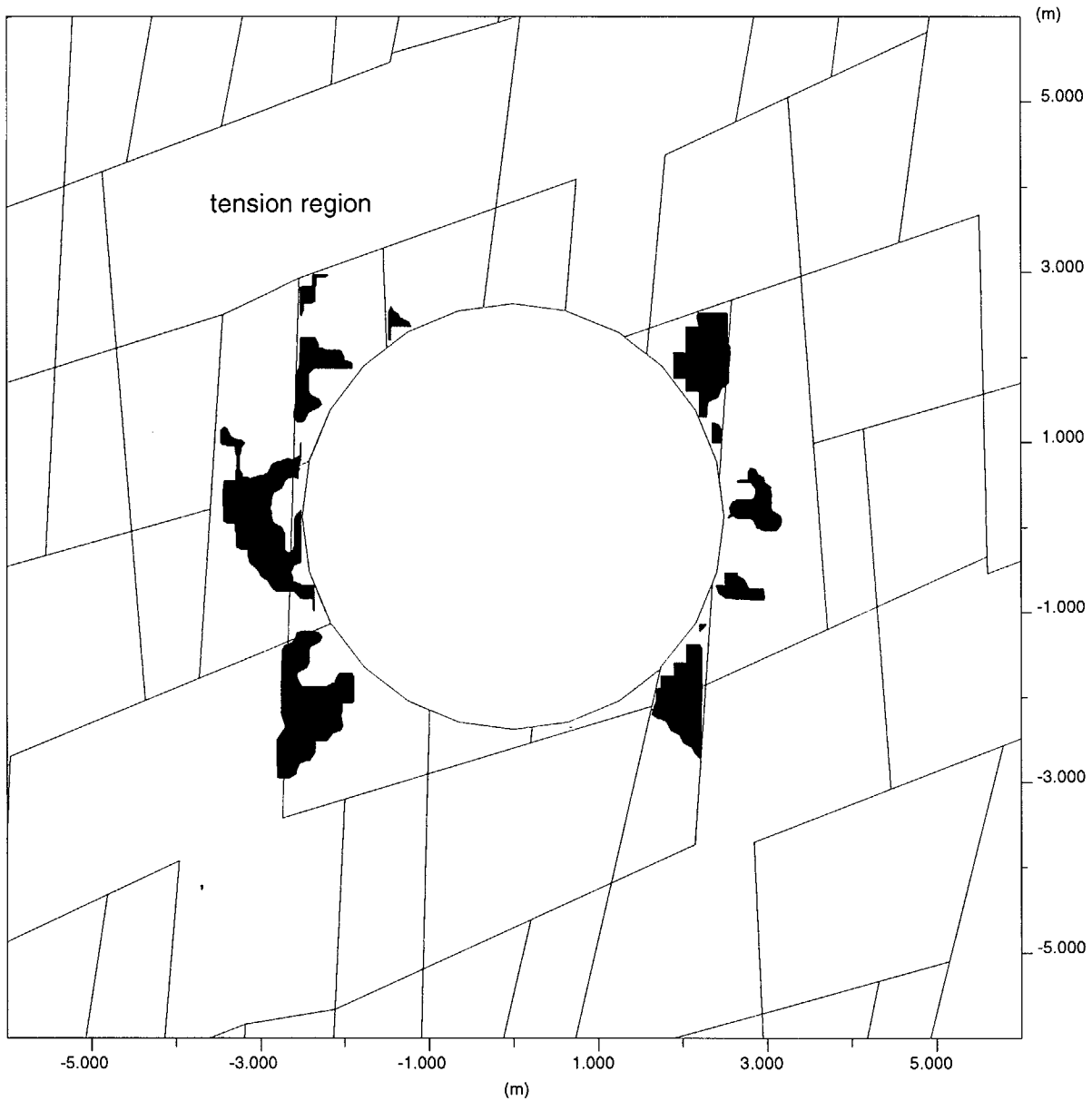

Figure 3-3a. Zones of tension (red) within the rock blocks for base case strong rock-mass model

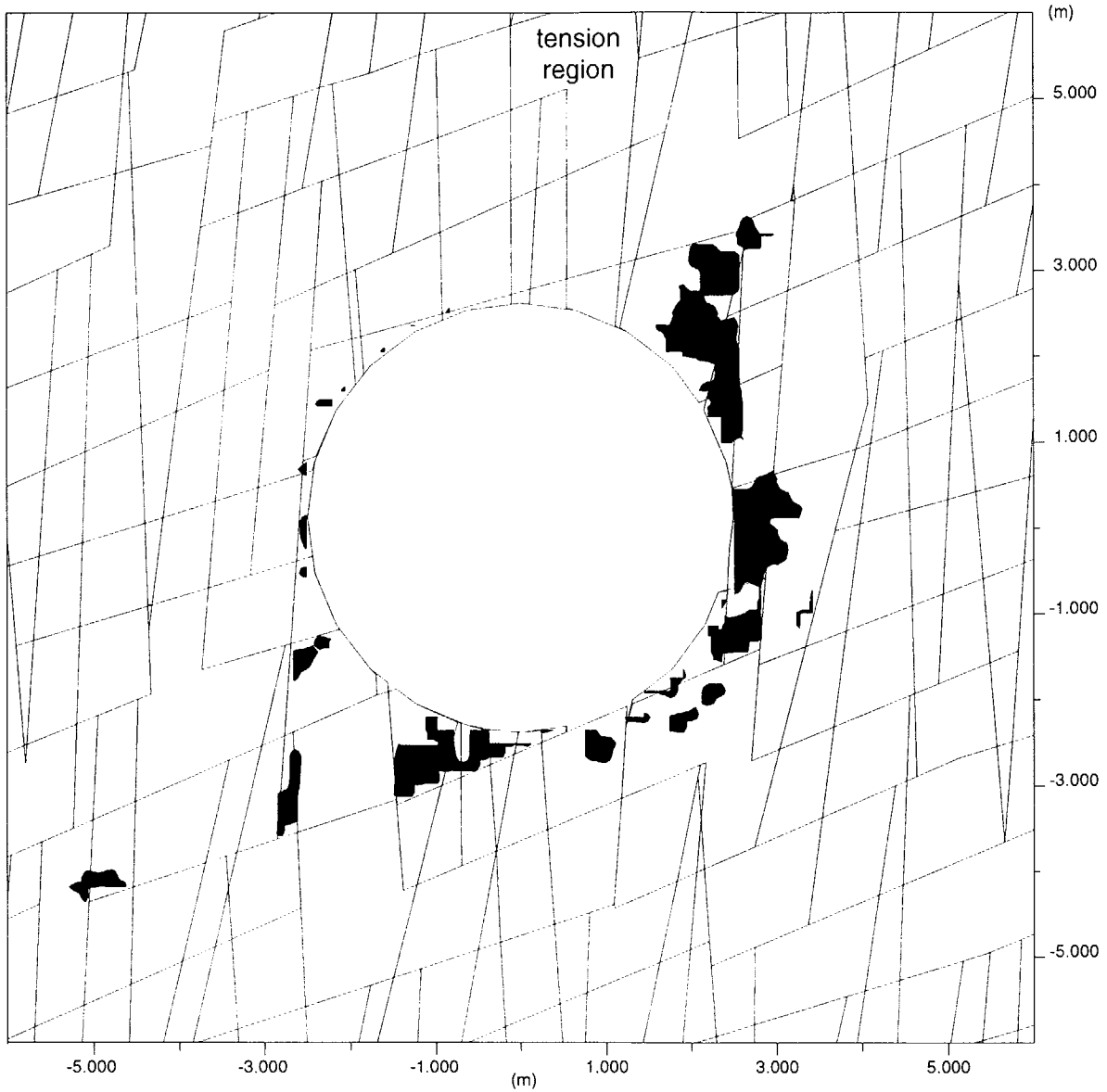

Figure 3-3b. Zones of tension (red) within rock blocks for base case weak rock-mass model (maximum tensile stress ranges from 6.5 to 7.5 MPa)

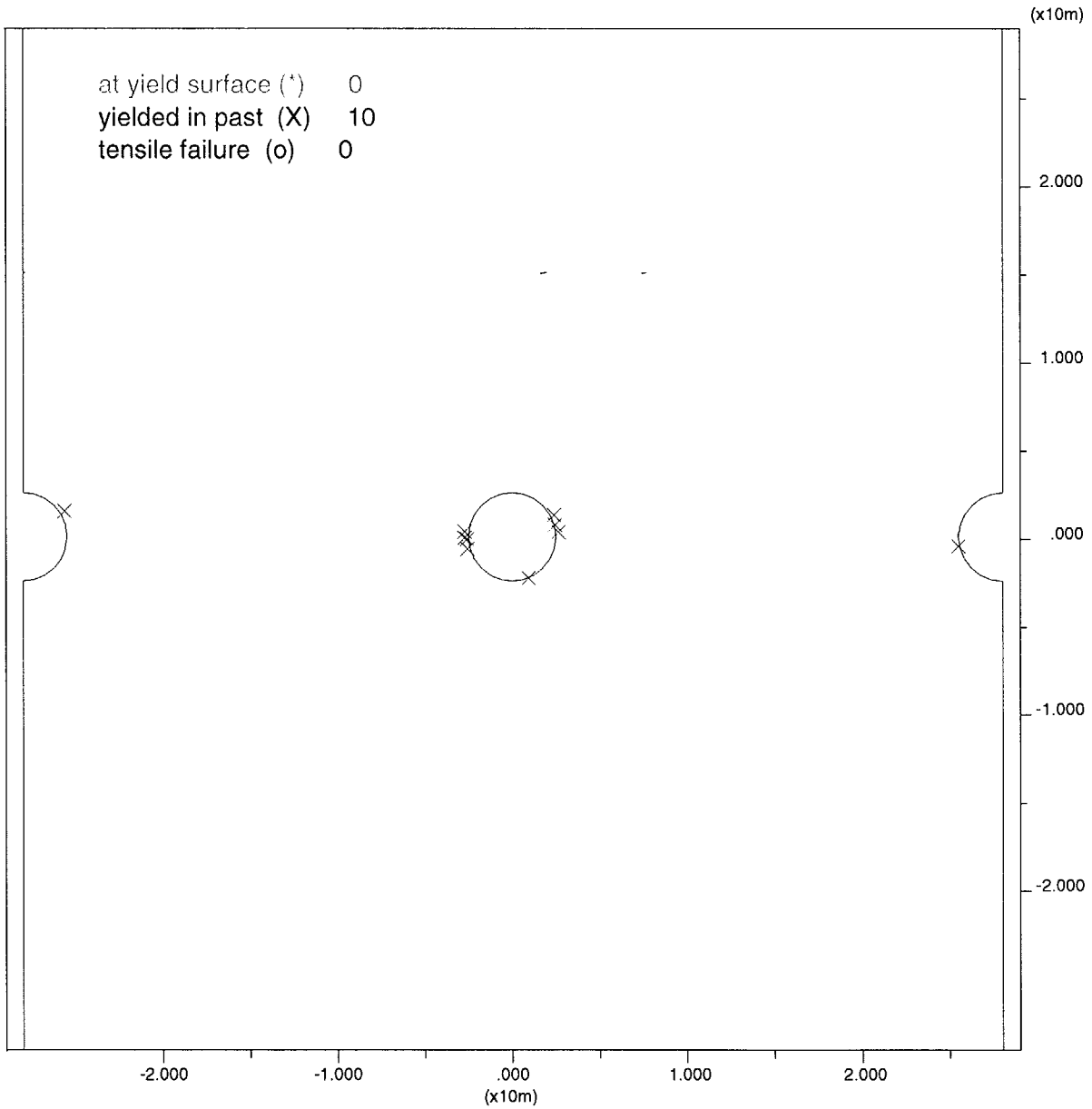

Figure 3-4a. Failure zones after 150 yr of thermal load assuming strong rock-mass model throughout

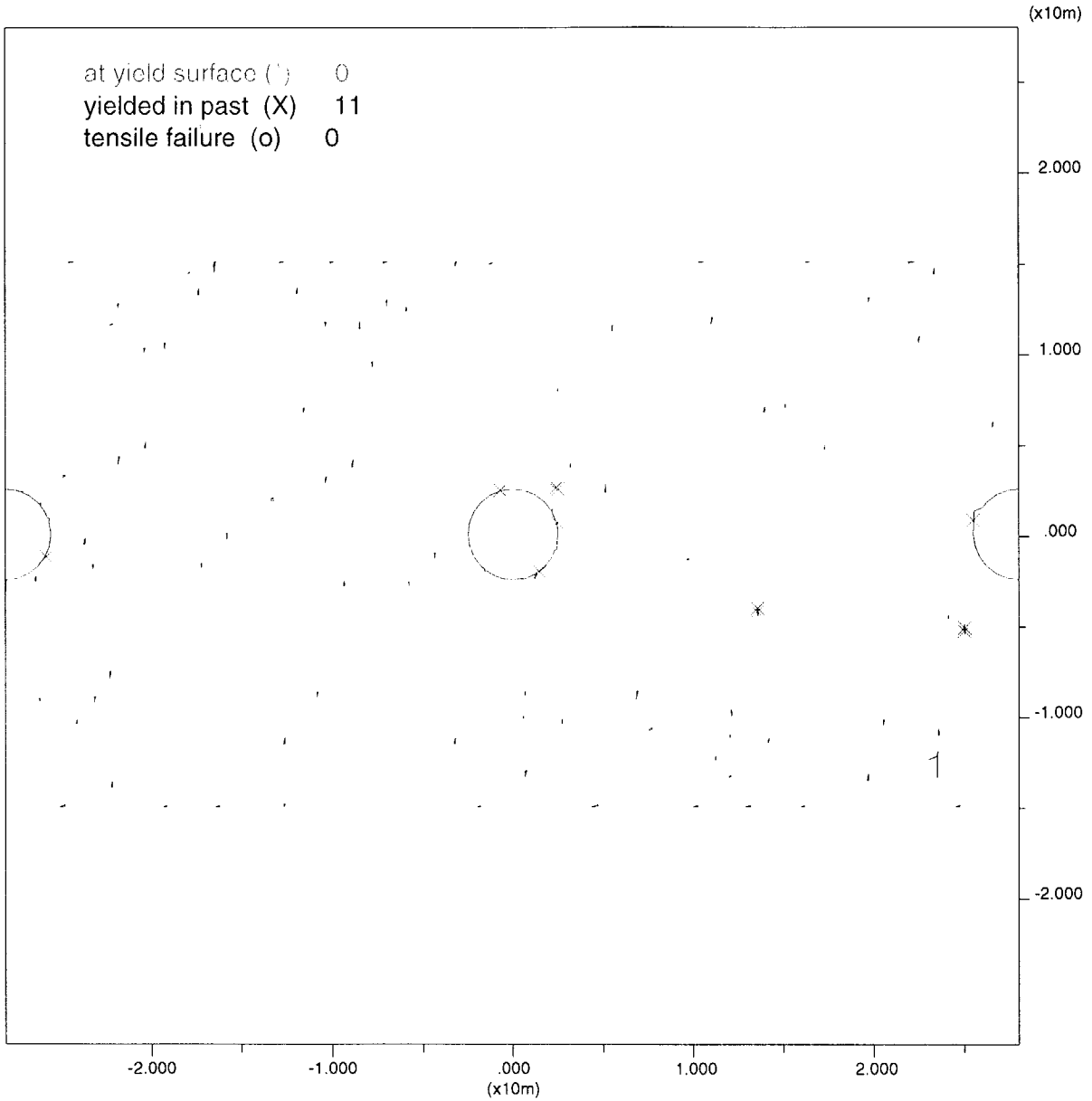

Figure 3-4b. Failure zones after 150 yr of thermal load assuming weak rock-mass model throughout

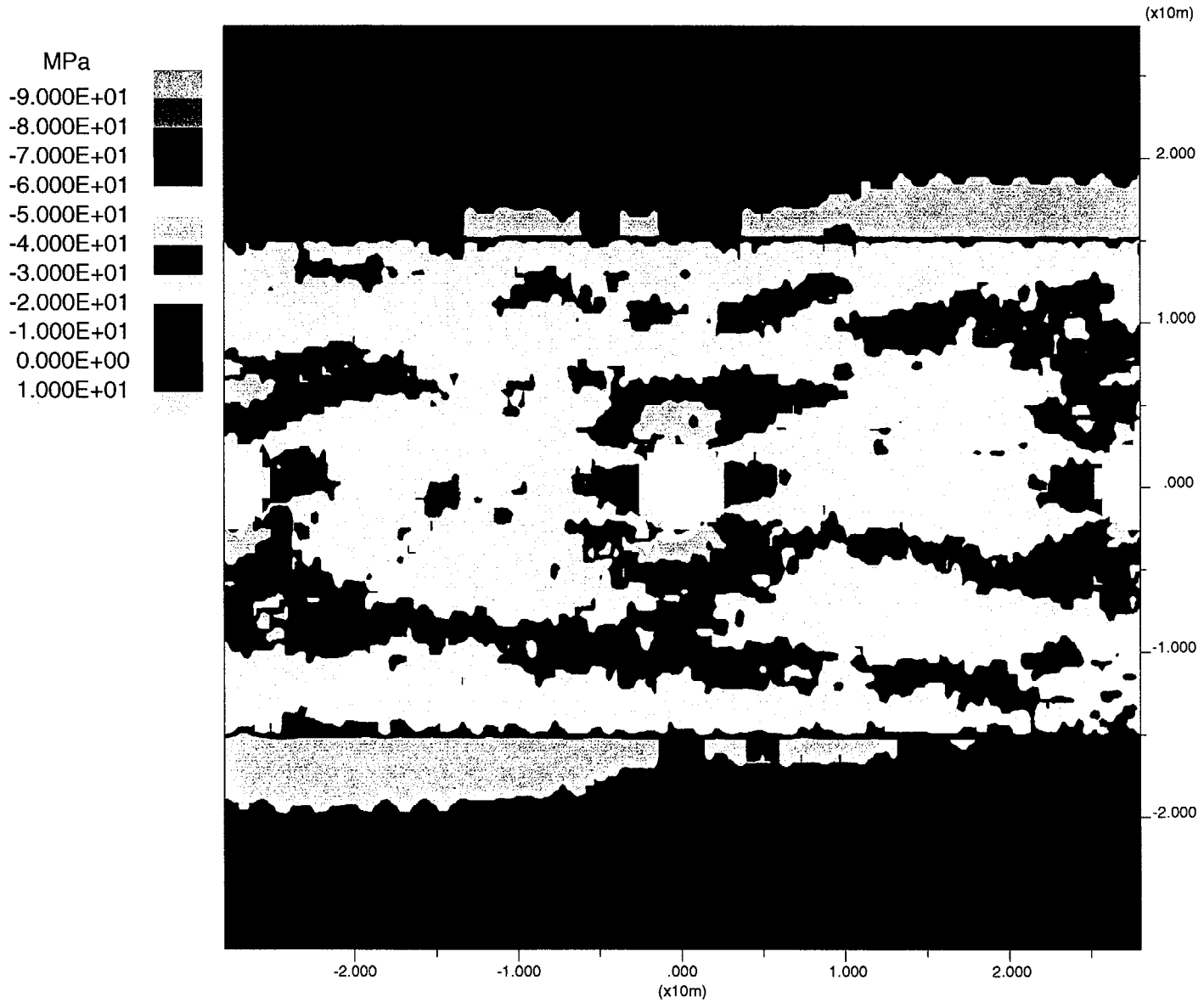

Figure 3-5a. Major principal stress countours (compression negative) at 100 yr after thermal load assuming strong rock-mass model throughout

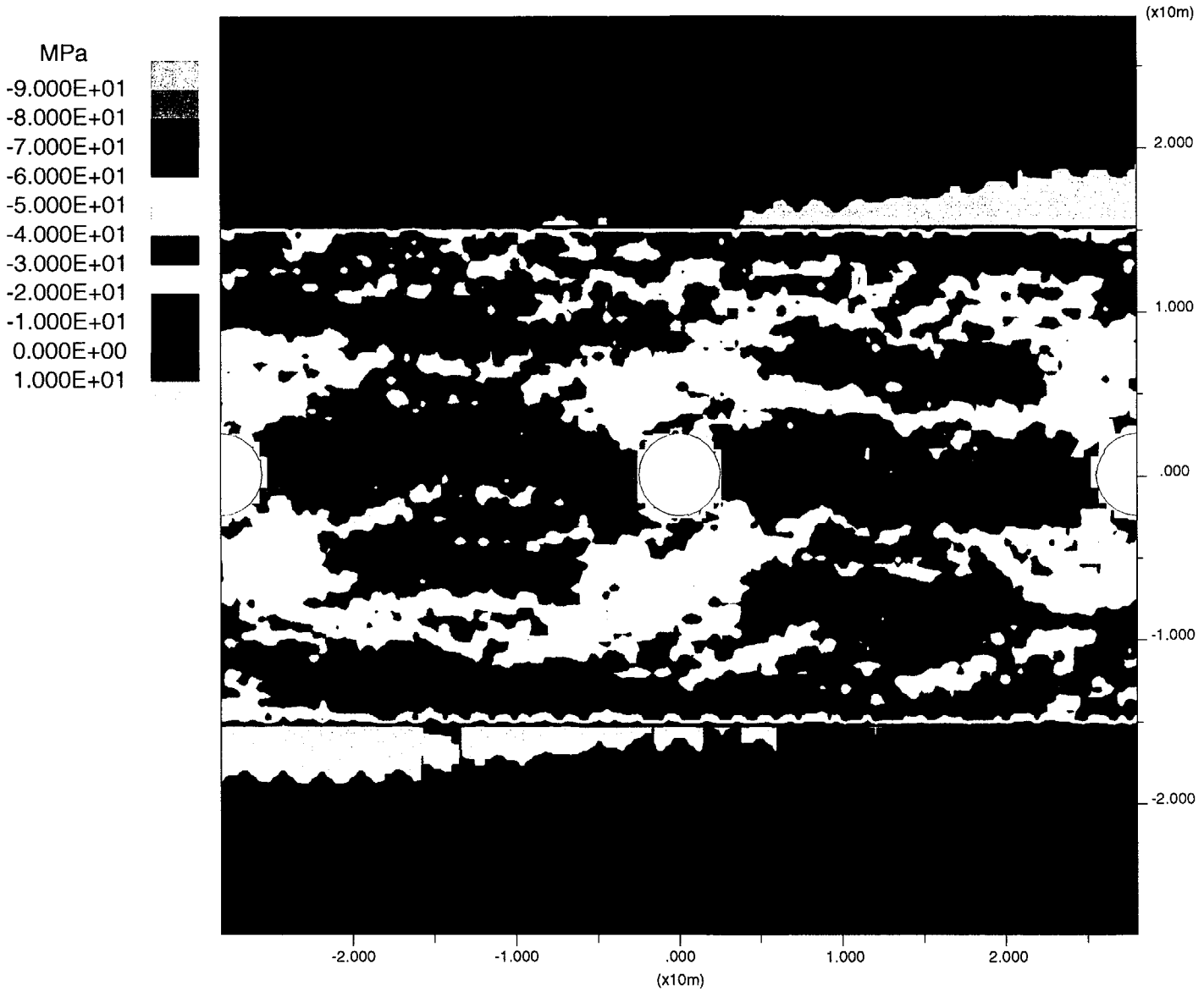

Figure 3-5b. Major principal stress countours (compression negative) at 100 yr after thermal load assuming weak rock-mass model throughout

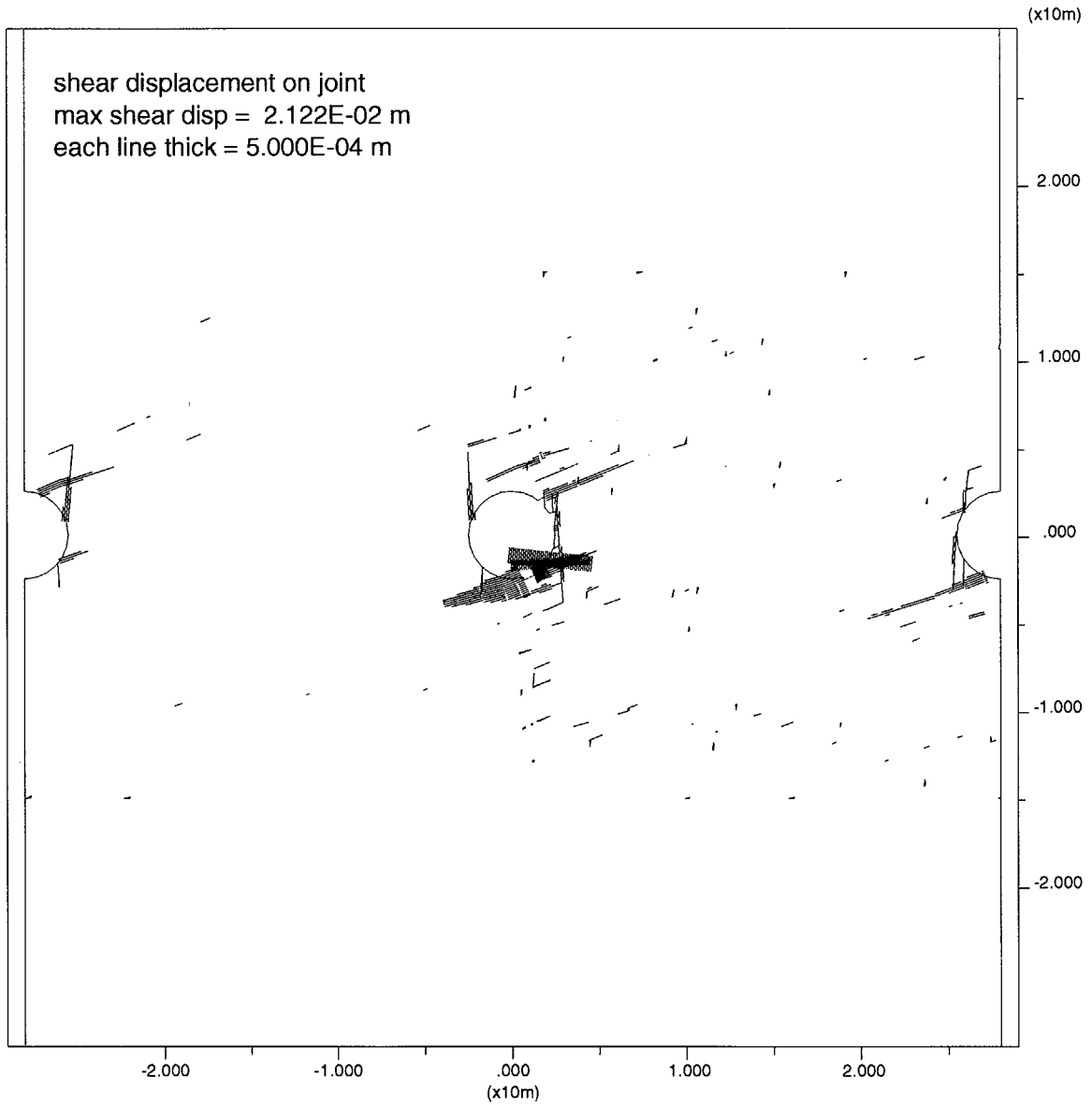

Figure 3-6. Joint shear displacements (m) after 150 yr of thermal loading based on vertical rock transitional zone through centerline of middle emplacement drift

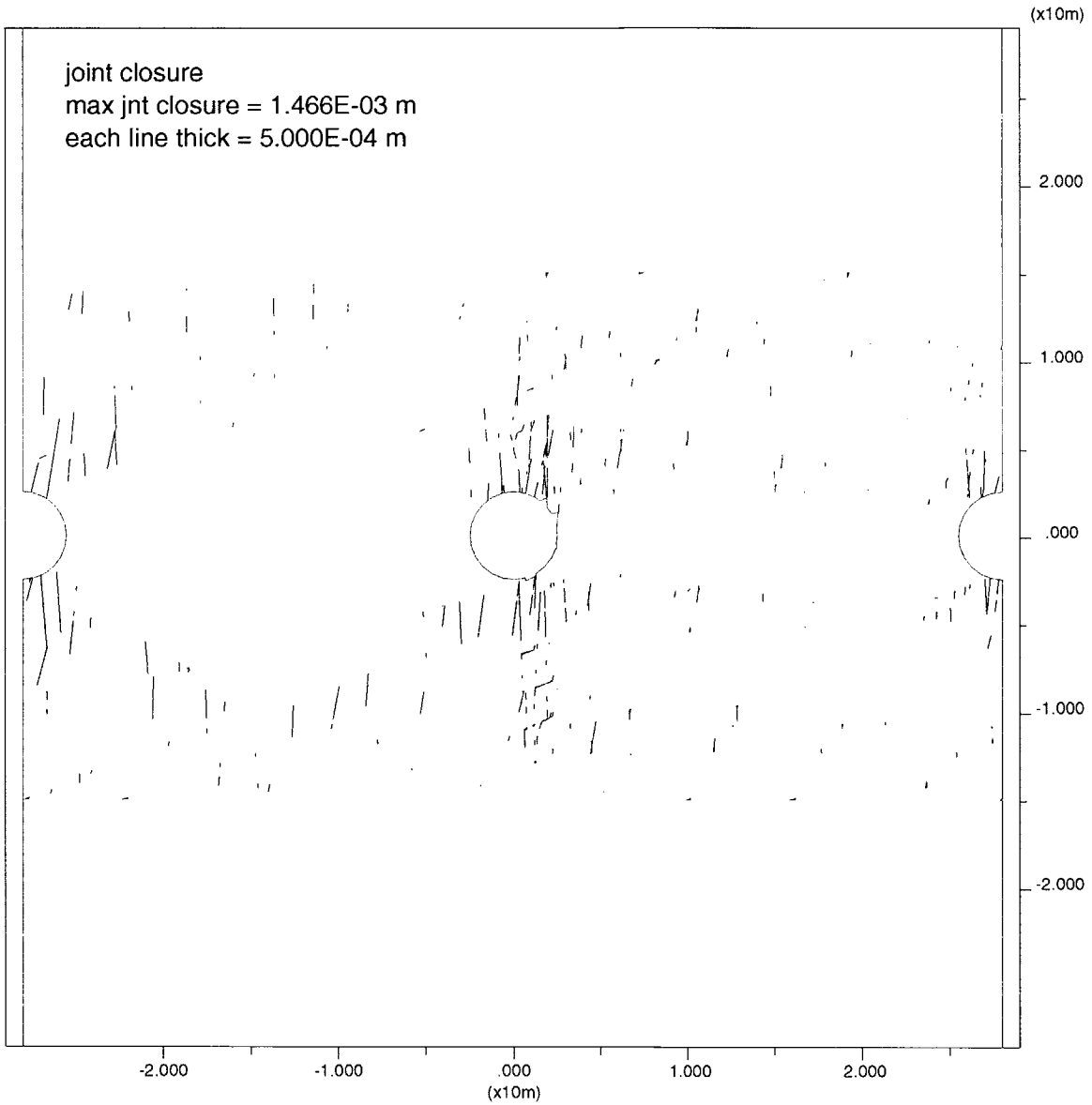

Figure 3-7. Joint closure (m) after 150 yr of thermal loading based on vertical rock transitional zone through centerline of middle emplacement drift

on either side. Also, some small segments of joint closure between the middle and right drift (i.e., the weak rock-mass region) are an artifact of the UDEC model. These segments are located around very small blocks created during the joint generation that were ultimately deleted to maintain a reasonable time step for the analyses.

Figure 3-8 shows the tensile stress zones around the central drift containing the transition. It can be seen that the region of tension is somewhat greater than for either of the two base case simulations (figures 3-3a and 3-3b). Tensile stress zones exist in both sidewalls of the drift, the drift floor, and the upper right and left portions of the roof. Maximum tensile stress values around the drift are approximately 7.25 MPa. A Mohr-Coulomb rock failure plot (figure 3-9a) indicates minor yielding in the drift floor in the weak rock region. Also, minor zones of yielding are predicted above the roof of the central tunnel along the transition, but on the weak rock zone side. Time histories of horizontal stress in the immediate roof of the central drift in the transitional model indicate a maximum horizontal compressive stress of approximately 55 MPa, lower than for either of the two base case simulations. This lower compressive stress field trend is also evident from a contour plot of the maximum principal stresses (figure 3-9b). Thus, it appears that the stress regime around the central drift in the transitional model might be better in terms of lower overall compressive stresses, but worse in terms of a larger region of tension immediately around the drift (although little to no tensile failure is predicted considering the rock strength properties of table 2-2).

3.2.1.1 Effect of Reduced Rock Block and Joint Strength Parameters on Rock-Mass Behavior in the 3-Drift Transitional Zone Model

To investigate the effect of rock-mass degradation with time during the thermal loading period, a TM simulation was conducted using the 3-drift transitional zone model with reduced rock block and joint strength parameters. As discussed in section 2.1, rock block compressive and tensile strengths and rock block friction angle and joint friction angle were reduced to one-half their reference values. Reduced values for rock block cohesion were derived from standard equations based on the uniaxial compressive strength and friction angle. Figure 3-10a shows zones of rock block failure after the 150-yr thermal loading time. Compared with figure 3-9a which is based on the reference rock and joint strength properties, a significant increase in the number of zone failures from plastic yield as well as from tension is indicated. These zone failures appear to indicate that the emplacement drifts would be unstable without the benefit of adequate rock support. Figure 3-10a shows the number of zone failures in yield and tension is higher in the weak rock region (i.e., to the right of the transitional zone located vertically through the central drift). Essentially no portion of the drift perimeter in the weak rock-mass region is without tensile failure or yielding. Plots of gridpoint velocity vectors indicate wedge collapse of blocks in the upper right roof region of the drifts based on the input joint set geometry. The maximum joint closure at 150 yr for the reduced strength simulation more than doubles from the reference transitional zone simulation discussed in section 3.2.1 to approximately 3.3 mm, although the region over which the high joint closures occur is similar. However, as shown in figure 3-10b, both the region and magnitude of joint shear displacements are higher for the reduced strength transitional zone simulation compared with the reference property strength transitional zone model (figure 3-6). Also, as shown in figure 3-11a, the zone of tension extends more or less completely around the central drift for the reduced strength transitional zone simulation.

3.2.1.2 Effect of Joint Stiffness on Rock-Mass Behavior in the 3-Drift Transitional Zone Model

UDEC simulations were performed to investigate the impact of varying the joint normal and joint shear stiffness on the rock-mass behavior in the transitional zone area over the 150-yr thermal loading period. Two

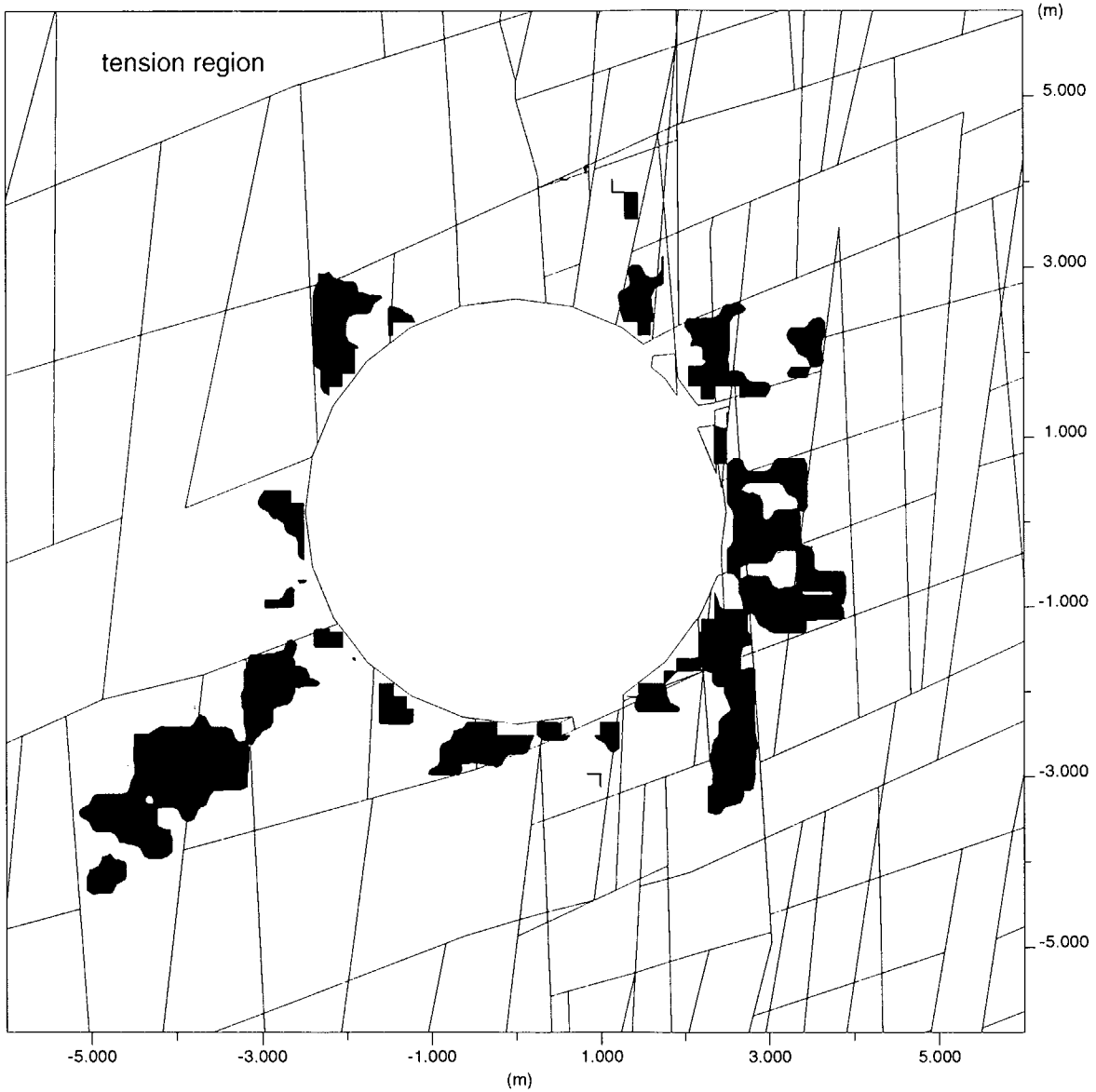

Figure 3-8. Region of tension after 150 yr of thermal loading based on vertical rock transitional zone through centerline of middle emplacement drift

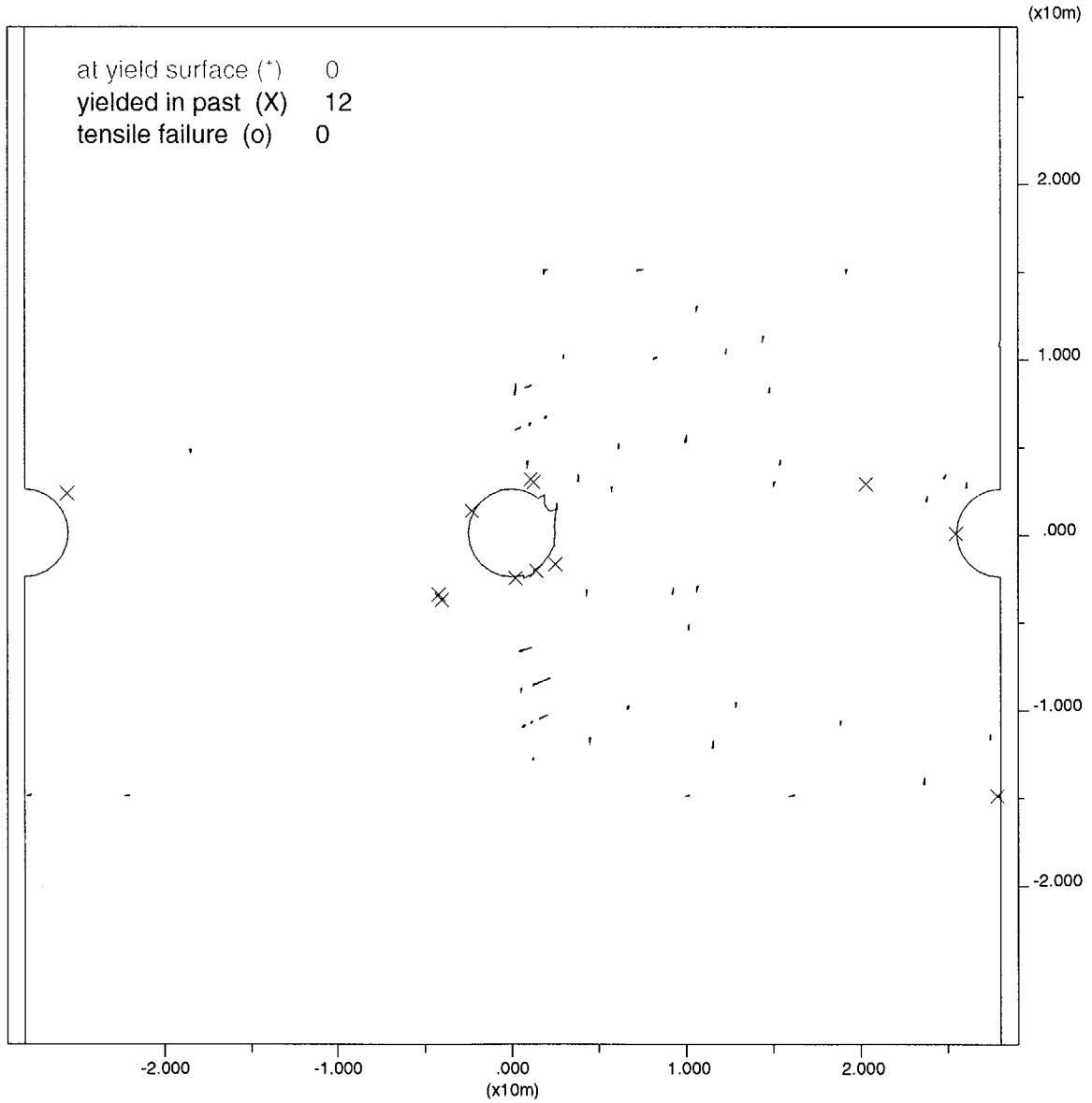

Figure 3-9a. Three-drift transitional zone thermal-mechanical analysis results using reference rock and joint strength parameters showing failure zones after 150 yr

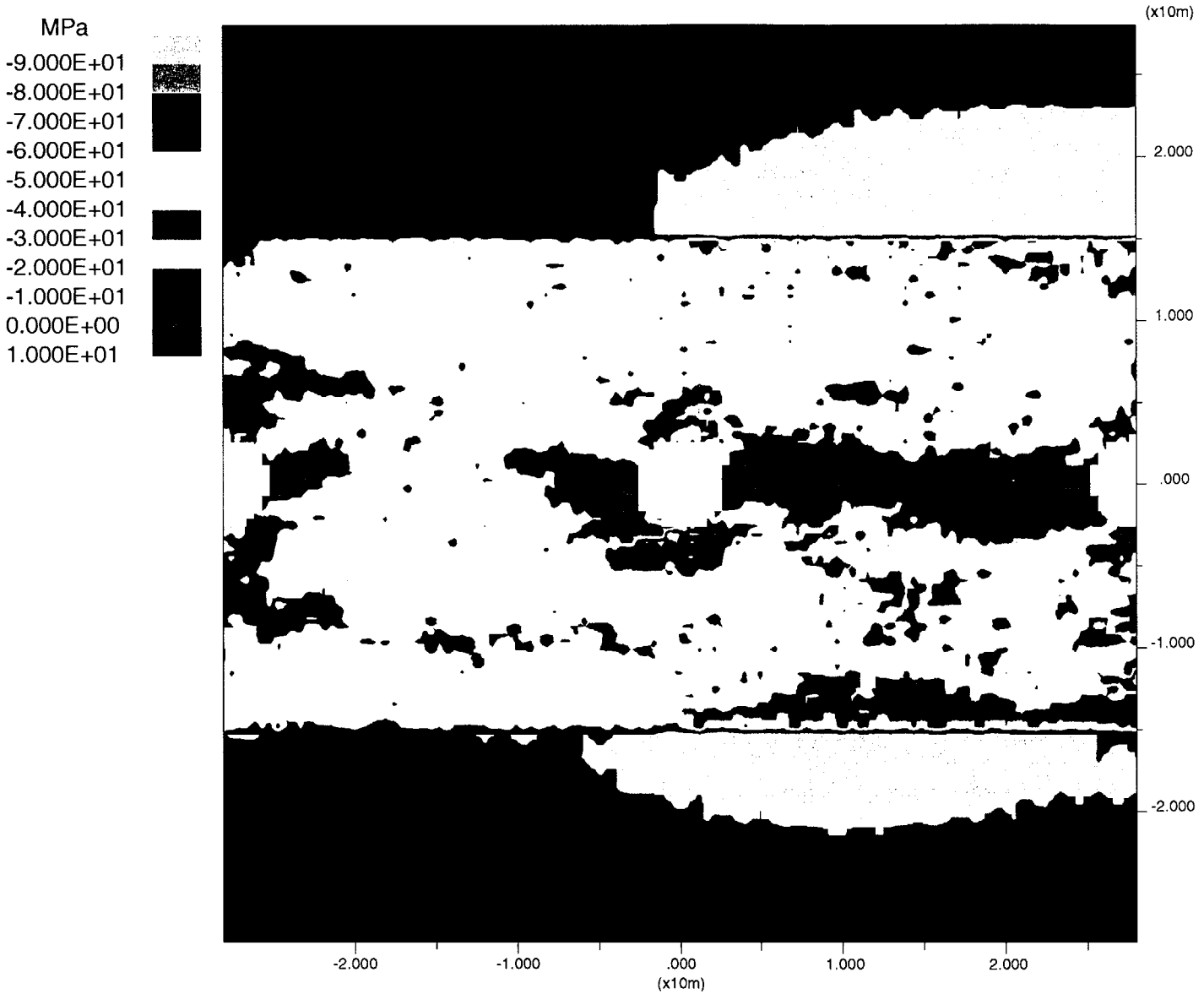

Figure 3-9b. Three-drift transitional zone thermal-mechanical analysis results using reference rock and joint strength parameters showing contours of major principal stresses after 100 yr

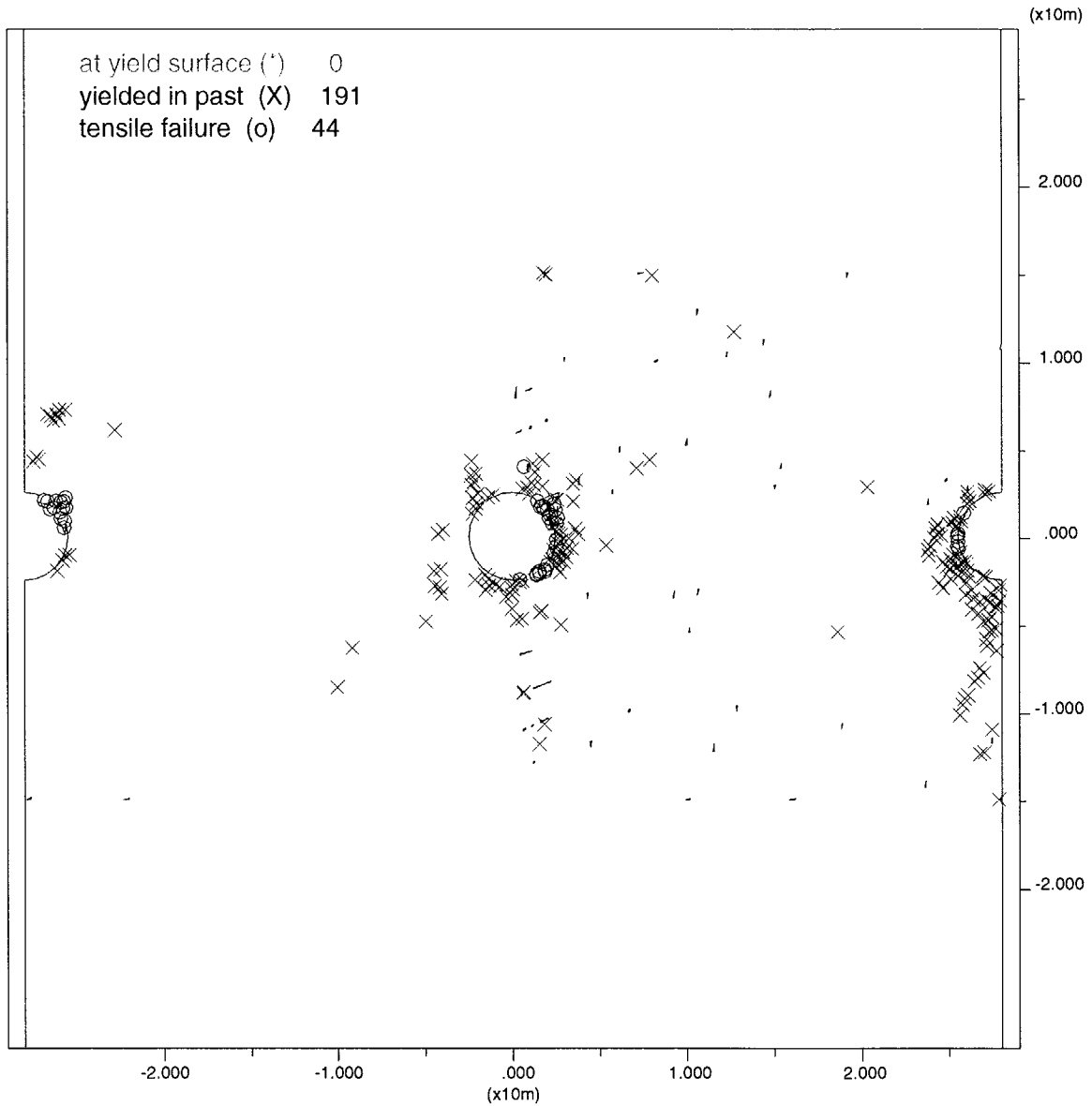

Figure 3-10a. Failure zones after 150 yr of thermal load using 3-drift transitional zone model with reduced rock and joint strength parameters

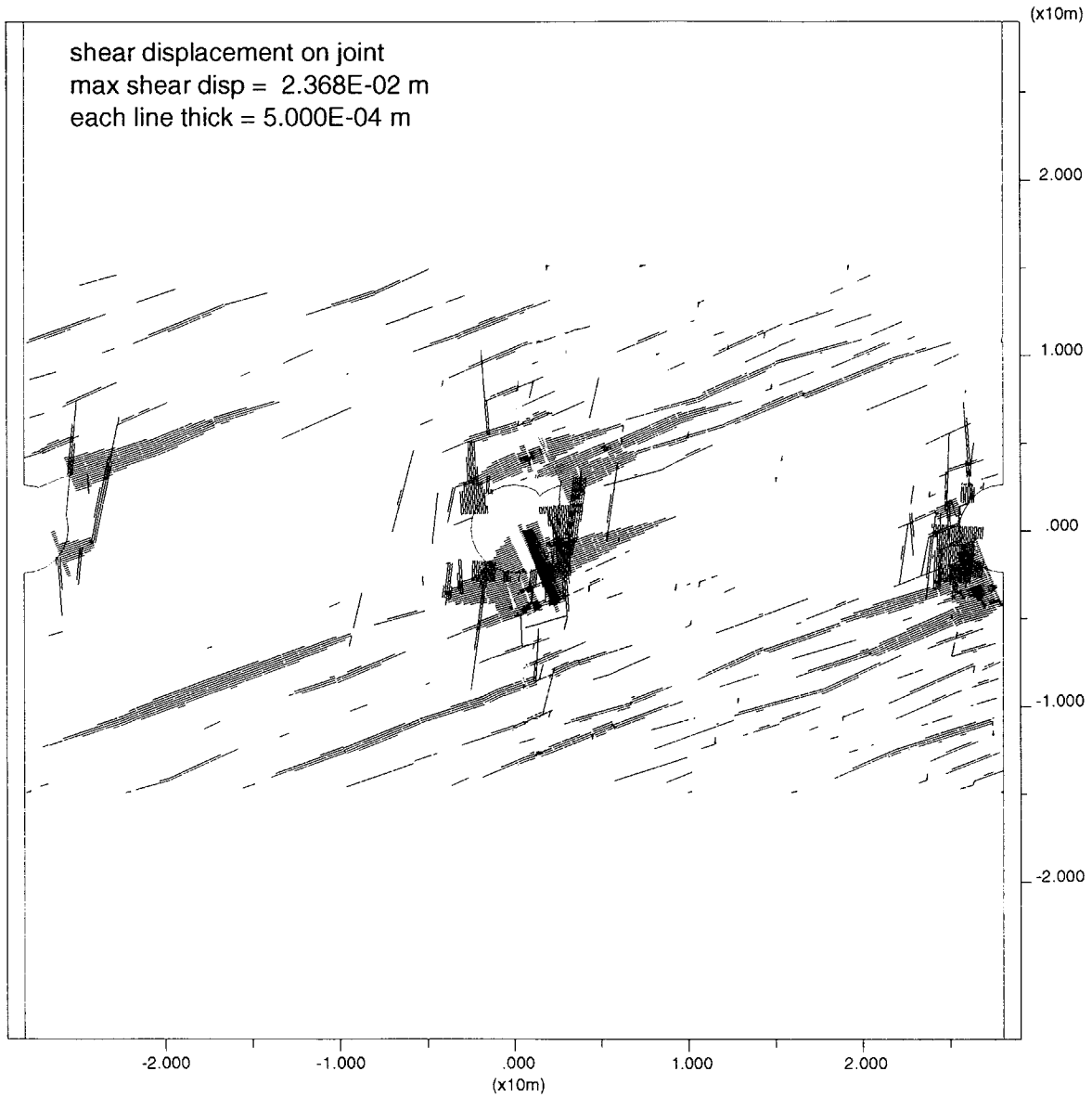

Figure 3-10b. Three-drift transitional zone thermal-mechanical analysis results at 150 yr using reduced rock and joint strength properties showing joint shear displacement (m)

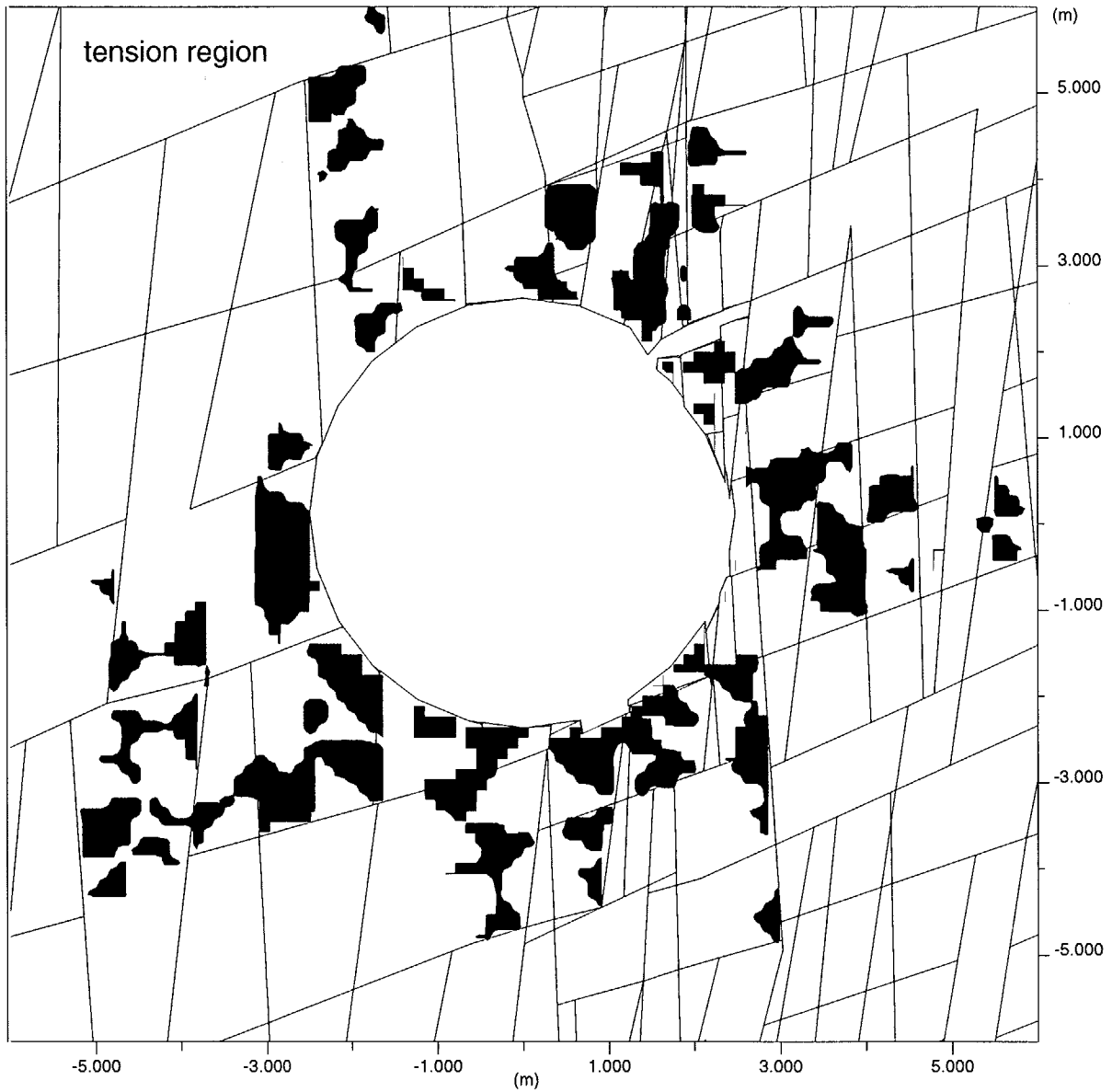

Figure 3-11a. Three-drift transitional zone thermal-mechanical analysis results at 150 yr using reduced rock and joint strength properties showing tensile strength regions

analyses were performed, one increasing both the joint normal and joint shear stiffnesses by a factor of 10 from the reference values (table 2-3) and the second decreasing the stiffnesses by a factor of 10 from the reference values. This factor of 10 increase or decrease in joint siffnesses was arbitrarily chosen. As joint stiffnesses are typically a nonlinear function of stress, the intent was to cover the potential range of stiffness values encountered at different thermal stress levels, since only constant stiffness values were incorporated into the analyses. The reference values were assumed for all other rock strength and joint strength parameters. Figures 3-11b and 3-12a show joint shear displacement and zone failure plots, respectively, after 150 yr for the case in which both the joint normal and shear stiffnesses were increased by a factor of 10. Similar to the results obtained from reducing the rock and joint strength properties, increasing the joint stiffnesses also results in a larger area over which shearing along the subhorizontal joint set takes place as compared with figure 3-6. Little to no joint shearing occurs between the drifts, with the majority occurring above and below, in the immediate roof and floor. Figure 3-12a shows that the number of failure zones also increases slightly, although not necessarily around the perimeters of the drifts, as compared to figure 3-4a. The maximum joint closure is below the 5.0E-4m (0.5-mm) cutoff used in the plotting. Figures 3-12b and 3-13 show joint shear displacement and failure zone plots, respectively, after 150 yr for the case in which both the joint normal and joint shear stiffnesses are reduced by a factor of 10 from their reference values. Comparing figure 3-12b with figure 3-6, one can see that reducing the joint stiffnesses appears to concentrate the shear displacements around joints near the drifts themselves, especially around the central drift with rock transition. Also, shearing along subvertical joints occurs above and below the central drift during the thermal loading period, whereas for the reference property simulations, the subvertical joint shearing was primarily due to excavation. The number of zone failures in yield and tension increase from the reference transitional zone simulation (figure 3-4a) and are more concentrated around the portions of the drifts in the weak rock-mass region. The maximum joint closure at 150 yr is approximately 3.75 mm.

3.2.1.3 Rock Bolt Reinforcement in the 3-Drift Transitional Zone Model

Permanent reinforcement for the waste emplacement drifts either in the form of rock bolts or concrete liners will be necessary to maintain the option for waste retrievability. Depending on the emplacement period, preclosure operation could extend upwards of 100 to 150 yr. This transitional zone rock-mass behavior study examined reinforcement only in the form of fully grouted rock bolts installed uniformly above the springline of the emplacement tunnels. The rock bolts were assumed to be 2.5 m long and on 1-m centers. Because the bolts were on 1-m centers, no adjustment to bolt or grout properties was necessary along the axis of the drifts (i.e., perpendicular to the 2D plane of the study). Satisfying these spacing requirements necessitated eight rock bolts above the springline of the drifts. The global reinforcement option within UDEC was used for the analyses, which applies reinforcement over the full grouted length of the bolt, rather than the local reinforcement scheme, which applies reinforcement only at the intersection of the bolt with a fracture trace. The global reinforcement in UDEC is developed for a cable bolt with axial stiffness and negligible shear stiffness. The global reinforcement option rather than the local reinforcement option was used in this analysis. Actual bolt properties were used rather than typical cable properties to better represent the reinforcement behavior above the drifts. This type of rock bolt has primarily axial stiffness and little shear stiffness. Each bolt was divided into 12 elements in which axial tensile failure of the steel bolt or shear failure of the grout could take place. If failure within the fully grouted bolt was predicted in one particular element, the remaining section(s) of the bolt could function to provide reinforcement to that section of the rock mass.

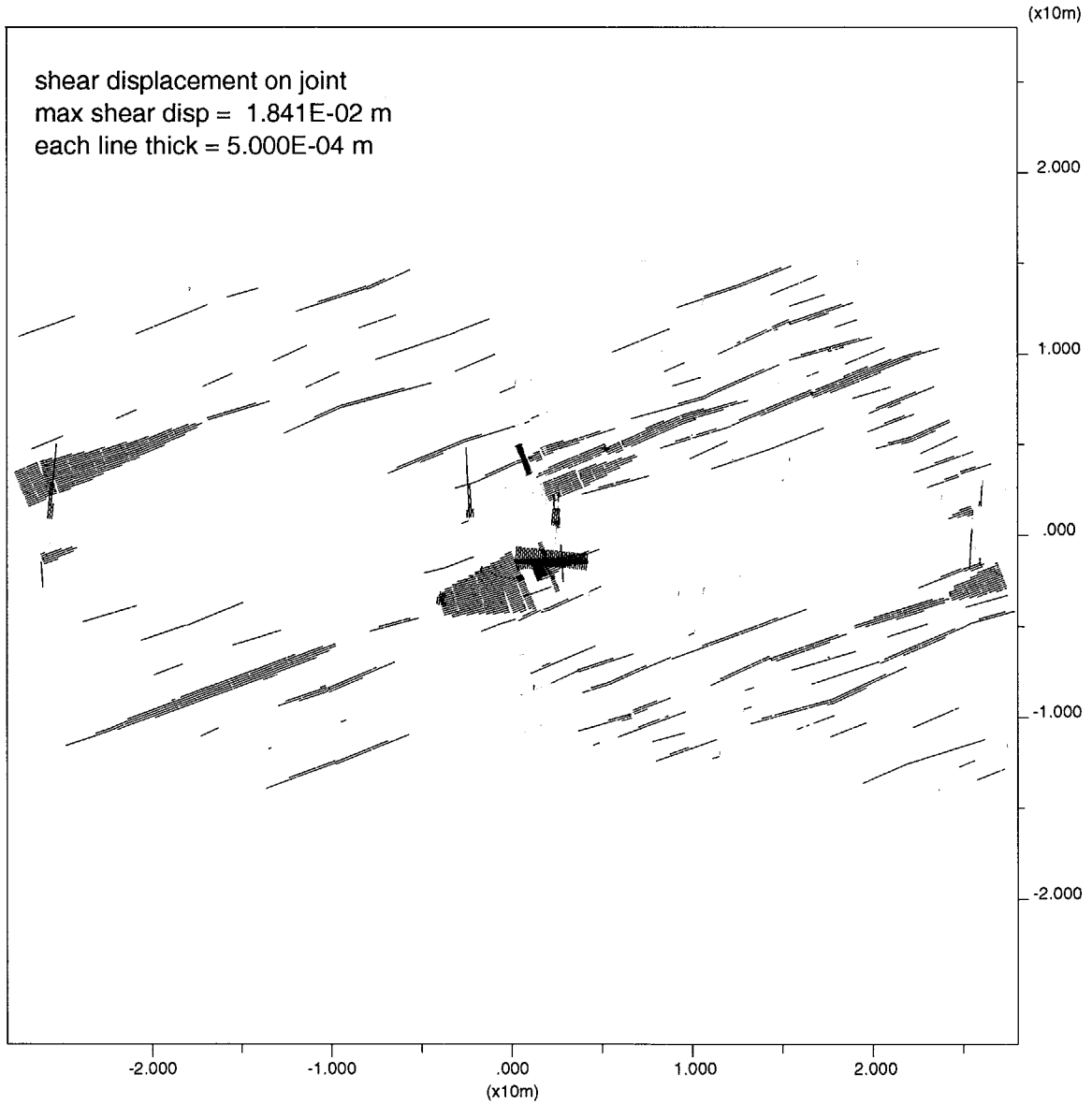

Figure 3-11b. Three-drift transitional zone thermal-mechanical analysis results at 150 yr using high joint stiffness properties showing joint shear displacements (m)

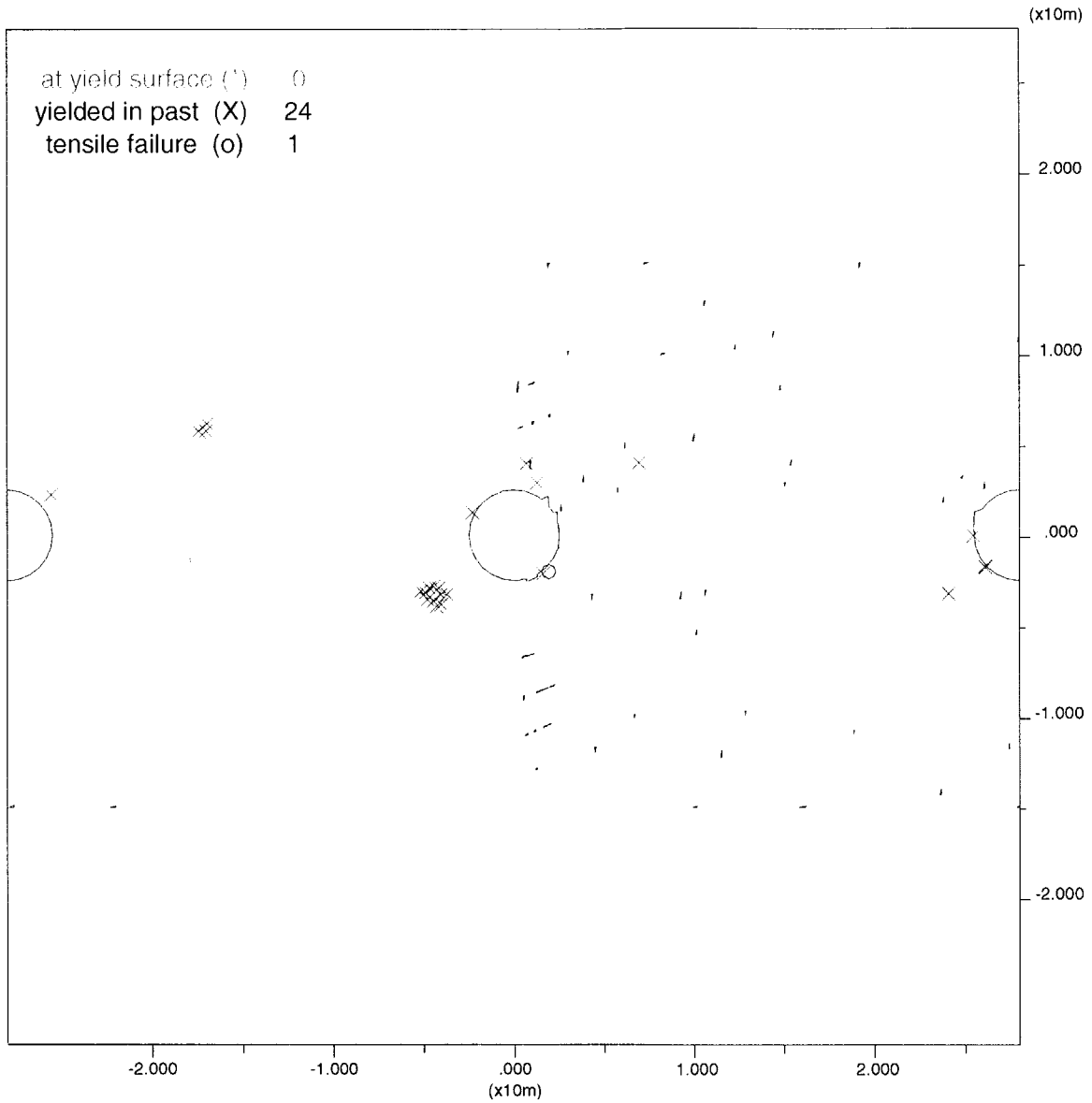

Figure 3-12a. Three-drift transitional zone thermal-mechanical analyses results at 150 yr using high joint stiffness properties showing failure zones

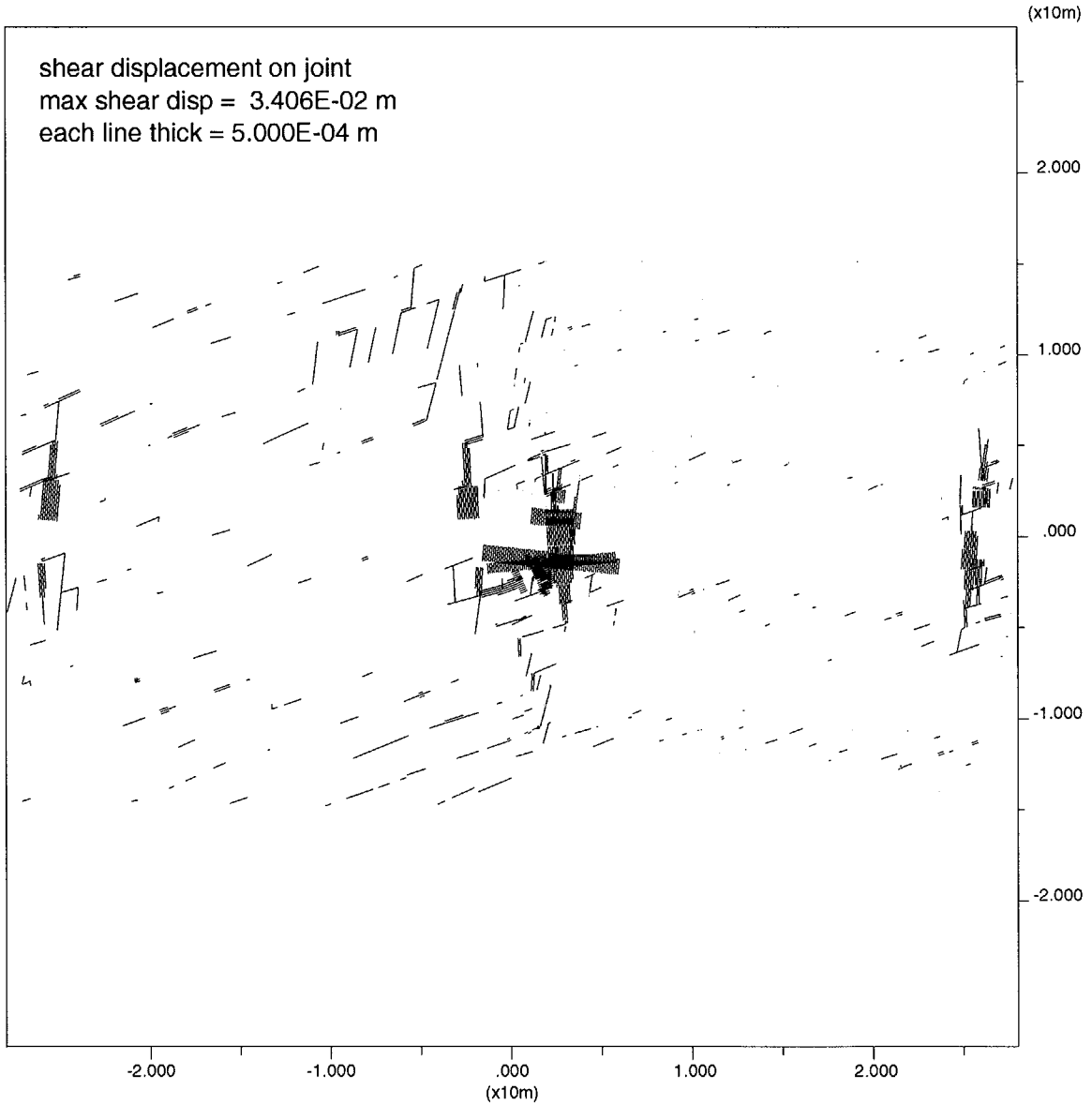

Figure 3-12b. Three-drift transitional zone thermal-mechanical analyses results at 150 yr using low joint stiffness properties showing joint shear displacements (m)

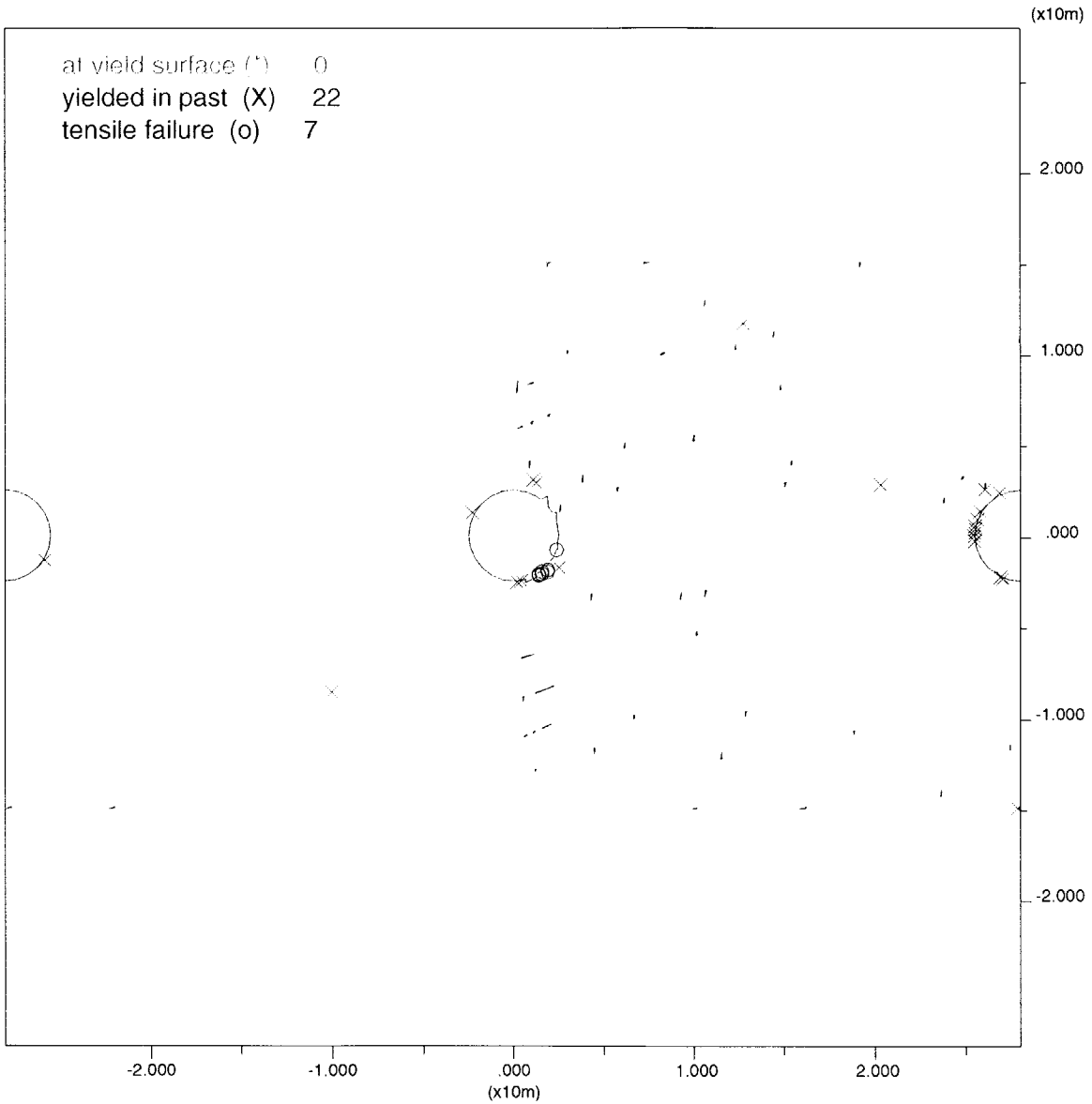

Figure 3-13. Three-drift transitional zone thermal-mechanical analyses results at 150 yr using low joint stiffness properties showing failure zones

Additional stiffness and strength properties used for the steel bolts and grout were previously discussed in section 2.1 and tabulated in table 2-4. The rock bolt TM analyses were not carried out to the full 150 yr of simulation time, as significant tensile failure of the bolts and shear failure of the grout occurred well before 150 yr. Although it would have been beneficial to run the rock bolt analyses using both the reference rock and joint strength properties and reduced strength properties, the analysis of bolts in conjunction with reduced rock and joint strength parameters only was performed. Results are presented for the axial forces within the bolts, axial tensile bolt failures, and grout failure. Figures 3-14a and 3-14b show the development of axial tensile forces within the bolts above the springline of the central tunnel after drift excavation and 30 yr after application of the thermal load, respectively. After excavation, axial forces develop in portions of only a few bolts around the central drift with the rock transitional zone. The length of the rectangular bar corresponds to the magnitude of the axial force. In any particular bolt for this analysis, the maximum axial bolt force is tensile (i.e., as indicated in figure 3-14a by the largest bar graph plots along a particular section of the bolt, regardless of whether the largest bar graph points to the left or right along the bolt itself). Bar graphs in the opposite direction are indicative of axial compression on that segment of the bolt. Figure 3-14b shows axial tensile force buildup at 30 yr along essentially the full length of all bolts as a result of upward thermal expansion of the rock mass. Again, in figure 3-14b, the maximum axial bolt forces in any bolt after this thermal loading time are tensile, regardless of which direction the largest bar graph spikes point. Any bar graph spikes in the opposite direction of the tensile bar graph spikes indicate a compressive bolt force. Figures 3-15a and 3-15b show locations of axial tensile failure within the bolts for these same two time periods. After drift excavation (figure 3-15a), a few bolts are predicted to fail in tension at select locations, slightly more so on the right, weak rock-mass side of the transitional zone. After 30 yr (figure 3-15b), all bolts have failed in tension in at least one location, with bolts in the weak rock-mass region failing in tension at several locations. Additional base case simulations would be required to verify whether the higher number of bolt axial tensile failures in the weak rock-mass side were due to the transitional zone effect or to the joint spacings in either of the two rock-mass regions. Finally, figures 3-16a and 3-16b show grout failures after drift excavation and after 30 yr of heating. While only a slight amount of grout failure is predicted after excavation (figure 3-16a), a significant portion of the length of all bolts shows failure of the grout after 30 yr of heating (figure 3-16b) from thermal expansion of the rock mass. While the rock bolts above might be able to contain any failed rock zones around the emplacement drifts after their excavation, they would appear to be inadequate (based on the bolt size and grout strength properties assumed) to contain the failed rock zones as discussed in section 3.2.1.1 after thermal loading and rock-mass expansion.

The results presented in the preceding paragraph assume a degraded rock mass after excavation and throughout the heating period (i.e., reduced intact rock strength and joint strength properties were used). Analyses were not performed to show how much less bolt and grout failure would occur if the full-strength rock and joint strength parameters were used, although similar expansion of the rock mass around the emplacement drifts occurs regardless of the rock strength properties assumed. The results presented would indicate further analyses are required to include consideration of a larger-diameter (higher-yield-strength) bolt and higher-shear-strength grout as well.

3.2.2 Transitional Zone Midway Between Emplacement Drifts (4-Drift Transitional Zone Model)

The impact of a vertical transitional zone located midway between two emplacement drifts (see figure 2-2) on the overall TM rock-mass behavior was also analyzed. Again, the first TM analyses using

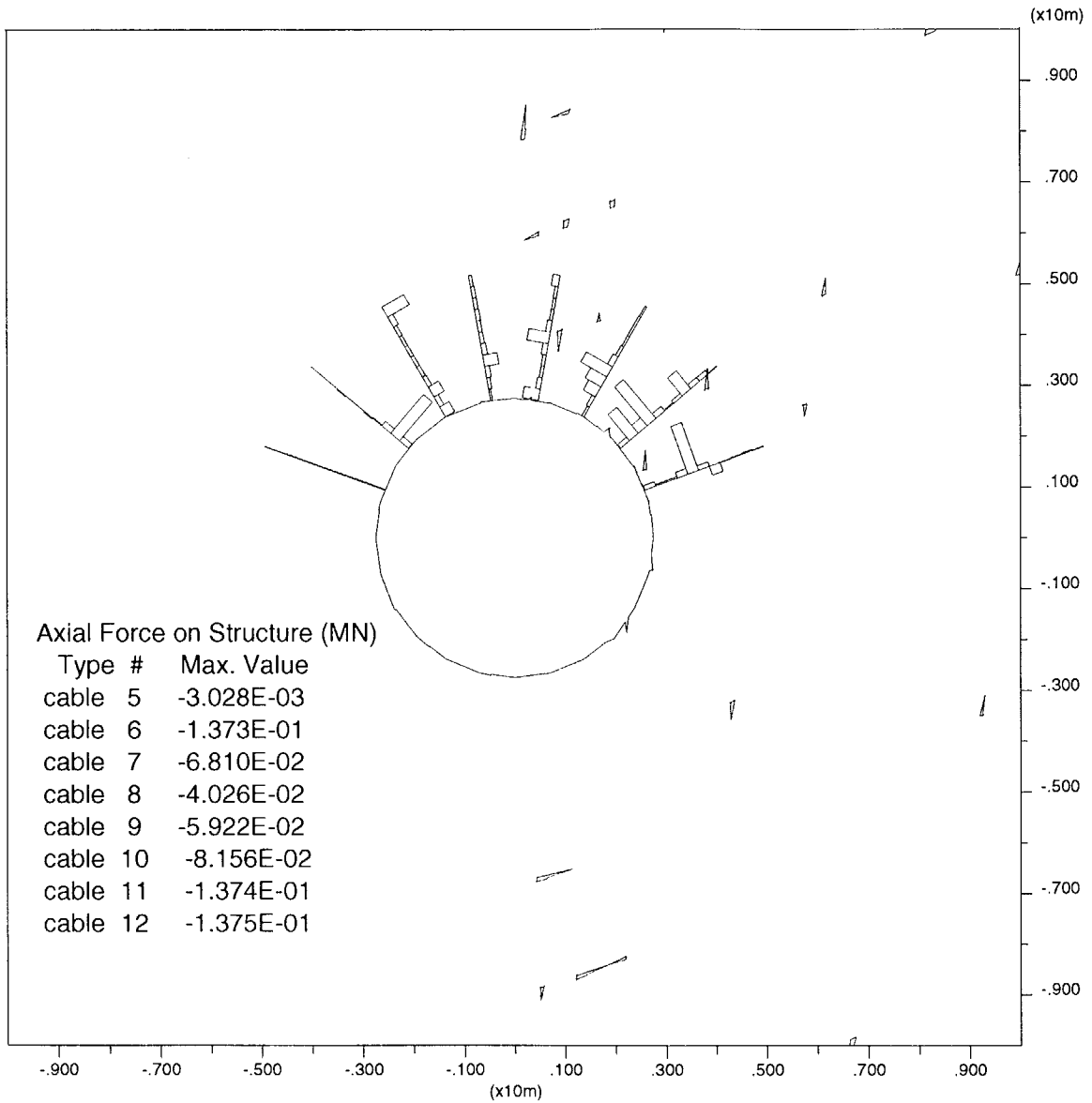

Figure 3-14a. Axial tensile forces (MN) within bolts above center drift of the 3-drift rock-mass transitional model after drift excavation

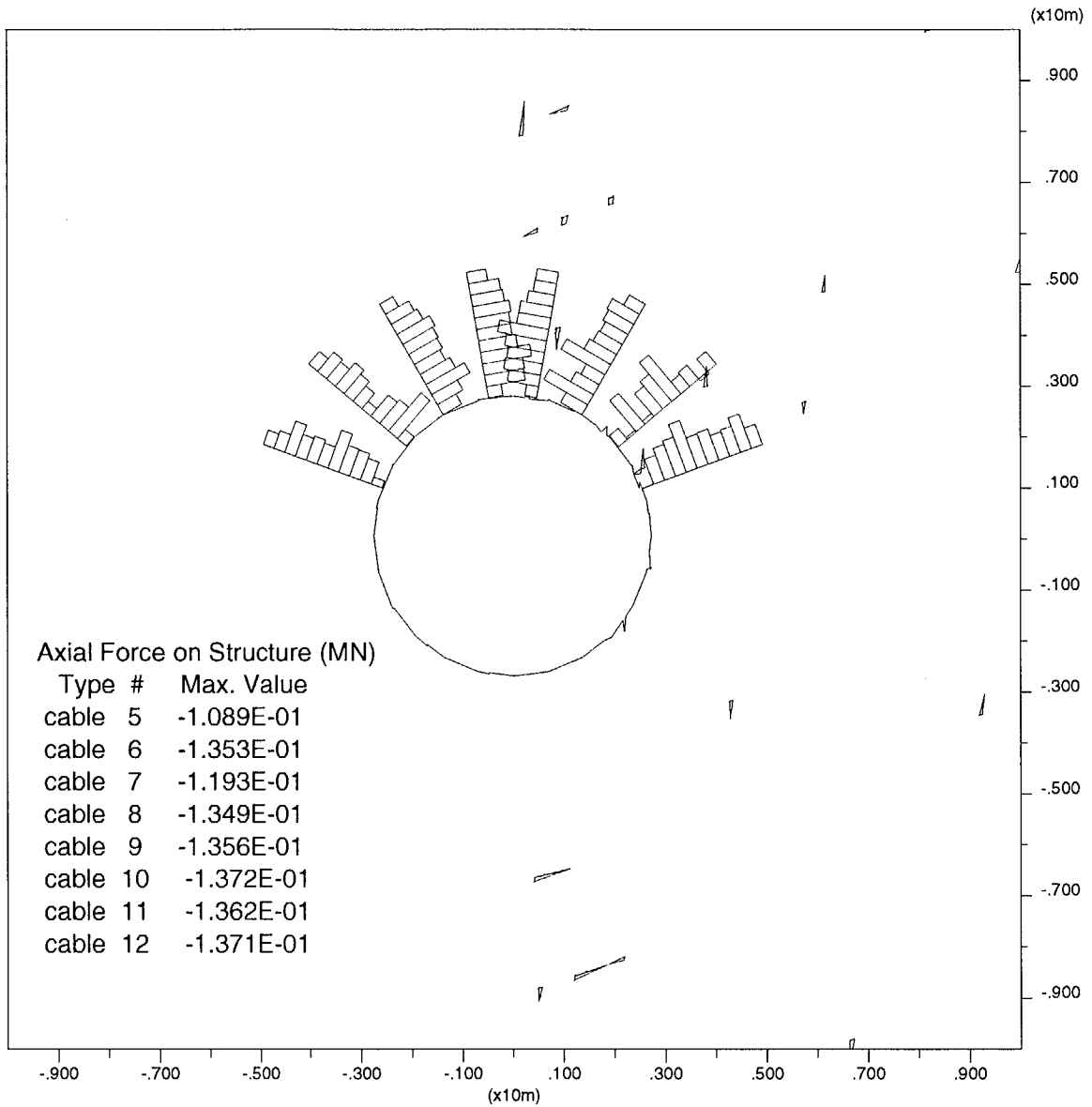

Figure 3-14b. Axial tensile forces (MN) within bolts above center drift of the 3-drift rock-mass transitional model after 30 yr of thermal load

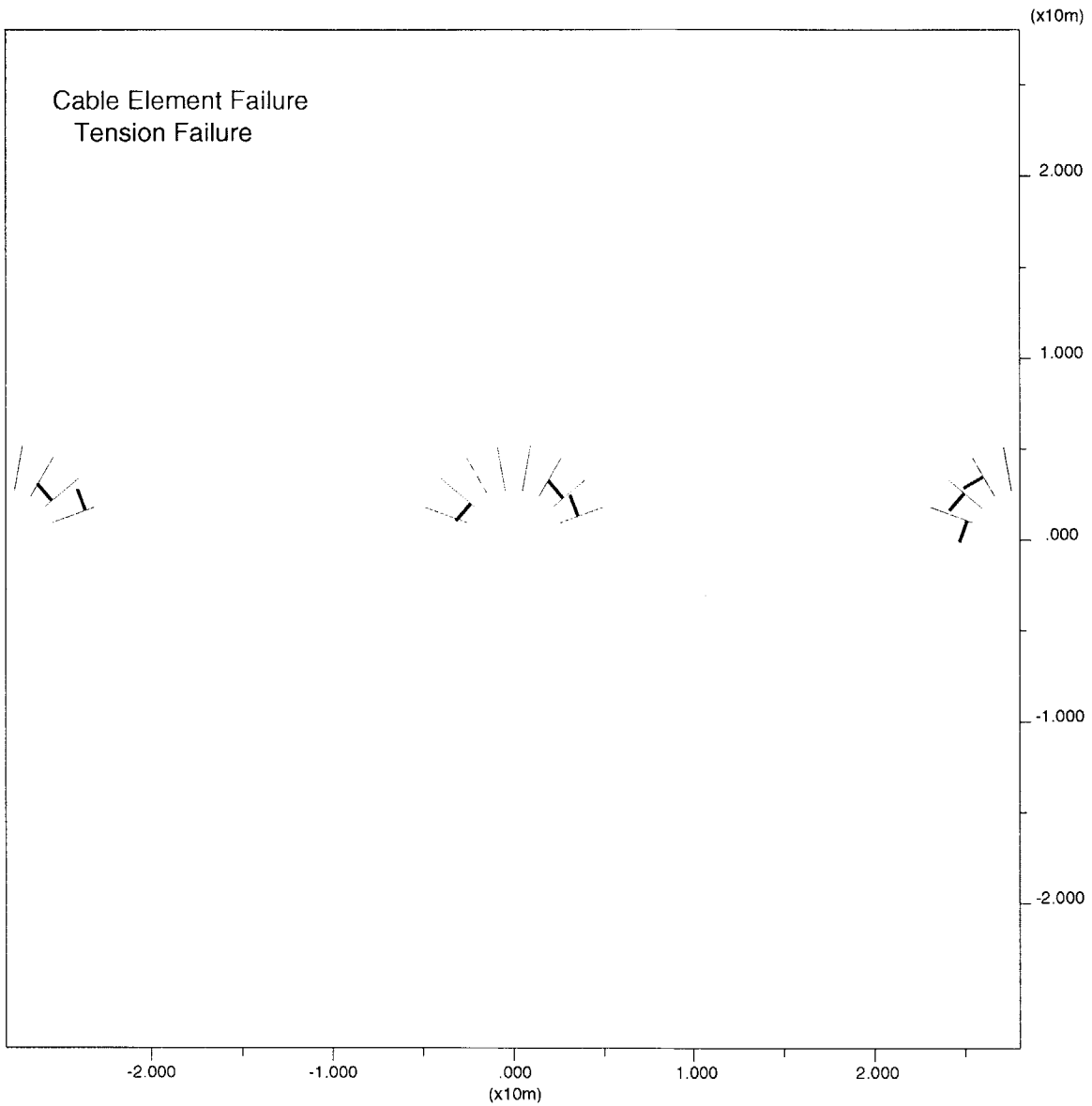

Figure 3-15a. Axial tensile failure locations within bolts above drifts in the 3-drift rock-mass transitional model after drift excavation

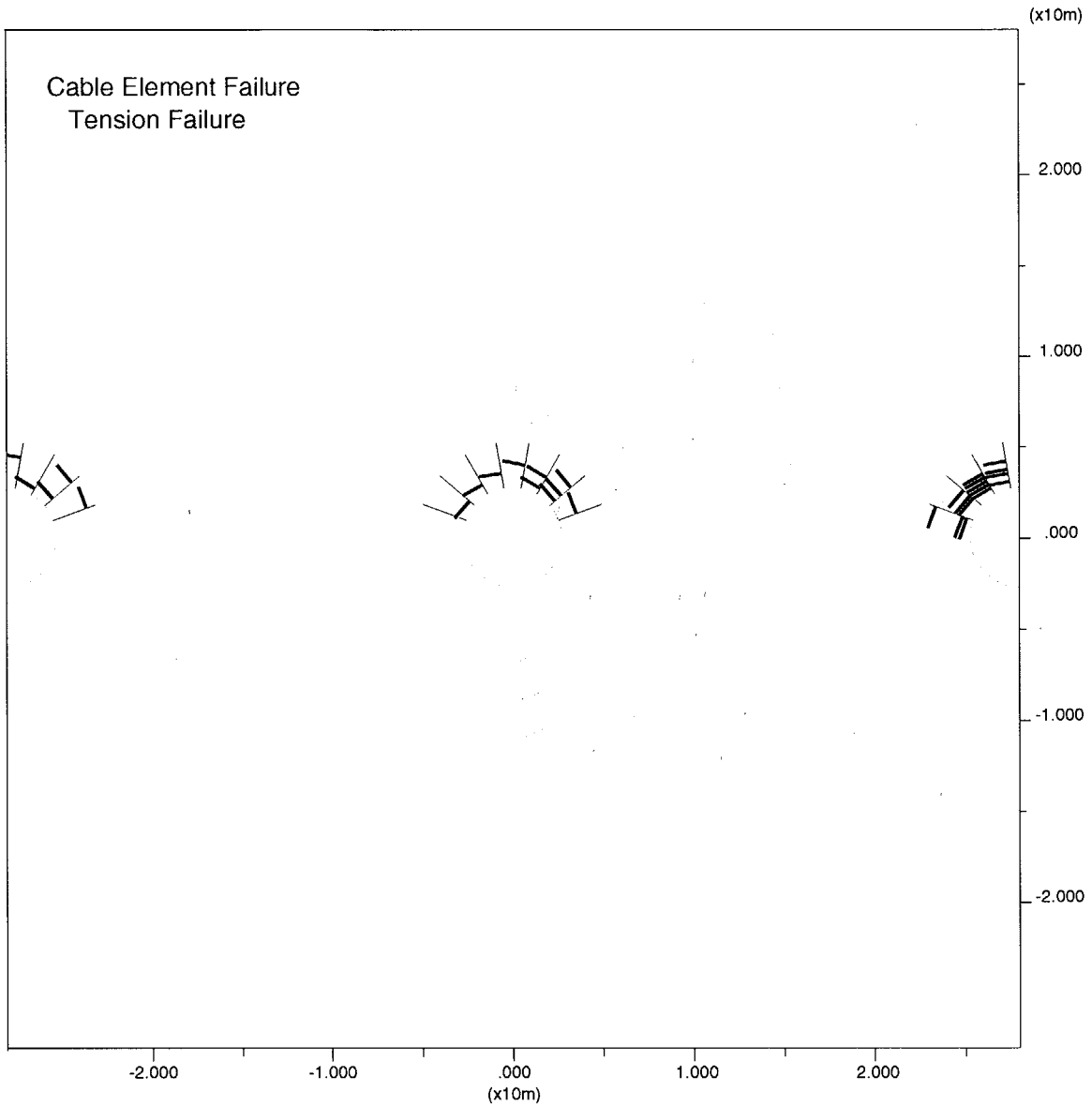

Figure 3-15b. Axial tensile failure locations within bolts above drifts in the 3-drift rock-mass transitional model after 30 yr of thermal load

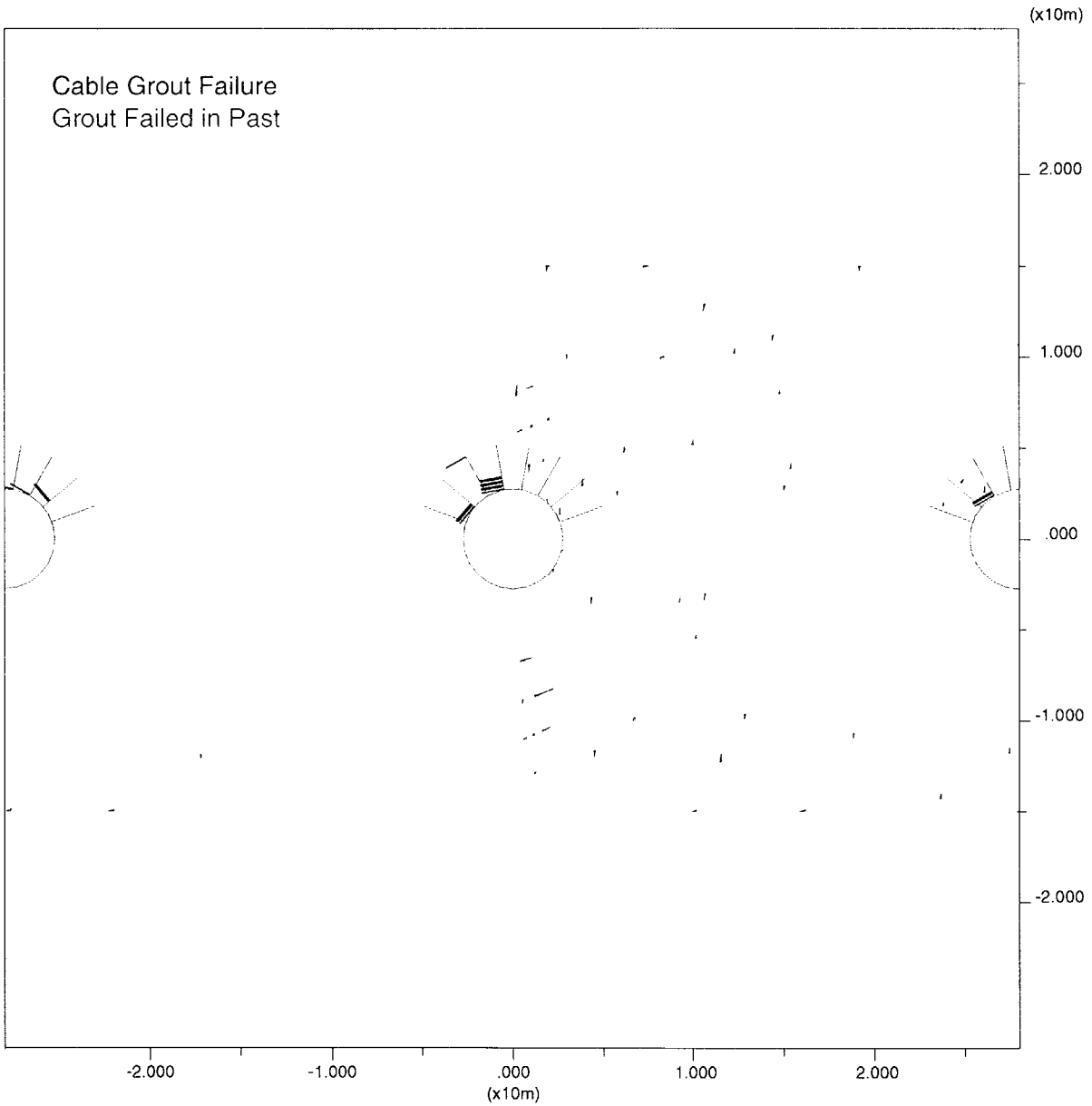

Figure 3-16a. Grout failure locations around bolts above drifts in the 3-drift rock-mass transitional model after drift excavation

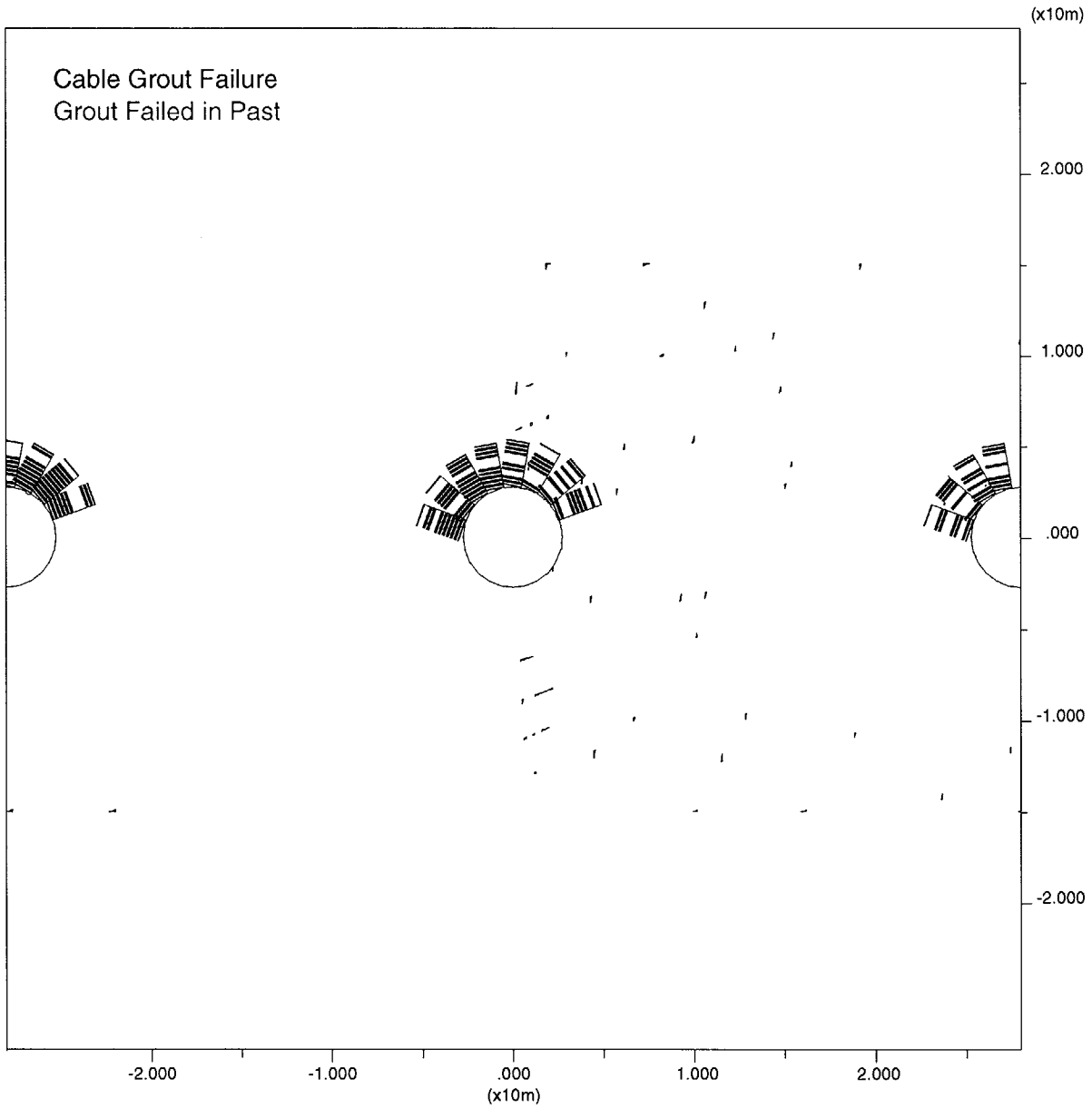

Figure 3-16b. Grout failure locations around bolts above drifts in the 3-drift rock-mass transitional model after 30 yr of thermal load

this geometric configuration utilized the reference rock strength and joint strength properties listed in tables 2-2 and 2-3. Figure 3-17 shows a plot of the joint shear displacements around the two drifts on either side of the transition; the left drift located in a strong rock mass and the right drift located in a weak rock mass. Because of computational problems during the computer run, results for this reference case analysis could only be carried out to a thermal time of 100 yr. Results show a maximum joint shear displacement of 6.6×10^{-3} m (6.6 mm) at 100 yr, which is smaller than the 1.85 cm calculated for the 3-drift transitional zone model discussed in section 3.2.1 for the same 100-yr period. A vertical transition located midway between drifts results in a much lower magnitude and extent of shearing along the subhorizontal joints around the drift in the strong rock mass (left drift in figure 3-17) compared to those around the drift in the weak rock mass (right drift in figure 3-17). Again, some of the small joint shear displacements further away from the drifts are caused by the small voids created in the rock mass from deletion of very small blocks during the analysis setup.

Figure 3-18 depicts joint closure around the two drifts on either side of the vertical transition after 100 yr. The maximum joint closure for this 4-drift transitional zone model at 100 yr is approximately 2.35 mm, compared to 1.45 mm for the 3-drift transitional zone model at the same time period.

Contour plots of tensile zone regions around the two drifts on either side of the transitional zone are shown in Figures 3-19a and b for the drifts in the strong and weak rock-mass regions, respectively, at 100 yr. Figure 3-19a shows that the transition zone midway between the drifts effectively reduces the tensile zone region around the drift located in the strong rock-mass region. This region of tension is smaller than that shown in the figure 3-3a base case simulation depicting similar tension contours for a drift located completely in the strong rock-mass region. However, the tensile zone region around the drift to the right of the transition and in the weak rock-mass region (figure 3-19b) is greater than that predicted for the base case simulation with a drift located solely in the weak rock-mass region (figure 3-3b). Maximum tensile stress values calculated for this transitional zone analysis are slightly lower (approximately 5 MPa) than those calculated for the previous transitional zone and base case analyses, which were on the order of 6.5 to 7.5 MPa. Mohr-Coulomb failure in the form of yielding is predicted in a few zones along the right sidewall of the drift to the left of the transitional zone in the strong rock (figure 3-20), while none is indicated directly around the perimeter of the drift to the right of the transitional zone in the weak rock. Time histories of horizontal compressive stresses in the immediate roof of these two drifts show a maximum horizontal compressive stress of approximately 65 MPa in the roof of the drift on the left of the transition (i.e., in strong rock) and a maximum horizontal stress of only 41 MPa in the roof of the tunnel to the right of the transitional zone (i.e., in weak rock).

3.2.2.1 Effect of Reduced Rock Block and Joint Strength Parameters on Rock-Mass Behavior in the 4-Drift Transitional Zone Model

Similar to what was performed for the 3-drift transitional zone model, a case was run for the 4-drift transitional zone model with reduced rock strength as well as joint strength parameters. The TM analysis was carried out to 150 yr of thermal loading. Similar to the results for the reference case run, the reduced rock and joint strength run results in significantly more deformation, slip, and yielding around the drifts in the weak rock to the right of the transitional zone. Figure 3-21a shows plastic yield and tensile failure indices after 150 yr of thermal loading. Although yield failure is indicated around both drifts on either side of the transitional zone, it is greater in the right tunnel on the weak side of the rock transition. Also, more tensile rock failure in the floor of the tunnels on the weak rock-mass side of the transition is indicated, as well as wedge collapse of rock in the roof of these drifts. Figure 3-21b shows that the extent and magnitude of shearing along joints around

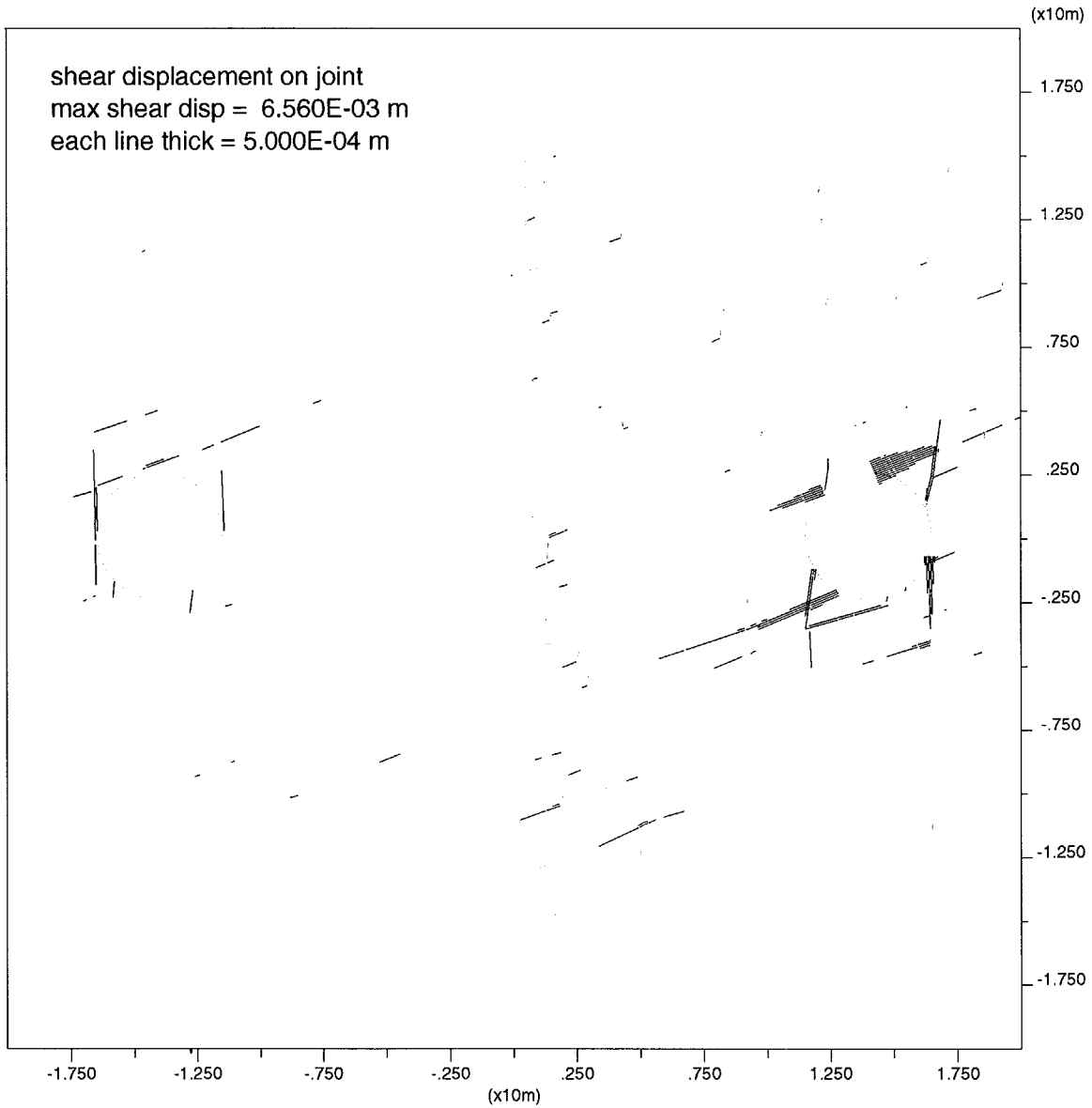

Figure 3-17. Joint shear displacements (m) after 100 yr of thermal loading based on vertical rock transitional zone midway between emplacement drifts (4-drift transitional zone model)

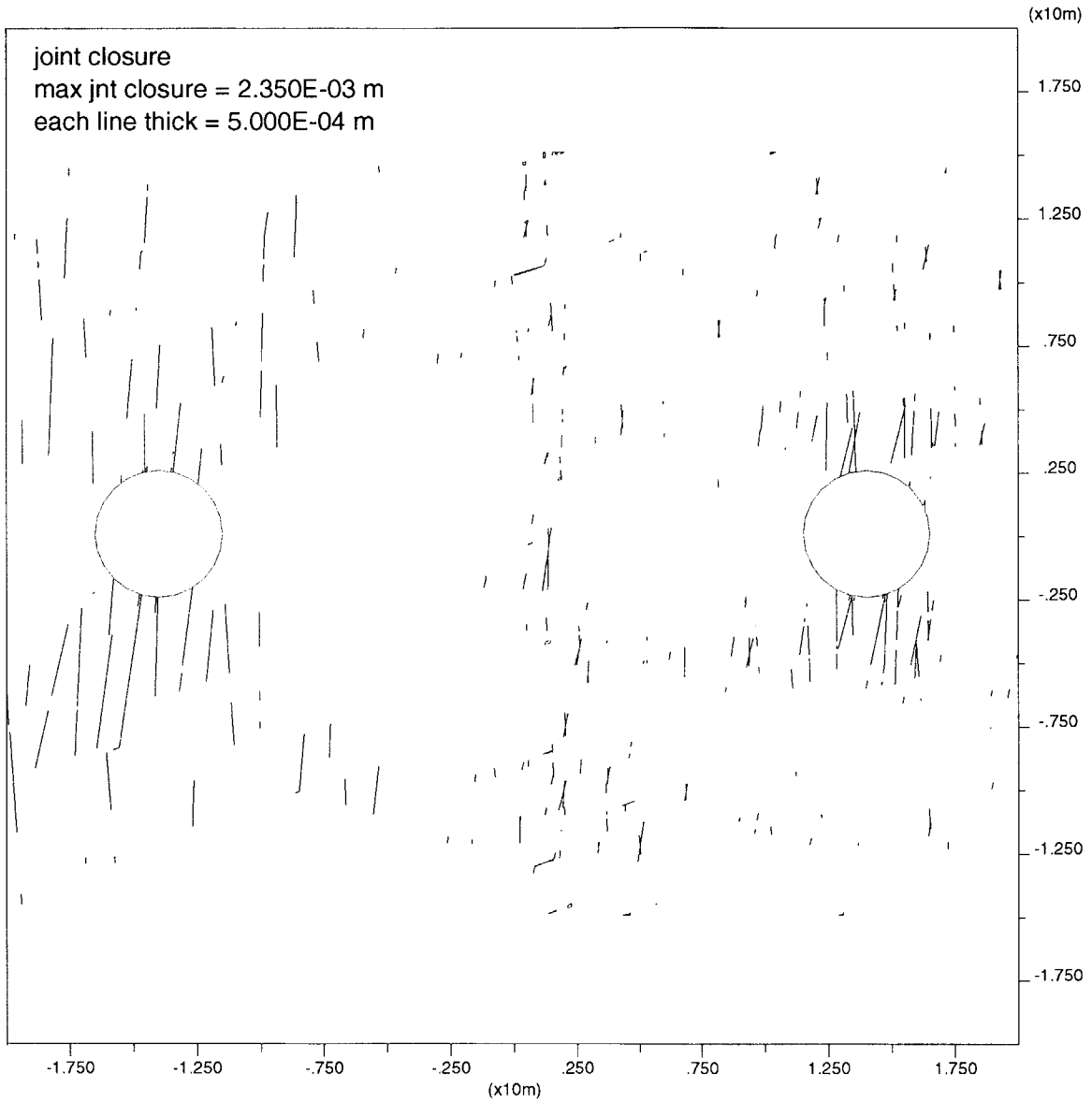

Figure 3-18. Joint closures (m) after 100 yr of thermal loading based on vertical rock transitional zone midway between emplacement drifts (4-drift transitional zone model)

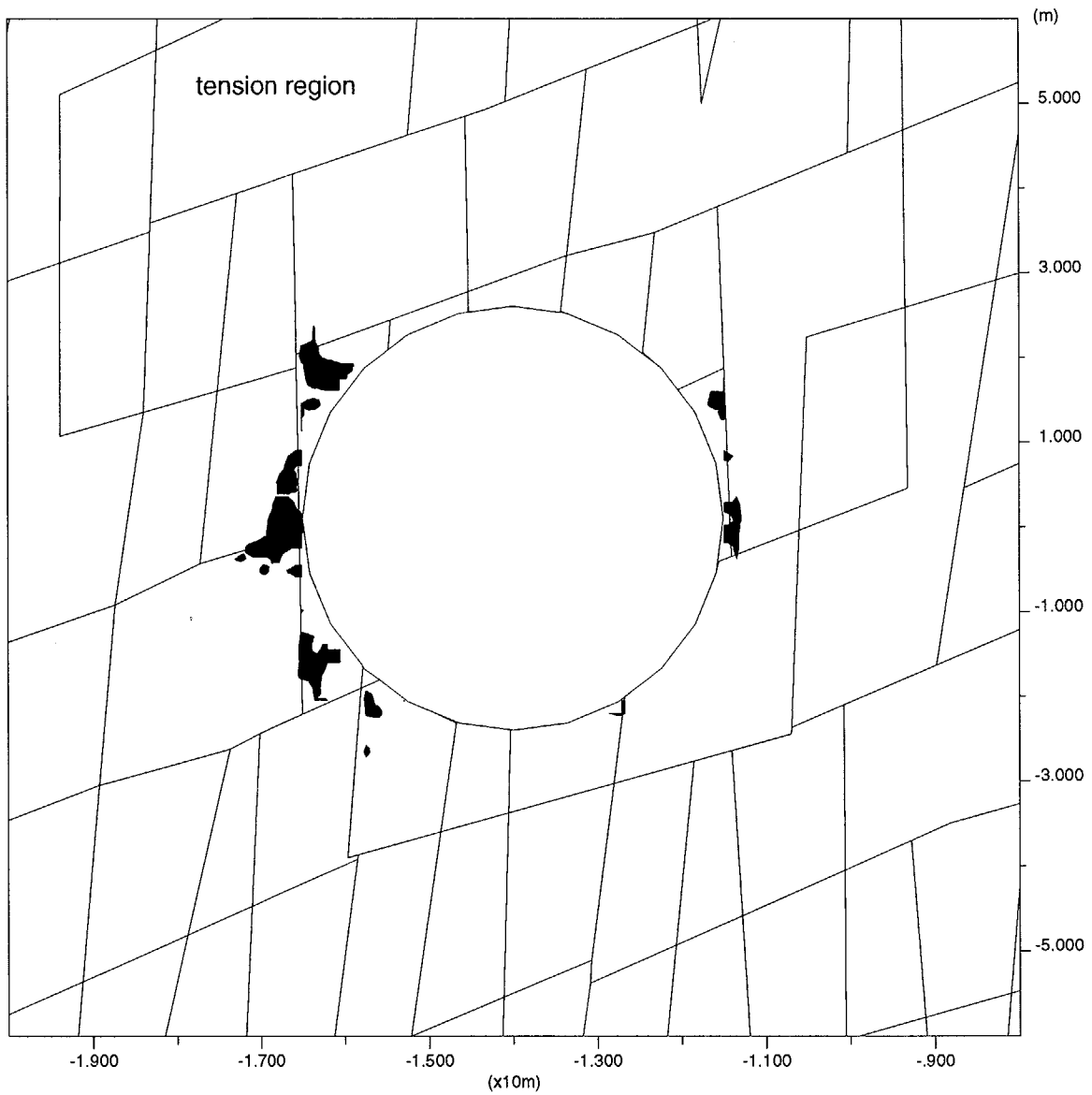

Figure 3-19a. Zones of tensile stress (red) after 100 yr of heating around the drift to the left of the transitional zone (i.e., in strong rock)

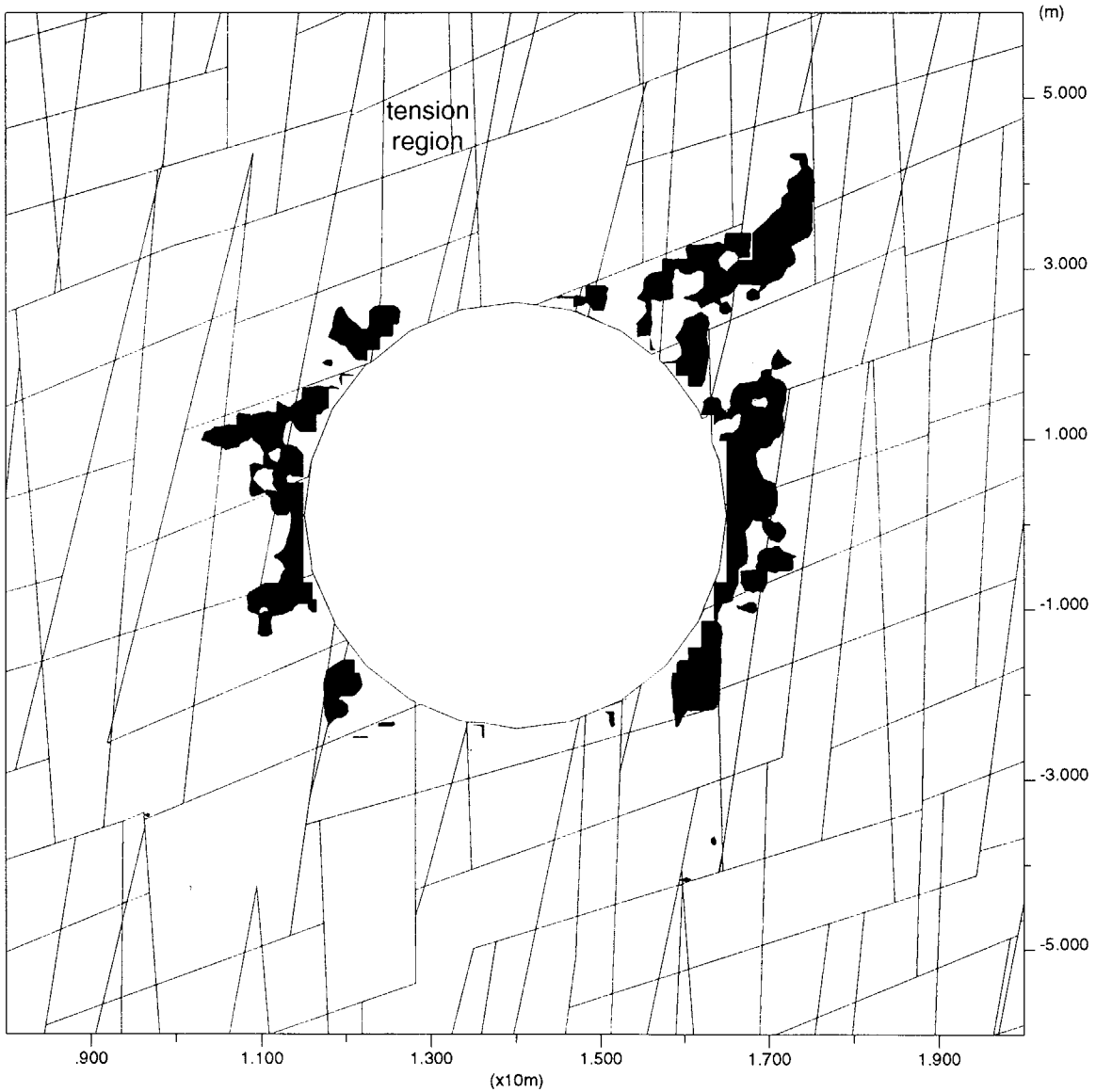

Figure 3-19b. Zones of tensile stress (red) after 100 yr of heating around the drift to the right of the transitional zone (i.e., in weak rock) for the 4-drift transitional zone model

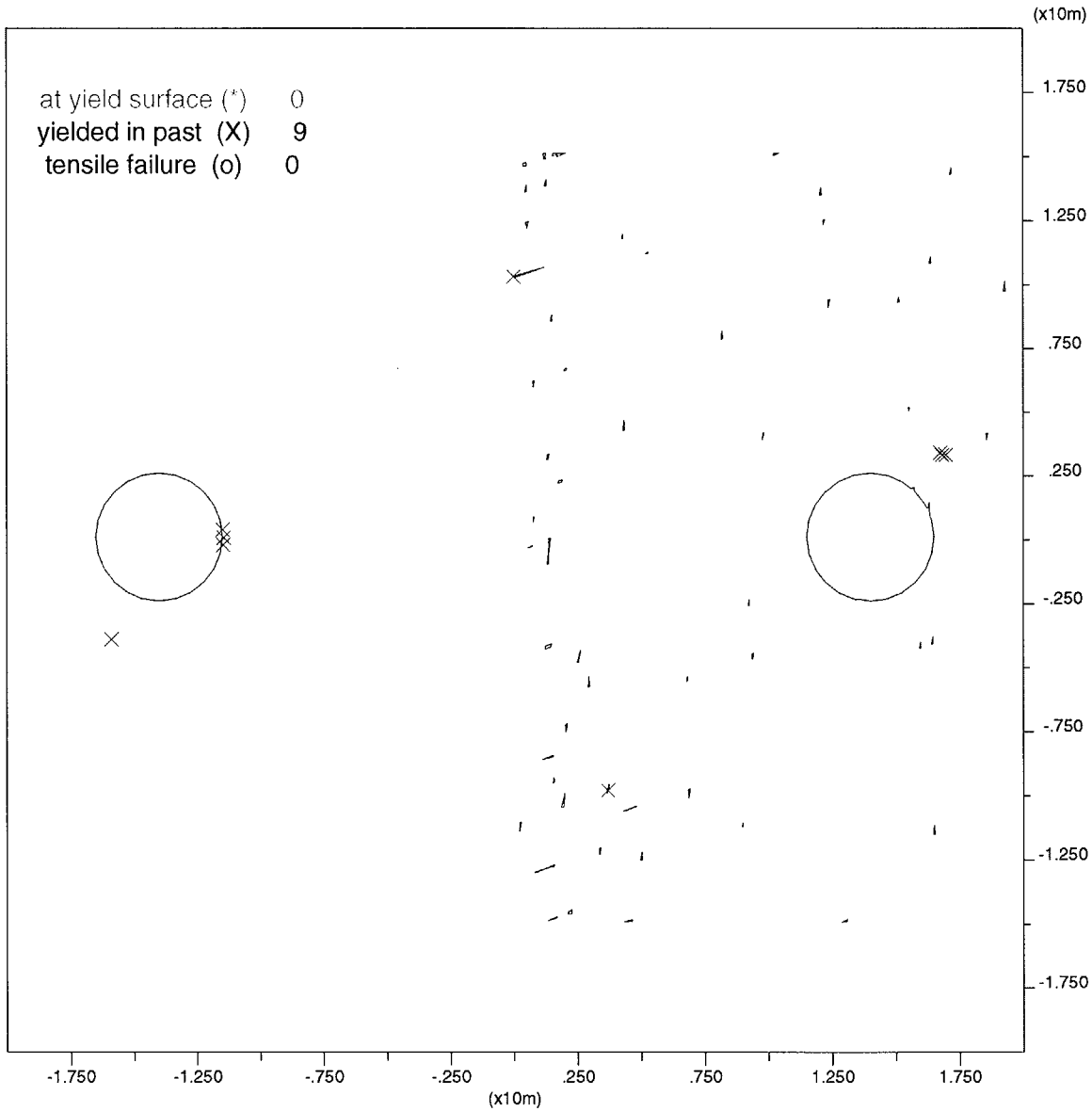

Figure 3-20. Failure zones after 150 yr of thermal load using 4-drift transitional zone model with reference rock and joint strength parameters

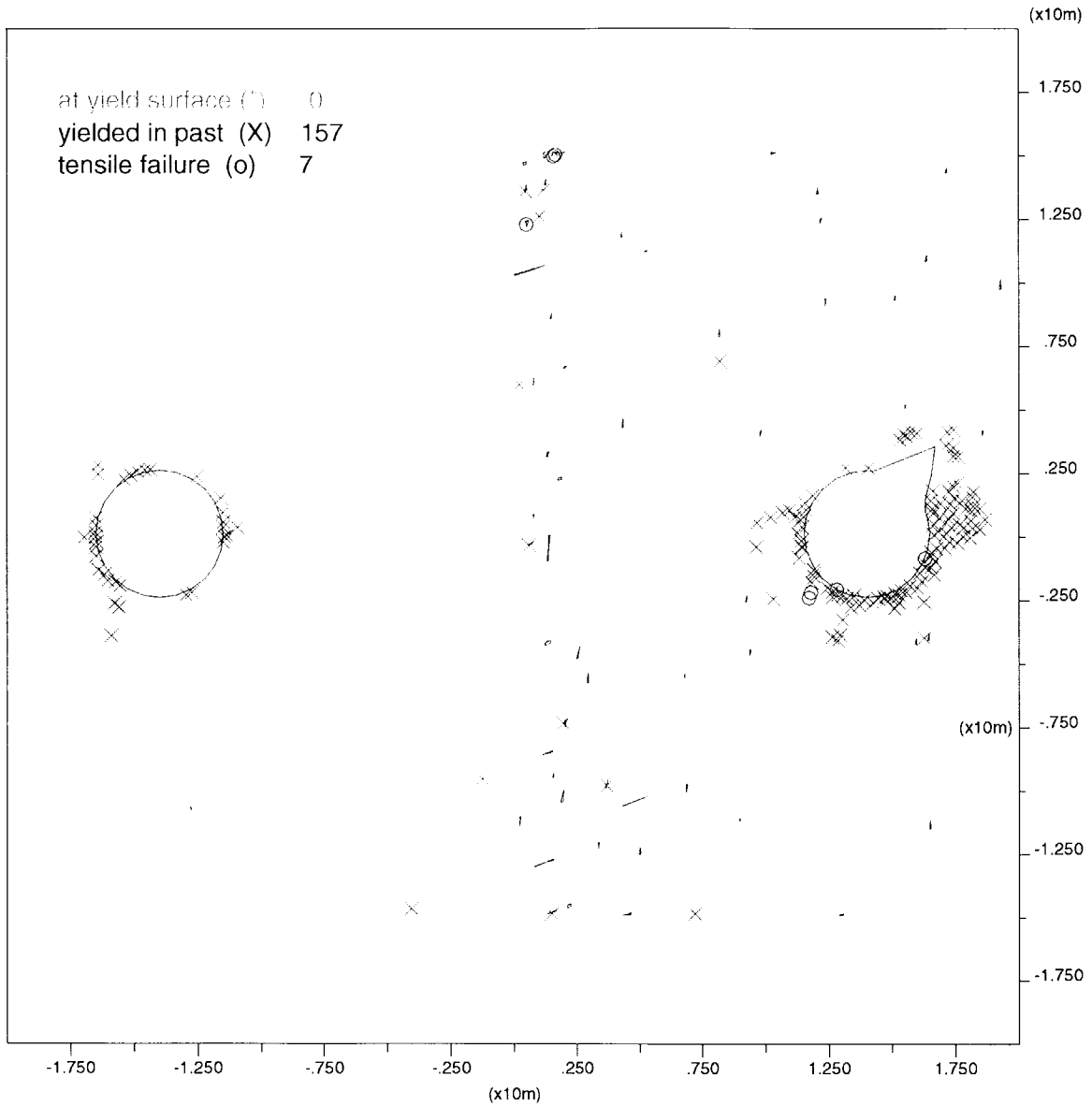

Figure 3-21a. Failure zones after 150 yr of thermal load using 4-drift transitional zone model with reduced rock and joint strength parameters

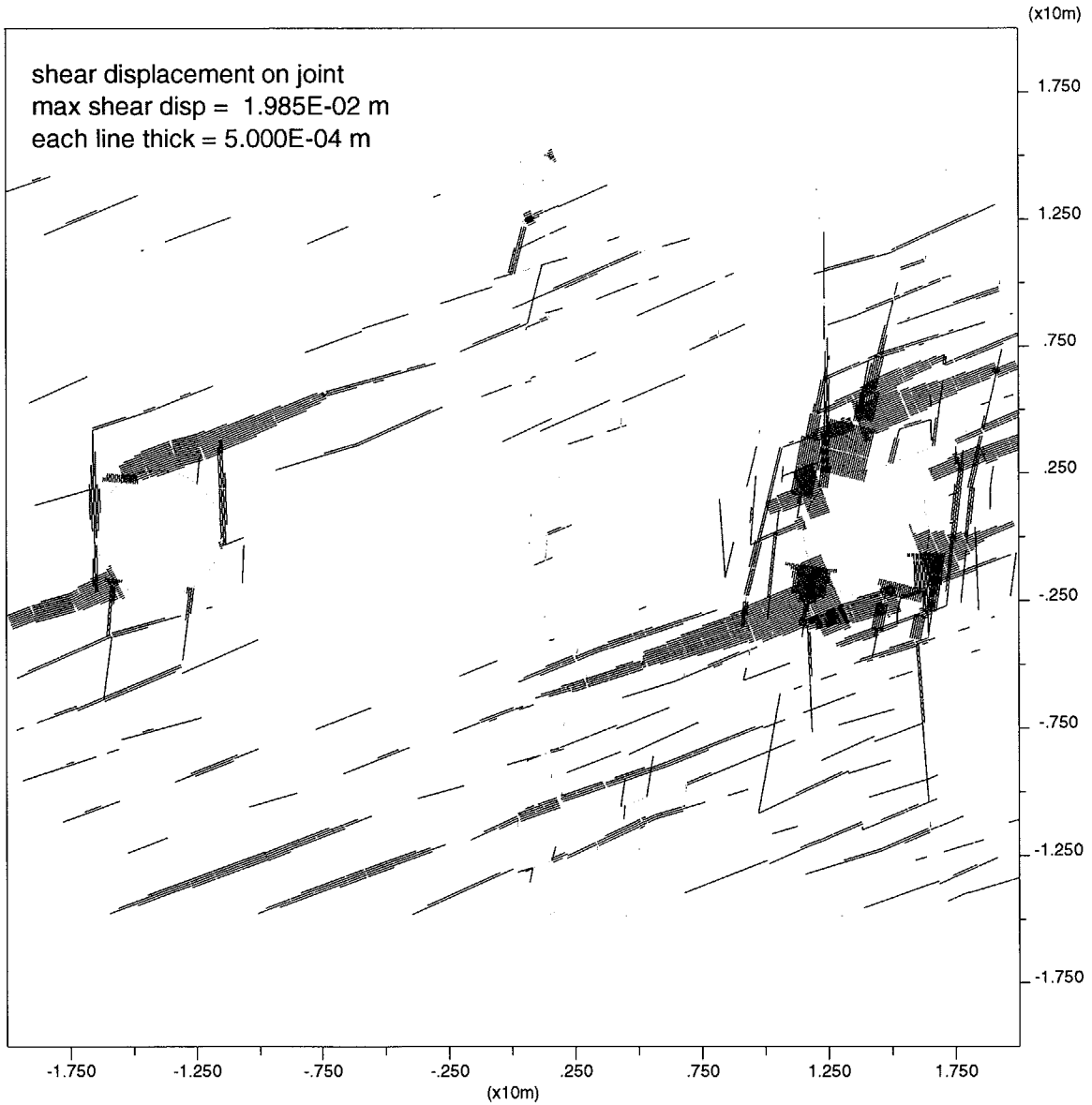

Figure 3-21b. Four-drift transitional zone thermal-mechanical analyses results at 150 yr using reduced rock and joint strength properties showing joint shear displacements (m)

the right tunnel in weak rock is significantly larger than around the left-most drift in strong rock, which includes shearing on both the subhorizontal and subvertical joints. Likewise, a contour plot of tensile stress regions again shows the right drift under a great deal more tension than the left drift on either side of the transitional zone (figure 3-22). At 150 yr, the horizontal stress has dropped significantly in the roof of the right drift in weak rock compared to that in the roof of the left drift in strong rock (15 MPa versus 54 MPa, respectively). Again, base case TM simulations could not be conducted for all the corresponding transitional model simulations discussed above (i.e., reduced intact rock and joint strength parameters) due to time constraints and long computer run times. Thus, it is not possible to confirm that all the TM effects discussed in this section are due solely to a rock-mass strength transition or whether they would also exist around emplacement drifts modeled in either a strong rock-mass region (coarse jointing) or weak rock-mass region (fine jointing). Future studies should continue with a suite of base case studies to clarify rock transitional zone effects.

3.2.2.2 Rock Bolt Reinforcement in the 4-Drift Transitional Zone Model

A simulation with fully grouted rock bolt reinforcement in conjunction with the 4-drift transitional zone model incorporating reduced rock and joint strength properties was conducted for 30 yr after onset of thermal loading. Axial bolt forces and indications of failures in either the steel bolts or grout were monitored in the two drifts on either side of the transitional zone. After excavation, the axial loading on the bolts in the drift to the right of the transition (weak rock) was greater than on those bolts supporting the roof of the drift in the left tunnel (strong rock). More than half the bolts in the roof of this right side drift showed indications of axial tensile failure, at some location along the bolt, while no axial tensile failure existed in the bolts supporting the drift on the left side of the transition after drift excavation. Little to no grout failure was predicted after excavation above either drift. After applying the thermal load for 30 yr, axial tensile failure was predicted at one or more locations in all bolts above the drift in the weak rock mass, while approximately half the bolts above the drift in the strong rock mass showed axial failure. Some grout failure was predicted around all bolts supporting both drifts, but the extent of grout failure did not appear to be as great as that for the fully grouted rock bolt simulations conducted for the 3-drift transitional zone model. Additional analyses are necessary to evaluate larger-diameter, higher-tensile strength bolts and possibly higher-shear-strength concrete grout. Comparing the discussion of results in this section with those for the 3-drift transition zone rock bolt simulations (section 3.2.1.3), the transition zone appears to have some effect on rock bolt behavior on either side of such a transition (i.e., after excavation bolt failures are indicated on the strong rock-mass side of the 3-drift rock transitional zone model but not on the strong rock-mass side of the 4-drift rock transitional zone model).

3.3 EFFECTS OF A TRANSITIONAL ZONE

Selected results for maximum and minimum principal stresses, maximum displacement vectors, maximum joint normal closure and joint shear displacements, and amount of rock yielding and tensile failure are tabulated in table 3-1 both after drift excavation equilibrium and after 150-yr thermal loading equilibrium. The results do not necessarily represent the maximum values throughout the entire TM analyses, as results were saved only at select output times, and time histories only at select locations were monitored. Much of the effect of the transitional zone and its location was discussed in section 3.2. Some additional quantitative results are added here. Table 3-1 shows that at 150 yr, the minimum compressive stresses in the 3-drift transitional zone model (Cases #3 and #4) are lower than those for either base case simulation (Cases #1 and #2). However, for the 4-drift transitional zone model (Cases #7 and #8), the minimum compressive principal stresses at this same time are higher than for the 3-drift transition simulation (Cases #3 and #4). No definite trends in

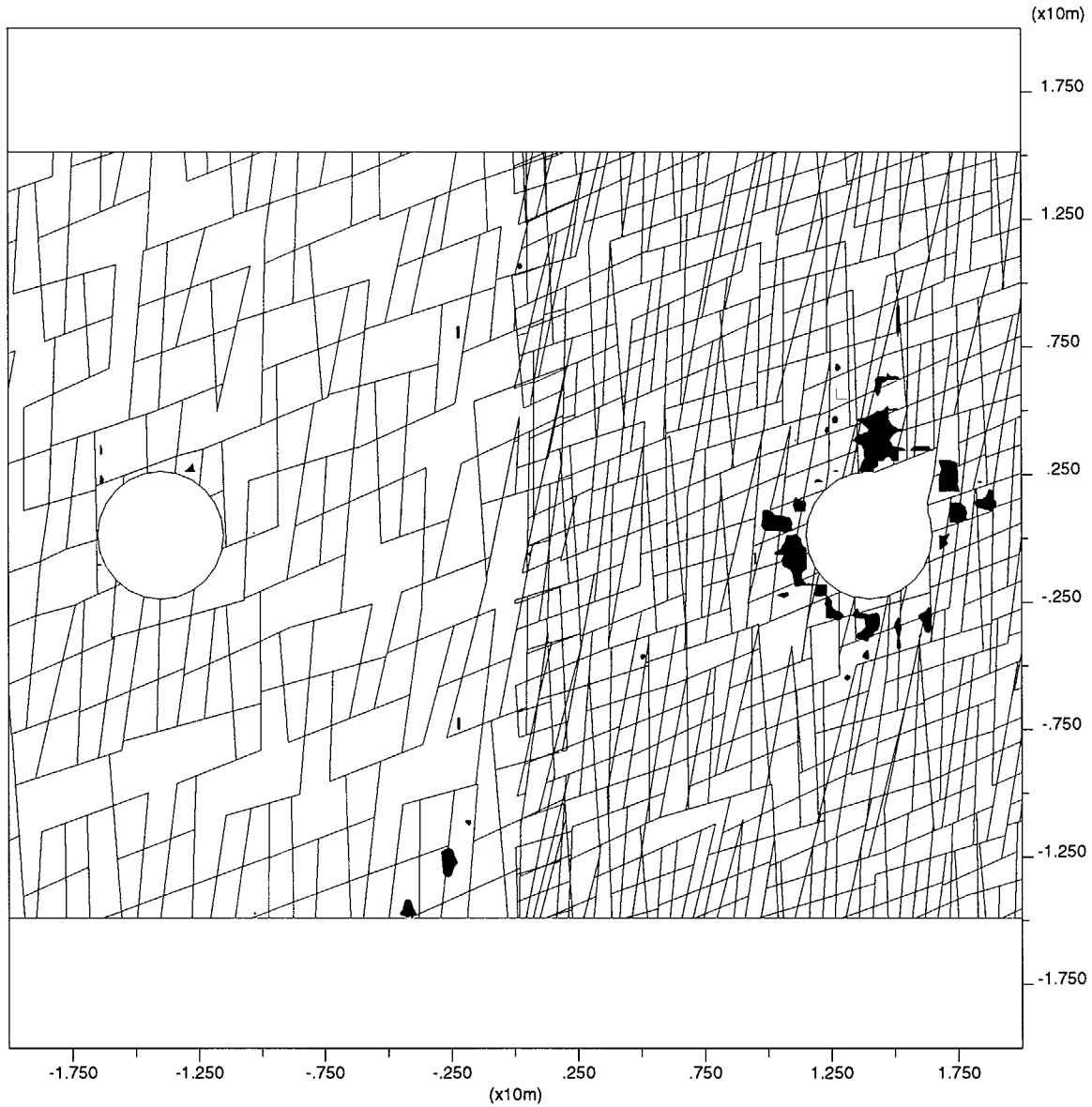

Figure 3-22. Four-drift transitional zone thermal-mechanical analyses results at 150 yr using reduced rock and joint strength properties showing contours of tensile stress regions

the tensile stress magnitudes (i.e., maximum principal stress) can be drawn from table 3-1. However, as discussed in section 3.2, the transitional zone Cases #3 and #4 result in a larger tensile stress zone region around the drift with the rock strength transition than that predicted for either of the two base case simulations. Also, as discussed in the previous section, the transitional zone Cases #7 and #8 resulted in very little tension around the drift to the left of the transition (i.e., in strong rock) and a larger zone of tension around the drift to the right of the transition (i.e, in weak rock).

As seen in table 3-1, the magnitudes of joint shear displacements are higher for the transitional zone simulations than for the base case simulations. The large joint shear displacement and maximum displacement vector for Case #8 at 150 yr was a result of some floor heave after rock failure occurred in one of the drifts in the weak rock to the right of the rock transition line. The number of rock failures in the form of plastic yield or tensile failure around the drifts increased somewhat when the joint normal and shear stiffnesses were either increased or decreased in magnitude. The number of rock failures increased significantly when the reduced rock and joint strength properties were substituted for the reference strength properties. The presence of the rock strength transition appeared to concentrate on rock failure around the drifts or drift portions on the weak side of the rock strength transition, although additional base case simulation is necessary to quantify or verify this finding. Some collapse of rock blocks above the drifts in the form of wedges was indicated after excavation and/or thermal loading for both of the rock transition model simulations. In performing distinct element analyses of a highly jointed rock mass, the maximum values of stresses, joint shear displacements, and joint closures as presented in table 3-1 are to some degree controlled by the particular geometry of the joints in the model. As such, a slightly different random generation of joints using the same mean and standard deviations for the joint set parameters would likely lead to different maximum values, though on a larger scale (i.e., drift scale or larger), the general trends in stress, displacement, and failure patterns should be similar. Much of the qualitative discussion of the transitional zone effects in the previous sections should be valid regardless of minor alterations (realizations) in the joint patterns (assuming the same governing parameters are used in the joint set generation). However, maximum values of such parameters as principal stresses, joint shear and closure displacements, etc., should be viewed in light of this analysis approach as opposed to standard continuum numerical methods. However, it is beneficial to present maximum values in this type of analysis, as the general trends in comparing such values among the different transitional zone cases or between the transitional zone cases and the base cases should hold with different joint pattern realizations (assuming the same joint set input parameters) discussed above.

Table 3-1. Tabulated comparison of select thermal-mechanical results with and without rock-mass transitional zone

Simulation Run*	Time	†Minimum Principal Stress (MPa)	‡Maximum Principal Stress (MPa)	§Maximum Displace-ment Vector (cm)	Maximum Joint Closure (mm)	Maximum Joint Shear Displace-ment (mm)	# Mohr-Coulomb Failure Zones	
							Yield	Tension
Case #1	Excavation	-28.0	2.9	0.3	0.4	3.3	0	0
	150 yr	-106.4	6.0	16.0	2.8	8.6	11	0
Case #2	Excavation	-25.3	1.4	0.2	0.3	2.52	0	0
	150 yr	-99.3	5.2	16.6	1.9	6.1	10	0
Case #3	Excavation	-33.7	2.3	0.7	0.5	5.5	0	0
	150 yr	-59.9	5.2	16.7	1.5	21.2	12	0
Case #4	Excavation	-19.7	2.9	0.5	0.6	5.1	1	0
	150 yr	-64.9	3.2	16.9	3.3	23.7	191	44
Case #5	Excavation	-33.1	1.7	0.4	0.1	2.8	0	0
	150 yr	-106.7	6.6	17.4	0.8	18.4	24	3
Case #6	Excavation	-31.2	4.0	1.0	4.4	12.8	0	0
	150 yr	-48.1	4.8	16.3	3.7	12.6	22	9
Case #7	Excavation	-38.5	1.8	0.2	0.7	2.2	0	0
	100 yr	-87.8	8.7	15.7	2.4	6.6	11	0
Case #8	Excavation	-45.1	2.1	0.8	1.2	5.5	0	0
	150 yr	-97.9	4.0	32.9	2.0	121.9	254	68

*Case # Definitions:
- #1 — Base case weak rock (3-drift)
- #2 — Base case strong rock (3-drift)
- #3 — 3-drift transitional model, reference strength properties
- #4 — 3-drift transitional model, reduced strength properties
- #5 — 3-drift transitional model, reference strength properties, high joint stiffnesses
- #6 — 3-drift transitional model, reference strength properties, low joint stiffnesses
- #7 — 4-drift transitional model, reference strength properties
- #8 — 4-drift transitional model, reduced strength properties

†Minimum principal stress is compression

‡Maximum principal stress is tension

§Maximum displacement vector is downward (negative) roof displacement after excavation, and upward (positive) displacement due to thermal expansion at 50-yr thermal loading state

4 CONCLUSIONS

A series of analyses was performed using UDEC to investigate the impact of a transitional area between a strong and weak rock mass at or near underground waste emplacement drifts on the overall TM behavior of such drifts. Two different locations for such a rock transitional zone were investigated: a vertical transition through the center of a drift and a vertical transition midway between two drifts. A thermal loading of 85 MTU/acre was applied and, to the extent possible, analyses were carried out to 150 yr. Limited base case TM analyses were also performed to compare differences with those analyses that were conducted with the transitional zone. The impact of reference (i.e., laboratory test) rock block and joint strength parameters, reduced rock block and joint strength parameters, variable joint stiffness, and fully grouted rock bolt reinforcement on the overall TM behavior of the rock mass surrounding the emplacement drifts in the transitional zone are also analyzed.

For the 3-drift model, with the transitional rock-mass region located about the vertical centerline of the middle drift, the zones of tension and the shearing along joints were more extensive around this center drift than for either of the base case simulations performed. However, based on the reference strength properties used, no tensile failures after 150 yr were predicted for the transitional model or either of the base case models, and only a few zones around the drifts were predicted to fail in yield in either the base case runs or the transitional model run. Analyses using the reduced rock block and joint strength properties showed extensive rock yielding as well as tensile failure after 150 yr in the transitional zone model, with the number of zones showing yield or tensile failure somewhat higher on the weak rock-mass side of the transitional zone. This reduced-strength property simulation also resulted in a larger zone of tension around the central drift, as well as a much larger extent of shearing along both the subhorizontal and subvertical joints than predicted using the reference-strength property simulation.

Increasing the joint normal and shear stiffnesses by a factor of 10 resulted in a much larger region over which shearing along subhorizontal joints occurred, with the maximum shear displacements located around the central drift in which the transition is located. The number of yield zones increased slightly, the majority of them located on the strong rock-mass side of the transition. Decreasing the joint normal and shear stiffnesses by a factor of 10 resulted in shearing along both subhorizontal as well as subvertical joints, which was more concentrated around the drifts (the most being around the central drift where the rock-mass transition was located). The number of zone yield and tensile failures again increased slightly from the reference transitional zone simulation, with the majority of them located around the drifts or portion of the drifts on the weak rock-mass side of the transition. Fully grouted rock bolts (2.5 m in length on 1.0-m centers) were incorporated above the springline of the drifts in the 3-drift transitional model with reduced-strength properties. The bolts incorporated into the model were typical of #6 alloy steel bars (0.75-in.-diameter and 70,000-psi-tensile yield strength). After drift excavation, a few bolts showed axial failure of the steel as well as some failure of the grout. During the thermal loading phase, rapid development of axial forces in the steel could be seen over the full 2.5-m length of all bolts. After 30 yr of heating, the thermal expansion of the rock mass resulted in failure of the grout along essentially the full length of all bolts on either side of the transitional zone. At this thermal time, all bolts show axial failure in at least one location, and in multiple locations on the weak rock-mass side of the transitional zone. It is not known if the same bolt/grout failure behavior would result if the reference rock strength and joint strength parameters had been used.

For the 4-drift model with the transitional zone located midway between the two central drifts, the TM analyses using the reference rock and joint strength properties showed that the magnitude and extent of shearing along joints as well as the extent of tensile stresses was greater around the drift in the weak rock-mass side of the

transition (i.e., to the right of the transition location). Similar TM simulations with this 4-drift model using the reduced rock and joint strength properties showed even more yielding/tensile rock failure, joint shearing, and tensile regions around the drift on the weak side of the rock strength transition line. Some bolts reinforcing drifts in the weak rock-mass region showed axial failure after drift excavation. Again, after 30 yr of heating, and perhaps sooner, nearly all bolts reinforcing drifts on either side of the transition showed axial and grout failure from thermal expansion of the rock mass, with more axial tensile bolt failures predicted on the weak rock-mass side of the transition.

In summary, based on the 150-yr TM analyses performed, any adverse conditions within the transitional zone between strong and weak rock-mass categories appear to be much more pronounced for rock and joint strength conditions and joint stiffness conditions that are weaker than for the reference values used (i.e., those derived from laboratory testing on small rock specimens). Such weak rock and joint strength conditions might be expected to exist later in the proposed repository preclosure period as a result of degradation to the rock block and rock joints/joint asperities due to a prolonged high-temperature environment (creating enhanced microfracturing and geochemical and geohydrologic changes within the rock). However, the potential for rock-mass strength reduction under long-term thermal loading should be confirmed through heater tests currently being conducted within the ESF. Assuming rock degradation does exist, the adverse conditions created in the transitional zone are predicted to be in the form of increased zones of rock tension around drifts directly within the transitional zone as well as in adjacent drifts on the weak rock-mass side of the transition, and results should also include increased rock failure in both yield and tension around the entire perimeter of such drifts. In addition, much larger joint shear displacements along subhorizontal, and to some extent, subvertical joints around drifts located directly within the transition and adjacent drifts on the weak rock-mass side of the transition, are predicted to occur. The larger degree of shearing along joints indicates the need for rock bolt reinforcement that has not only a high axial strength but also a high resistance to shearing at the joint intersections. The predicted rock failure around these drifts indicates the need for additional rock reinforcement between the grouted rock bolts (e.g., wire mesh or steel straps). Finally, the floor of such drifts showed rock failure and joint shearing. Rock bolting into the floor of such drifts might be prudent to aid in preventing shifting or uplift of the floor which could damage the pedestals on which the waste canisters rest. Assuming there was little to no degradation in rock/joint strengths within the 150-yr simulation time, the presence of a rock transition zone appears to have a minimal impact from a design standpoint, although sufficient diameter/strength rock bolts would have to be incorporated to withstand the rock thermal expansion. Considering the highly fractured nature of the rock surrounding the waste emplacement drifts, other numerical approaches (i.e., finite elements) do not appear to be as useful or accurate as distinct element methods such as UDEC. Three-dimensional analyses of a rock strength transition zone would be beneficial but would most likely be difficult to analyze.

In these TM analyses, the rock-mass moduli on either side of the transitional zone were set by adjusting the fracture frequency and, in some cases, the joint normal stiffness, while keeping the rock block moduli fixed. The fracture frequency in the weak rock-mass region was set as high as feasible from a computational point considering the number of drifts and size of the fractured model that was used. Future data may allow development of a better approach to adjusting the rock block modulus based on the nominal block size to account for much more closely spaced joints/microfractures that could not be incorporated into this TM analyses. Additional analyses should also investigate other size rock bolts and grout strengths to determine which would be most effective during the thermal loading period. It should be noted that base case simulations were not run for the reduced rock and joint strength transitional simulations, for joint stiffness variation transitional cases, or for the rock bolt reinforcement transitional cases. As a result, it is not clear whether all of the effects/differences in results on either side of the rock transition presented in section 3.2 are the result of the rock-mass strength transition or whether they may also be caused by the different degree of jointing in these regions.

5 REFERENCES

Anna, L.O. 1998. *Preliminary Three-Dimensional Discrete Fracture Model of Topopah Spring Tuff in the Exploratory Studies Facility, Yucca Mountain Area, Nye County, Nevada.* USGS Open-File Report 97-834. Washington, DC: U.S. Geological Survey.

Beason, R., and K. Hoeg. 1997. Previous Mapping Efforts. *Handout and Presentation at the U.S. Department of Energy/Nuclear Regulatory Commission Appendix 7 Meetings, October 16, 1997.* Washington, DC: Nuclear Regulatory Commission.

Brechtel, C.E., M. Lin, E. Martin, D.S. Kessel. 1995. *Geotechnical Characterization of the North Ramp of the Exploratory Studies Facility.* SAND95–0488/1. Albuquerque, NM: Sandia National Laboratories.

Carter, N.L. 1975. High-temperature flow of rocks. *Reviews of Geophysics and Space Physics* 14(3): 301–360.

Carter, N.L. 1976. Steady state flow of rocks. *Reviews of Geophysics and Space Physics*. 14(3): 344–349.

Chen, R. 1999. Analyses of drift stability and rockfall due to earthquake ground motion at Yucca Mountain, Nevada. *Proceedings of the 37th U.S. Rock Mechanics Symposium, Rock Mechanics for Industry, Vail, Colorado, June 5–9, 1999.* B. Amadei, R.L. Kranz, G.A. Scott, and P.H. Smeallie, eds.: 759–766.

Ghosh, A., S.M. Hsiung, and A.H. Chowdhury. 1996. *Seismic Response of Rock Joints and Jointed Rock Mass*. NUREG/CR–6388. San Antonio, TX: Center for Nuclear Waste Regulatory Analyses.

Civilian Radioactive Waste Management System Management and Operating Contractor. 1997.*Confirmation of Empirical Design Methodologies.* BABEE–01717–5705–00002. Revision 00. Las Vegas, NV: Civilian Radioactive Waste Management System Management and Operating Contractor.

Civilian Radioactive Waste Management System Management and Operating Contractor. 1999. *License Application Design Selection Report.* B00000000–01717–4600–00123. Revision 01. Las Vegas, NV: Civilian Radioactive Waste Management System Management and Operating Contractor.

Hoek, E., and E.T. Brown. 1982. *Underground Excavations in Rock.* Hertford, England: Stephen Austin and Son, Ltd.

Hsiung, S.M., and T.M. Shih. 1979. Creep study on Shin Pin Seah sandstone.*Journal of Mining and Metallurgy*: in Chinese.

Hsiung, S.M., W. Blake, A.H. Chowdhury, and T.J. Williams. 1992. Effects of mining-induced seismic events on a deep underground mine. *PAGEOPH* 139(3/4): 741–762.

Itasca Consulting Group, Inc. 1996. *UDEC Universal Distinct Element Code. Version 3.0. Volume I: User's Manual.* Minneapolis, MN: Itasca Consulting Group, Inc.

Jaeger, J.C., and N.G.W. Cook. 1979. *Fundamentals of Rock Mechanics*. 3rd Edition. London, UK: Chapman and Hall, Ltd.

Kana, D.D., B.H.G. Brady, B.W. Vanzant, and P.K. Nair. 1991. *Critical Assessment of Seismic and Geomechanics Literature Related to a High-Level Nuclear Waste Underground Repository*. NUREG/CR-5440. Washington, DC: Nuclear Regulatory Commission.

Kana, D.D., D.J. Fox, S.M. Hsiung, and A.H. Chowdhury. 1995. *An Experimental Model Study of Seismic Response of an Underground Opening in Jointed Rock*. CNWRA 95-012. San Antonio, TX: Center for Nuclear Waste Regulatory Analyses.

Kemeny, J., and N. Cook. 1990. Rock mechanics and crustal stress. *Demonstration of Risk-Based Approach to High-Level Waste Repository Evaluation.* R.K. McGuire, ed. EPRI NP-7057. Golden, CO: Risk Engineering Inc.: 5-1-5-20.

Lin. M., M.P. Hardy, and S.J. Bauer. 1993. *Fracture Analysis and Rock Quality Designation Estimation for the Yucca Mountain Site Characterization Project*. SAND92-0449. Albuquerque, NM: Sandia National Laboratories.

Martin, III, R.J. 1972. Time-dependent crack growth in quartz and its application to the creep of rocks. *Journal of Geophysical Research* 77(8).

Price, R.H., J.R. Connolly, and K. Keil. 1987. *Petrologic and Mechanical Properties of Outcrop Samples of the Welded, Devitrified Topopah Spring Member of the Paintbrush Tuff*. SAND86-1131. Albuquerque, NM: Sandia National Laboratories.

Pye, J.H., D.C. Kicker, and G.H. Nieder-Westermann. 1997. Plans for mapping of subsurface facilities. *Notes from U.S. Department of Energy/Nuclear Regulatory Commission Appendix 7 Discussions. October 16, 1997.* Washington, DC: Nuclear Regulatory Commission.

Spiegel, L., and G.F. Limbrunner. 1998. *Reinforced Concrete Design.* 4th Edition. Columbus, OH: Prentice Hall.

U.S. Department of Energy. 1997. *Repository Ground Support Analysis for Viability Assessment.* Document No. BCAA00000-01717-0200-00004. Revision 00. Las Vegas, NV: U.S. Department of Energy.

U.S. Department of Energy. 1998a. *Viability Assessment of a Repository at Yucca Mountain*. DOE/RW-0508. Las Vegas, NV: U.S. Department of Energy.

U.S. Department of Energy. 1998b. *Repository Thermal Loading Management Analysis.* B00000000-01717-0200-00135. Revision 0. Las Vegas, NV: U.S. Department of Energy.

APPENDIX A

UDEC INPUT DATA FILE FOR 3-TUNNEL MODEL WITH TRANSITIONAL ZONE ALONG VERTICAL CENTERLINE OF DRIFT

APPENDIX A
UDEC INPUT DATA FILE FOR 3-TUNNEL MODEL WITH TRANSITIONAL ZONE ALONG VERTICAL CENTERLINE OF DRIFT

```
************************************************************
*UDEC Version 3.0 Input Data File
*3 tunnel drift scale T-M model with strong rock/weak rock transition along vertical centerline
*of central tunnel.
*
* Objective - Evaluate transition zone between a strong TSW2 category rock versus a weaker TSW2
* category rock  in which the dividing line between the two categories occurs through the vertical axis
* of the central tunnel.  Approach is to incorporate two different joint sets (one being
* 85 degrees measured ccw from horizontal axis and the other being 20 degrees (as taken
* from Table 1 (Chen, 1999).  As listed in this table, mean fracture spacings were on the order
* of 0.4 m for the 85 degree joint set and 0.75 m for the 20 degree joint set, both with standard
* deviations of 0.1 m.
*
*  Strong rock -   Joint Set #1 - (mean orientation 85 degrees ccw from horizontal, joint spacing = 1.0 m)
*                  Joint Set #2 - (mean orientation 20 degrees ccw from horizontal, joint spacing = 2.0 m)
*
*          Equivalent rock mass modulus (Em) in the horizontal direction where 1/Em = 1/Er + 1/(Kn*S)
*                  and Er = 3.303e+04 MPa [Intact Rock Young's Modulus]
*                      Kn = 5.0e+04 MPa/m  [Joint normal stiffness]
*                      S = 1.0 m [Sub-vertical joint spacing]
*  ------>             Em = 19.890 GPa   (horizontal direction)
*
*  Weak  rock -   Joint Set #1 - (mean orientation 85 degrees ccw from horizontal, joint spacing = 0.5 m)
*                 Joint Set #2 - (mean orientation 20 degrees ccw from horizontal, joint spacing = 1.0 m)
*
*                    Assuming S=0.5 m [Sub-vertical joint spacing]
*  -------->          Em = 14.230 GPa (horizontal direction)
*
* Note: small standard deviation in joint orientation allowed (10 degrees for 85 degree joint set, and 5
* degrees for the 20 degree joint set). Also, mean joint trace lengths of 7.5 m was assigned to 85 degree
* joint set and 5.0 m to the 20 degree joint set, both with a standard deviation of 1.0 m.
************************************************************
*
*********************
* Part I:
*********************
set log tm_3tun.log
set plot po
start
************************************************************************
```

```
* Title and block definition for Lwp=18 m, Ldrift=28 m
**********************************************************************
head
3 Tunnel T-M Analysis - strong/weak rock transition zone along center tunnel vert. axis
config thermal
*
* Size of problem domain is -28 m < x < 28 m;  -225 m < y < 311 m
*  - Vertical boundaries are located along symmetry lines assuming
*    28 m drift spacings
*
round 0.0145
set ovtol 1.0
*
**************
* Part I - In situ loading and excavation of tunnels
*************
block -28,-225 -28,311 28,311 28,-225
* create splits at all rock formation boundaries TCw --> CHnz
split -28,275 28,275
split -28,236.9 28,236.9
split -28,106.8 28,106.8
split -28,-82.5 28,-82.5
split -28,-98.3 28,-98.3
split -28,-103.5 28,-103.5
split -28,-207.5 28,-207.5
split -28,-225 28,-225
*
* create additional horizontal cracks to bound fractured from non-fractured region
split -28,15 28,15
split -28,-15 28,-15
split -28,-25 28,-25
split -28,25 28,25
*
* create jointing around tunnels
jregion -28,-15 -28,15 2.5,15 2.5,-15
jset 85.0,10.0 7.5,1.0 -0.2,0.0 1.0,0.0 -28,-15
jset 20.0,5.0 5.0,1.0 -0.2,0.0 2.0,0.0 -28,-15
*
jregion 0,-15 0,15 28,15 28,-15
jset 85.0,10.0 7.5,1.0 -0.2,0.0 0.5,0.0 -28,-15
jset 20.0,5.0 5.0,1.0 -0.2,0.0 1.0,0.0 -28,-15
*
tunnel -28 0 2.5 24
tunnel 0 0 2.5 24
tunnel 28 0 2.5 24
del area 1.5e-2
jd
```

```
* additional cracks to break up large block below central tunnel created from above jset commands
crack -1.331,-11.75 -0.2323,-11.38
crack -1.781,-9.778 -0.5083,-9.212
crack -1.293,-7.336 -0.239,-7.0
crack -0.1845,5.747 0.2659,3.796
crack -0.4784,-3.028 0.2773,-2.742
crack -0.4784,-3.028 -0.8401,-5.071
crack -0.8401,-5.071 0.02847,-4.791
save 3tun_jnt.sav
jd
*
* ****************************
*  auto generation of zones
* ****************************
gen ann -28 0 0 5.0 edge 1.0
gen ann 0 0 0 5.0 edge 0.75
gen ann 28 0 0 5.0 edge 0.75
gen region -28 -15 -28 15 28 15 28 -15 edge 1.0
*
gen region -28 15 -28 25 28 25 28 15 quad 2.5
gen region -28 -25 -28 -15 28 -15 28 -25 quad 2.5
gen region -28 -225 -28 -25 28 -25 28 -225 quad 10.0
gen region -28 25 -28 311 28 311 28 25  quad 10.0
save 3tun_zon.sav
pr max
*
*****************************************************
* apply mechanical boundary conditions (units, MPa)
*****************************************************
grav 0.0 -9.81
insitu stress -1.89 0.0 -7.0 ygrad 0.006077 0.0 0.022508 szz -1.89 &
zgrad 0.0 0.006077
bound -28 28 310 312 stress -1.89 0.0 -7.0 ygrad 0.006077 0.0 0.022508
bound -28 28 -226 -224 yvel=0.0
bound -28.5 -27.5 -225 312 xvel=0.0
bound 27.5 28.5 -225 312 xvel=0.0
*
*
*************************************************************************
* define mechanical and thermal material properties for joints/intact blocks
*************************************************************************
*
*  material 1 = rock
*
change -29 29 -16 16 jcons=5
**
**** TCw unit ****
```

```
prop mat=1 k=18.3908e3 g=13.2231e3 d=0.002274
prop mat=1 cond=1.59 thexp=6.0e-06 spec=9.32e08
*
**** PTn unit ****
prop mat=2 k=18.3908e3 g=13.2231e3 d=0.002274
prop mat=2 cond=0.85 thexp=6.0e-06 spec=9.32e08
*
**** TSw1 unit *****
prop mat=3 k=18.3908e3 g=13.2231e3 d=0.002274
prop mat=3 cond=1.60 thexp=6.0e-06 spec=9.32e08
*
**** TSw2 unit ****
prop mat=4 k=18.3908e3 g=13.2231e3 d=0.002274
prop mat=4 cond=2.10 thexp=6.0e-06 spec=9.32e08
*
****TSw3 unit ****
prop mat=5 k=18.3908e3 g=13.2231e3 d=0.002274
prop mat=5 cond=1.28 thexp=6.0e-06 spec=9.32e08
*
**** CHn1v unit ****
prop mat=6 k=18.3908e3 g=13.2231e3 d=0.002274
prop mat=6 cond=1.20 thexp=6.0e-06 spec=9.32e08
*
**** CHn1z unit ****
prop mat=7 k=18.3908e3 g=13.2231e3 d=0.002274
prop mat=7 cond=1.28 thexp=6.0e-06 spec=9.32e08
*
**** CHnz unit ****
prop mat=8 k=18.3908e3 g=13.2231e3 d=0.002274
prop mat=8 cond=1.56 thexp=6.0e-06 spec=9.32e08
*
**** joint properties TSw2 welded unit ****
prop jmat=4 jks=5.0e4 jkn=5.0e4 kn=5.0e4 ks=5.0e4
prop jmat=4 jdil=0 jc=0.03 jfric=41.0 jtens=0.0
*
change mat=1 range -28 28 275.0 312.0
change mat=2 range -28 28 236.9 275.0
change mat=3 range -28 28 106.8 236.9
change mat=4 jmat=4 range -28 28 -82.5 106.8
change mat=5 range -28 28 -98.3 -82.5
change mat=6 range -28 28 -103.5 -98.3
change mat=7 range -28 28 -207.5 -103.5
change mat=8 range -28 28 -225 -207.5
*
set jcondf 5
*
* mohr-coulomb failure parameters TSw2 unit
```

```
*
prop mat=4 coh=36.9 fric=46.0 tens=8.91 dil=0
*
* assign high strength properties to fictitious horizontal joints separating rock units
*
change jmat=2 range -29 29 14.99 312
change jmat=2 range -29 29 -226 -14.99
prop jmat=2 jkn=1.0e5 jks=1.0e5 jcoh=1.0e20 jten=1.0e20 &
kn=5.0e4 ks=5.0e4

**********
* history records
**********
hist ncyc=10 unbal damp type 4
hist ydis 0 0 yvel 0 0 yacc 0 0 ydis 0 311 yvel 0 311 yacc 0 311
hist sxx 0.0 0.0 syy 0.0 0.0
*
**********
* initial cycling equilibrium
**********
damp auto
cycle 5000
save 3tun_ini.sav
*
**********
* remove tunnel blocks
**********
*
del ann -28 0 0 2.5
del ann 0 0 0 2.5
del ann 28 0 0 2.5
*
* reset displacements after applying in situ loading conditions
*
reset damp time hist dis rot
hist unbal damp
hist ydis 0.0 2.5 yvel 0 2.5 yacc 0 2.5 ydis 0.0 311.0
hist ydis -28.0 2.5 yvel -28.0 2.5
hist ydis 28.0 2.5 yvel 28.0 2.5
hist sxx 0.0 2.5 syy 0.0 2.5 syy 2.5 0.0 syy 5.0 0.0 syy 7.5 0.0 syy 10.0 0.0 syy 12.5 0.0
hist syy 15.0 0.0
*
* change Tsw2 material property to Mohr-Coulomb
change cons=3 range -28 28 -82.5 106.8
*
cycle 5000
*
```

```
sav 3tun_exc.sav
*
res 3tun_exc.sav
*
**********************
* Part II: Thermal
**********************
*
*************************************
* set thermal boundary and histories
*************************************
*
* set up thermal boundaries (default thermal b.c. are adiabatic)
*
*  Initial temperature at repository horizon taken to be approx, 25 C
*  Average ground surface temperature = 18.70 C
*  - temperature gradient taken to be 0.02 deg C/m
*
*  $$$ fish functions to set up initial temperature gradient $$$
*
def setup
  t_surf = 18.7      ; fixed ground surface temperature
  y_surf = 311.0     ; distance to ground surface from y-origin (i.e., repos. level)
  t_grad = 0.02      ; temperature gradient
  xr_beg = -28.0     ; start of x-range (m)
  xr_end = 28.0      ; end of x-range (m)
  delt_y = 5.0       ; increment in y to set initial grid node temperatures (m)
  num_inc = 108      ; number of increments in delt_y to reach base of model (311 < y < -225 m)
end
*
def init_tem
  yr_end = 310.0  ; starting y end range
  yr_beg = yr_end - delt_y   ; starting y beginning range
  loop ii (1, num_inc)
    yd_tem = y_surf - (0.5*(yr_end + yr_beg))   ;  depth location below surface to calculate initial temp
(midpoint of y range)
    item = t_surf + t_grad*yd_tem
    command
      pr item yd_tem yr_beg yr_end
      initem item xr_beg xr_end yr_beg yr_end
    endcommand
    yr_end = yr_end - delt_y
    yr_beg = yr_beg - delt_y
  endloop
end
*
setup
```

```
init_tem
print bound
*
initem 18.7 -29.0,29.0 310.0,312.0
initem 29.42 -29.0,29.0 -226.0,-224.0
tfix 18.70 range -29.0,29.0 310.0,312.0
tfix 29.42 range -29.0,29.0 -226.0,-224.0
*
thist ntcyc=10 tem 0 2.5 tem 0 5 tem 0 10 tem 0 25 tem 0 50 tem 0 100
thist tem 0 150 tem 0 200 tem 0 250 tem 0 311 tem 2.5 0 tem 5 0 tem 10 0
thist tem 14 0
thist tem -28 2.5 tem 28 2.5

*
**********
* apply heat flux to tunnel wall
**********
*
thapp ann   0.0 0.0 2.4 2.53 flux 43.18 -3.2197e-10
thapp ann -28.0 0.0 2.4 2.53 flux 43.18 -3.2197e-10
thapp ann  28.0 0.0 2.4 2.53 flux 43.18 -3.2197e-10
*
sav 3tun_tbc.sav
*
* run thermal time to 1 day (implicit) - explicit time step is too small (~10e-5 sec)
*
run age=8.64e4 delt=5.0 temp=10000 step=2000000 tol=0.025 impl
reset damp
cycle 5000
pr max
*
* run thermal time to 10 days
*
run age=8.64e5 delt=10.0 temp=10000 step=2000000 tol=0.025 impl
reset damp
cycle 5000
pr max
*
* run thermal time to 1 month
*
run age=2.592e6 delt=500.0 temp=10000 step=2000000 tol=0.025 impl
reset damp
cycle 5000
pr max
*
* run thermal time to 2 months
*
```

```
run age=5.184e6 delt=500.0 temp=10000 step=2000000 tol=0.025 impl
reset damp
cycle 5000
pr max
*
* run thermal time to 3 months
*
run age=7.776e6 delt=500.0  temp=10000 step=2000000 tol=0.025 impl
reset damp
cycle 5000
pr max
*
* run thermal time to 6 months
*
run age=1.5552e7 delt=1000.0  temp=10000 step=2000000 tol=0.025 impl
reset damp
cycle 5000
pr max
*
* run thermal time to 1 year
*
run age=3.1536e7 delt=1000.0  temp=10000 step=2000000 tol=0.025 impl
reset damp
cycle 5000
pr max
save 3tun_1y.sav
*
* run thermal time to 18 months
*
run age=4.7304e7 delt=1000.0  temp=10000 step=2000000 tol=0.025 impl
reset damp
cycle 5000
pr max
*
* run thermal time to 2 years
*
run age=6.3072e7 delt=1000.0  temp=10000 step=2000000 tol=0.025 impl
reset damp
cycle 5000
pr max
sav 3tun_2y.sav
*
* run thermal time to 3 years
*
run age=9.4608e7 delt=1000.0  temp=10000 step=2000000 tol=0.025 impl
reset damp
cycle 5000
```

```
sav 3tun_3y.sav
pr max
*
* run thermal time to 4 years
*
run age=1.26144e8 delt=1000.0  temp=10000 step=2000000 tol=0.025 impl
reset damp
cycle 5000
pr max
sav 3tun_4y.sav
*
* run thermal time to 5 years
*
run age=1.5768e8 delt=1000.0  temp=10000 step=2000000 tol=0.025 impl
reset damp
cycle 5000
pr max
sav 3tun_5y.sav
*
* run thermal time to 7.5 years
*
run age=2.3652e8 delt=1000.0 temp=10000 step=2000000 tol=0.025 impl
reset damp
cycle 5000
pr max
*
* run thermal time to 10 years
*
run age=3.1536e8 delt=1000.0 temp=10000 step=2000000 tol=0.025 impl
reset damp
cycle 5000
pr max
sav 3tun_10y.sav
*
* run thermal time to 20 years
*
run age=6.3072e8 delt=2000.0 temp=10000 step=2000000 tol=0.025 impl
reset damp
cycle 5000
pr max
save 3tun_20y.sav
*
* run thermal time to 30 years
*
run age=9.4608e8 delt=2000.0 temp=10000 step=2000000 tol=0.025 impl
reset damp
cycle 5000
```

```
pr max
sav 3tun_30y.sav
*
* run thermal time to 40 years
*
run age=12.6144e8 delt=2000.0 temp=10000 step=2000000 tol=0.025 impl
reset damp
cycle 5000
pr max
res 3tun_40y.sav
*
* run thermal time to 50 years
*
run age=1.5768e9 delt=7200.0 temp=10000 step=2000000 tol=0.025 impl
reset damp
cycle 6000
pr max
sav 3tun_50y.sav
ret
*
* run thermal time to 60 years
run age=1.89216e9 delt=7200.0 temp=10000 step=2000000 tol=0.025 impl
reset damp
cycle 6000
pr max
*sav 3tun_60y.sav
*
* run thermal time to 70 years
*
run age=2.20752e9 delt=7200.0 temp=10000 step=2000000 tol=0.025 impl
reset damp
cycle 6000
pr max
* sav 3tun_70y.sav
*
* run thermal time to 80 years
*
run age=2.52288e9 delt=7200.0 temp=10000 step=2000000 tol=0.025 impl
reset damp
cycle 6000
pr max
*
* run thermal time to 100 years
*
run age=3.1536e9 delt=7200.0 temp=10000 step=2000000 tol=0.025 impl
reset damp
cycle 6000
```

```
pr max
sav 3tun_100y.sav
return
*
```

APPENDIX B

UDEC INPUT DATA FILE FOR 4-TUNNEL MODEL WITH THE TRANSITIONAL ZONE LOCATED ALONG A VERTICAL LINE MIDWAY BETWEEN DRIFTS

APPENDIX B
UDEC INPUT DATA FILE FOR 4-TUNNEL MODEL WITH THE TRANSITIONAL ZONE LOCATED ALONG A VERTICAL LINE MIDWAY BETWEEN DRIFTS

```
************************************************************
* UDEC Version 3.0 Input Data File
* 4 tunnel drift scale T-M model with weak rock/strong rock transition zone midway between
* central tunnels
*
* Objective - Evaluate transition zone between a strong TSW2 category rock versus a weaker TSW2
* category rock  in which the dividing line between the two categories occurs between the two central
* tunnels.  Approach is to incorporate two different joint sets (one being 85 degrees measured ccw from
* horizontal axis and the other being 20 degrees (as taken from Table 1 (Chen, 1999).  As listed in this
* table, mean fracture spacings were on the order of 0.4 m for the 85 degree joint set and 0.75 m for the
20 * degree joint set, both with standard deviations of 0.1 m.
*
*  Strong rock -   Joint Set #1 - (mean orientation 85 degrees ccw from horizontal, joint spacing = 1.0 m)
*                  Joint Set #2 - (mean orientation 20 degrees ccw from horizontal, joint spacing = 2.0 m)
*
*         Equivalent rock mass modulus (Em) in the horizontal direction where 1/Em = 1/Er + 1/(Kn*S)
*                  and Er = 3.303e+04 MPa [Intact Rock Young's Modulus]
*                      Kn = 5.0e+04 MPa/m  [Joint normal stiffness]
*                      S = 1.0 m [Sub-vertical joint spacing]
*  ------>             Em = 19.890 GPa   (horizontal direction)
*
*  Weak  rock -   Joint Set #1 - (mean orientation 85 degrees ccw from horizontal, joint spacing = 0.5 m)
*                 Joint Set #2 - (mean orientation 20 degrees ccw from horizontal, joint spacing = 1.0 m)
*
*                    Assuming S=0.5 m [Sub-vertical joint spacing]
*  -------->          Em = 14.230 GPa (horizontal direction)
*
*  Note: small standard deviation in joint orientation allowed (10 degrees for 85 degree joint set, and 5
* degrees for the 20 degree joint set). Also, mean joint trace lengths of 7.5 m was assigned to 85 degree
* joint set and 5.0 m to the 20 degree joint set, both with a standard deviation of 1.0 m.
************************************************************
*
*********************
* Part I:
*********************
set log tm_4tun.log
set plot po
start
**********************************************************************
* Title and block definition for Lwp=18 m, Ldrift=28 m
```

```
**********************************************************************
head
4 Tunnel T-M Analysis - strong/weak rock transition between central two tunnels
config thermal
*
* Size of problem domain is -42 m < x < 42 m;  -225 m < y < 311 m
*  - Vertical boundaries are located along symmetry lines assuming
*    28 m drift spacings
*
round 0.0145
set ovtol 1.0
*
**************
* Part I - In situ loading and excavation of tunnels
*************
block -42,-225 -42,311 42,311 42,-225
* create splits at all rock formation boundaries TCw --> CHnz
split -42,275 42,275
split -42,236.9 42,236.9
split -42,106.8 42,106.8
split -42,-82.5 42,-82.5
split -42,-98.3 42,-98.3
split -42,-103.5 42,-103.5
split -42,-207.5 42,-207.5
split -42,-225 42,-225
*
* create additional horizontal cracks to bound fractured from non-fractured region
split -42,15 42,15
split -42,-15 42,-15
split -42,-25 42,-25
split -42,25 42,25
*
* create jointing around tunnels
jregion -42,-15 -42,15 2.5,15 2.5,-15
jset 85.0,10.0 7.5,1.0 -0.2,0.0 1.0,0.0 -28,-15
jset 20.0,5.0 5.0,1.0 -0.2,0.0 2.0,0.0 -28,-15
*
jregion 0,-15 0,15 42,15 42,-15
jset 85.0,10.0 7.5,1.0 -0.2,0.0 0.5,0.0 -28,-15
jset 20.0,5.0 5.0,1.0 -0.2,0.0 1.0,0.0 -28,-15
*
tunnel -42 0 2.5 24
tunnel -14 0 2.5 24
tunnel 14 0 2.5 24
tunnel 42 0 2.5 24
*
* add additional cracks to break up large blocks around 2 tunnels on left side of model (strong rock)
```

```
cr -11.75,4.891 -11.57,3.674
cr -18.74,-1.022 -18.40,1.251
cr -18.74,-1.022 -17.73,-0.5342
cr -17.37,-2.726 -18.93,-3.149
cr -39.08,-.1467 -39.09,-2.032
cr -37.78,0.5274 -36.28,1.250
cr -41.07,-4.648 -41.38,-7.236
cr -41.07,-4.648 -42.0,-4.90
cr -39.09,-2.032 -38.72,0.2527
cr -12.31,3.368 -13.36,3.097
cr -11.75,4.891 -12.31,3.368
*
del area 1.5e-2
jd
save 4tun_jnt.sav
*
* ****************************
*  auto generation of zones
* ****************************
gen ann -42 0 0 5.0 edge 1.0
gen ann -14 0 0 5.0 edge 1.0
gen ann  14 0 0 5.0 edge 1.0
gen ann  42 0 0 5.0 edge 1.0
gen region -42 -15 -42 15 42 15 42 -15 edge 1.25
*
gen region -42 15 -42 25 42 25 42 15 quad 2.5
gen region -42 -25 -42 -15 42 -15 42 -25 quad 2.5
gen region -42 -225 -42 -25 42 -25 42 -225 quad 10.0
gen region -42 25 -42 311 42 311 42 25  quad 10.0
save 4tun_zon.sav
pr max
*
*****************************************************
* apply mechanical boundary conditions (units, MPa)
*****************************************************
grav 0.0 -9.81
insitu stress -1.89 0.0 -7.0 ygrad 0.006077 0.0 0.022508 szz -1.89 &
zgrad 0.0 0.006077
bound -42 42 310 312 stress -1.89 0.0 -7.0 ygrad 0.006077 0.0 0.022508
bound -42 42 -226 -224 yvel=0.0
bound -42.5 -41.5 -225 312 xvel=0.0
bound 41.5 42.5 -225 312 xvel=0.0
*
*************************************************************************
* define mechanical and thermal material properties for joints/intact blocks
*************************************************************************
*
```

```
*  material 1 = rock
*
change -43 43 -16 16 jcons=5
**
**** TCw unit ****
prop mat=1 k=18.3908e3 g=13.2231e3 d=0.002274
prop mat=1 cond=1.59 thexp=6.0e-06 spec=9.32e08
*
**** PTn unit ****
prop mat=2 k=18.3908e3 g=13.2231e3 d=0.002274
prop mat=2 cond=0.85 thexp=6.0e-06 spec=9.32e08
*
**** TSw1 unit *****
prop mat=3 k=18.3908e3 g=13.2231e3 d=0.002274
prop mat=3 cond=1.60 thexp=6.0e-06 spec=9.32e08
*
**** TSw2 unit ****
prop mat=4 k=18.3908e3 g=13.2231e3 d=0.002274
prop mat=4 cond=2.10 thexp=6.0e-06 spec=9.32e08
*
****TSw3 unit ****
prop mat=5 k=18.3908e3 g=13.2231e3 d=0.002274
prop mat=5 cond=1.28 thexp=6.0e-06 spec=9.32e08
*
**** CHn1v unit ****
prop mat=6 k=18.3908e3 g=13.2231e3 d=0.002274
prop mat=6 cond=1.20 thexp=6.0e-06 spec=9.32e08
*
**** CHn1z unit ****
prop mat=7 k=18.3908e3 g=13.2231e3 d=0.002274
prop mat=7 cond=1.28 thexp=6.0e-06 spec=9.32e08
*
**** CHnz unit ****
prop mat=8 k=18.3908e3 g=13.2231e3 d=0.002274
prop mat=8 cond=1.56 thexp=6.0e-06 spec=9.32e08
*
**** joint properties TSw2 welded unit ****
prop jmat=4 jks=5.0e4 jkn=5.0e4 kn=5.0e4 ks=5.0e4
prop jmat=4 jdil=0 jc=0.03 jfric=41.0 jtens=0.0
*
change mat=1 range -42 42 275.0 312.0
change mat=2 range -42 42 236.9 275.0
change mat=3 range -42 42 106.8 236.9
change mat=4 jmat=4 range -42 42 -82.5 106.8
change mat=5 range -42 42 -98.3 -82.5
change mat=6 range -42 42 -103.5 -98.3
change mat=7 range -42 42 -207.5 -103.5
```

```
change mat=8 range -42 42 -225 -207.5
*
set jcondf 5
*
* mohr-coulomb failure parameters TSw2 unit
*
prop mat=4 coh=36.9 fric=46.0 tens=8.91 dil=0
*
* assign high strength properties to fictitious horizontal  joints separating rock units
*
change jmat=2 range -43 43 14.99 312
change jmat=2 range -43 43 -226 -14.99
prop jmat=2 jkn=1.0e5 jks=1.0e5 jcoh=1.0e20 jten=1.0e20 &
kn=5.0e4 ks=5.0e4

****************
* history records
****************
hist ncyc=10 unbal damp type 4
hist ydis 0 0 yvel 0 0 yacc 0 0 ydis 0 311 yvel 0 311 yacc 0 311
hist sxx 0.0 0.0 syy 0.0 0.0
*
*******************************
* initial cycling equilibrium
*******************************
damp auto
cycle 5000
save 4tun_ini.sav
*
************************
* remove tunnel blocks
************************
*
del ann -42 0 0 2.5
del ann -14 0 0 2.5
del ann  14 0 0 2.5
del ann  42 0 0 2.5
*
* reset displacements after applying in situ loading conditions
*
reset damp time hist dis rot
hist unbal damp
hist ydis -14 2.5 yvel -14 2.5 yacc -14 2.5 ydis 0.0 311.0
hist ydis -42 2.5 yvel -42 2.5
hist ydis  14 2.5 yvel  14 2.5
hist ydis  42 2.5 yvel  42 2.5
hist sxx -14 2.5 syy -14 2.5
```

```
hist sxx  14 2.5 syy 14 2.5
*
* change Tsw2 material property to Mohr-Coulomb
change cons=3 range -42 42 -82.5 106.8
*
cycle 6000
*
sav 4tun_exc.sav
*
res 4tun_exc.sav
*
**********************
* Part II: Thermal
**********************
*
*************************************
* set thermal boundary and histories
*************************************
*
* set up thermal boundaries (default thermal b.c. are adiabatic)
*
*  Initial temperature at repository horizon taken to be approx, 25 C
*  Average ground surface temperature = 18.70 C
*  - temperature gradient taken to be 0.02 deg C/m
*
*  $$$ fish functions to set up initial temperature gradient $$$
*
def setup
  t_surf = 18.7       ; fixed ground surface temperature
  y_surf = 311.0      ; distance to ground surface from y-origin (i.e., repos. level)
  t_grad = 0.02       ; temperature gradient
  xr_beg = -42.0      ; start of x-range (m)
  xr_end = 42.0       ; end of x-range (m)
  delt_y = 5.0        ; increment in y to set initial grid node temperatures (m)
  num_inc = 108       ; number of increments in delt_y to reach base of model (311 < y < -225 m)
end
*
def init_tem
  yr_end = 310.0  ; starting y end range
  yr_beg = yr_end - delt_y   ; starting y beginning range
  loop ii (1, num_inc)
    yd_tem = y_surf - (0.5*(yr_end + yr_beg))   ;  depth location below surface to calculate initial temp
(midpoint of y range)
    item = t_surf + t_grad*yd_tem
    command
      pr item yd_tem yr_beg yr_end
      initem item xr_beg xr_end yr_beg yr_end
```

```
    endcommand
    yr_end = yr_end - delt_y
    yr_beg = yr_beg - delt_y
  endloop
end
*
setup
init_tem
print bound
*
initem 18.7 -43.0,43.0 310.0,312.0
initem 29.42 -43.0,43.0 -226.0,-224.0
tfix 18.70 range -43.0,43.0 310.0,312.0
tfix 29.42 range -43.0,43.0 -226.0,-224.0
*
thist ntcyc=10 tem 0 0 tem 0 5 tem 0 10 tem 0 25 tem 0 50 tem 0 100
thist tem 0 150 tem 0 200 tem 0 250 tem 0 311
thist tem 14 2.5 tem -14 2.5
thist tem -42 2.5 tem 42 2.5
*
**********************************
* apply heat flux to tunnel wall
* heat load to represent 85 MTU/acre AML
**********************************
*
thapp ann -42.0 0.0 2.4 2.53 flux 43.18 -3.2197e-10
thapp ann -14.0 0.0 2.4 2.53 flux 43.18 -3.2197e-10
thapp ann  14.0 0.0 2.2 2.53 flux 43.18 -3.2197e-10
thapp ann  42.0 0.0 2.4 2.53 flux 43.18 -3.2197e-10
*
* run thermal time to 1 day
*
run age=8.64e4  delt=10.0 temp=10000 step=1000000 tol=0.025 impl
reset damp
cycle 5000
pr max
*
* run thermal time to 1 month
*
run age=2.592e6 delt=500.0 temp=10000 step=1000000 tol=0.025 impl
reset damp
cycle 5000
pr max
*
* run thermal time to 3 months
*
run age=7.776e6 delt=500.0  temp=10000 step=1000000 tol=0.025 impl
```

```
reset damp
cycle 5000
pr max
*
* run thermal time to 6 months
*
run age=1.5552e7 delt=1000.0  temp=10000 step=1000000 tol=0.025 impl
reset damp
cycle 5000
pr max

*
* run thermal time to 1 year
*
run age=3.1536e7 delt=1000.0  temp=10000 step=1000000 tol=0.025 impl
reset damp
cycle 5000
pr max
save 4tun_1y.sav
*
* run thermal time to 18 months
*
run age=4.7304e7 delt=1000.0  temp=10000 step=1000000 tol=0.025 impl
reset damp
cycle 5000
pr max
*
* run thermal time to 2 years
*
run age=6.3072e7 delt=1000.0  temp=10000 step=1000000 tol=0.025 impl
reset damp
cycle 5000
pr max
sav 4tun_2y.sav
*
* run thermal time to 3 years
*
run age=9.4608e7 delt=1000.0  temp=10000 step=1000000 tol=0.025 impl
reset damp
cycle 5000
sav 4tun_3y.sav
pr max
*
* run thermal time to 4 years
*
run age=1.26144e8 delt=1000.0  temp=10000 step=1000000 tol=0.025 impl
reset damp
```

```
cycle 5000
pr max
sav 4tun_4y.sav
*
* run thermal time to 5 years
*
run age=1.5768e8 delt=1000.0  temp=10000 step=1000000 tol=0.025 impl
reset damp
cycle 5000
pr max
res 4tun_5y.sav
*
* run thermal time to 7.5 years
*
run age=2.3652e8 delt=1500.0 temp=10000 step=1000000 tol=0.025 impl
reset damp
cycle 5000
pr max
*
* run thermal time to 10 years
*
run age=3.1536e8 delt=1500.0 temp=10000 step=1000000 tol=0.025 impl
reset damp
cycle 5000
pr max
sav 4tun_10y.sav
*
* run thermal time to 20 years
*
del bl 578915
del bl 578606
cycle 500
run age=6.3072e8 delt=1750.0 temp=10000 step=2000000 tol=0.029 impl
reset damp
cycle 5000
pr max
save 4tun_20y.sav
*
* run thermal time to 30 years
*
run age=9.4608e8 delt=1750.0 temp=10000 step=3000000 tol=0.029 impl
reset damp
cycle 5000
pr max
sav 4tun_30y.sav
*
* run thermal time to 40 years
```

```
*
run age=12.6144e8 delt=1750.0 temp=10000 step=4000000 tol=0.029 impl
reset damp
cycle 6000
pr max
sav 4tun_40y.sav
*
* run thermal time to 50 years
*
run age=1.5768e9 delt=1750.0 temp=10000 step=4000000 tol=0.029 impl
reset damp
cycle 6000
pr max
sav 4tun_50y.sav
ret
*
* run thermal time to 60 years
run age=1.89216e9 delt=1500.0 temp=10000 step=1000000 tol=0.025 impl
reset damp
cycle 5000
pr max
*sav 4tun_60y.sav
*
* run thermal time to 70 years
*
run age=2.20752e9 delt=1500.0 temp=10000 step=1000000 tol=0.025 impl
reset damp
cycle 5000
pr max
* sav 4tun_70y.sav
*
* run thermal time to 80 years
*
run age=2.52288e9 delt=1500.0 temp=10000 step=1000000 tol=0.025 impl
reset damp
cycle 5000
pr max
* sav 4tun_80y.sav
*
* run thermal time to 100 years
*
run age=3.1536e9 delt=1500.0 temp=10000 step=1000000 tol=0.025 impl
reset damp
cycle 5000
pr max
sav 4tun_100y.sav
return
```